



Virginia Commonwealth University
VCU Scholars Compass

Theses and Dissertations

Graduate School

1988

**ELECTROCHEMICAL AND SURFACE ENHANCED RESONANCE
RAMAN STUDY OF HEME PROTEINS AT BARE METAL
ELECTRODES**

David Edward Reed

Follow this and additional works at: <https://scholarscompass.vcu.edu/etd>

 Part of the [Chemistry Commons](#)

© The Author


Downloaded from

<https://scholarscompass.vcu.edu/etd/5260>

This Dissertation is brought to you for free and open access by the Graduate School at VCU Scholars Compass. It has been accepted for inclusion in Theses and Dissertations by an authorized administrator of VCU Scholars Compass. For more information, please contact libcompass@vcu.edu.

COLLEGE OF HUMANITIES AND SCIENCES
VIRGINIA COMMONWEALTH UNIVERSITY

This is to certify that the dissertation prepared by David E. Reed entitled "Electrochemical and Surface Enhanced Resonance Raman Study of Heme Proteins at Bare Metal Electrodes" has been approved by his committee as satisfactory completion of the dissertation requirement for the degree of Doctor of Philosophy.



Director of Dissertation




Committee Member



Committee Member



Committee Member



Committee Member



Committee Member



Department Chairman



College Dean

5-31-88

Date

© David E. Reed 1988

All Rights Reserved

ELECTROCHEMICAL AND SURFACE ENHANCED RESONANCE RAMAN
STUDY OF HEME PROTEINS AT BARE METAL ELECTRODES

A dissertation submitted in partial fulfillment of the
requirements for the degree of Doctor of Philosophy at
Virginia Commonwealth University.

By

David Edward Reed
A.S., Virginia Western Community College, 1979
B.S., Virginia Commonwealth University, 1983

Director: Dr. Fred M. Hawkrige
Professor of Chemistry

Virginia Commonwealth University
Richmond, Virginia
May 1988

ACKNOWLEDGEMENTS

I take this time to express gratitude to all those who have provided help in the course of my study at Virginia Commonwealth University. Special appreciation goes out to the faculty of the Department of Chemistry for their unlimited support and assistance. I am specially grateful to my advisor, Dr. Fred M. Hawkridge, for his guidance, constant encouragement and advise throughout my graduate career. I also wish to thank Dr. James Turner for the time and effort he spent in order to help me with the SERRS experiments, and Dr. Songchen Sun for sharing his knowledge in this area. I enjoyed the opportunity to work with Dr. Kent Koller and Dr. Bertha King, and would like to thank them and the other graduate students for their friendship.

Finally, special thanks go to my wife Patty and her family for their encouragement, understanding and patience throughout my graduate studies.

TABLE OF CONTENTS

	page
LIST OF TABLES	vi
LIST OF FIGURES	vii
LIST OF SYMBOLS	x
ABSTRACT	xiii
I. INTRODUCTION	1
A. Overview	1
B. Physiological Reactions of Cytochrome <u>c</u>	5
C. Structure of Cytochrome <u>c</u>	19
D. Properties of Cytochrome <u>c</u>	32
E. Conformational Changes of Cytochrome <u>c</u> with pH	40
F. Redox Conformational Changes of Cytochrome <u>c</u>	47
G. Electrode Reactions of Heme Proteins	52
H. Resonance Raman Spectroscopy of Heme Proteins	67
I. Surface Enhanced Resonance Raman Spectroscopy	77
II. EXPERIMENTAL	83
III. RESULTS AND DISCUSSION	98
A. Interfering Faradaic and Non-Faradaic Reactions at Silver Electrodes	98

TABLE OF CONTENTS (continued)

	page
B. Effects of Lyophilization on the Electron Transfer Kinetics of Cytochrome <u>c</u>	106
1. Evidence of a Contaminating Component after Lyophilization	106
2. Identity of the Contaminating Component	113
3. Mechanism for Decreased Electron Transfer After Lyophilization	117
C. Determination of Heterogeneous Electron Transfer Kinetic Parameters for Purified Cytochrome <u>c</u>	120
1. DCVA and Background Subtracted CV Responses of Purified Cytochrome <u>c</u> at Smooth Silver Electrodes	120
2. Reductive SPS/CA Responses of Purified Cytochrome <u>c</u> at Smooth Silver Electrodes	129
3. DCVA Response of Purified Cytochrome <u>c</u> at a Rough Silver Electrode	145
D. Adsorption Effects of Purified Cytochrome <u>c</u> at a Smooth Silver Electrode	148
E. Surface Enhanced Resonance Raman Spectroscopy of Cytochrome <u>c</u>	153
1. Studies of Silver Sol Suspensions for Purified Cytochrome <u>c</u>	153
2. Studies at Electrochemically Roughened Silver Electrodes for Purified Cytochrome <u>c</u>	160
3. Effect of Electric Field on Spin State of Cytochrome <u>c</u>	170
4. Importance of Sample Purification on SERRS Experiments	174
IV. SUMMARY AND CONCLUSIONS	178
REFERENCES	184

TABLE OF CONTENTS (continued)

	page
APPENDIX I. DATA ACQUISITION SYSTEMS	198
A. Setup of the Spectroelectrochemical System	198
B. Computational Algorithms for DCVA and SPS/CA Experiments	202
APPENDIX II. VIBRATIONAL MODES CORRESPONDING TO ν_3 AND ν_4 RR INDICATOR BANDS	220
APPENDIX REFERENCES	223
VITA	224

LIST OF TABLES

Table	page
1. Heterogeneous electron transfer kinetic parameters for chromatographically purified cytochrome <u>c</u> at a smooth silver electrode.....	144

LIST OF FIGURES

Figure	page
1. Schematic representation of the mitochondrial respiratory chain	6
2. Interaction of cytochrome <u>aa₃</u> with cytochrome <u>c</u> and dioxygen	11
3. Heme <u>c</u>	20
4. Molecular structure of cytochrome <u>c</u>	24
5. Visible absorption spectrum of cytochrome <u>c</u>	71
6. Resonance Raman spectra of cytochrome <u>c</u>	75
7. Spectroelectrochemical cell design	88
8. Cyclic voltammetry of a smooth silver electrode in degassed 0.05 M Na ₂ SO ₄ electrolyte	101
9. Derivative cyclic voltabsorptometry of purified and lyophilized cytochrome <u>c</u> at a smooth silver electrode.....	108
10. Cyclic voltammetry of adsorbed lyophilized cytochrome <u>c</u> at a smooth silver electrode.....	111
11. Derivative cyclic voltabsorptometry of deamidated and oligomeric forms of cytochrome <u>c</u> at a smooth silver electrode	114
12. Derivative cyclic voltabsorptometry and background subtracted cyclic voltammetry of purified cytochrome <u>c</u> at a smooth silver electrode.....	121
13. Plot of background subtracted cyclic voltammetry cathodic peak currents <u>vs.</u> concentration of purified cytochrome <u>c</u> at a smooth silver electrode.....	126

LIST OF FIGURES (continued)

Figure	page
14. Normalized absorbance vs. $\log [k_{f,h}(t/D_0)^{1/2}]$ working curves for SPS/CA experiments.....	133
15. SPS/CA absorbance vs. time response for the reduction of purified cytochrome <u>c</u> at a smooth silver electrode.....	136
16. Background subtracted (SPS/CA) responses for the reduction of purified cytochrome <u>c</u> at a smooth silver electrode.....	139
17. Plot of $\log k_{f,h}$ vs. η for SPS/CA reduction kinetics of purified cytochrome <u>c</u> at a smooth silver electrode.....	141
18. Derivative cyclic voltabsorptometry of purified cytochrome <u>c</u> at a roughened silver electrode.....	146
19. Derivative cyclic voltabsorptometry subtracted from cyclic voltammety response for purified cytochrome <u>c</u> at a smooth silver electrode.....	151
20. SERRS spectra of purified ferricytochrome <u>c</u> adsorbed on silver sol.....	154
21. Effect of Ag^+ ions on the resonance Raman spectra of purified ferricytochrome <u>c</u>	158
22. Comparison of SERRS and resonance Raman spectra of purified cytochrome <u>c</u> at a silver electrode.....	161
23. Potential dependence of SERRS spectra for purified cytochrome <u>c</u> at a silver electrode.....	166
24. Fractional reduction of adsorbed cytochrome <u>c</u> as a function of electrode potential of SERRS spectra from Figure 23.....	168

LIST OF FIGURES (continued)

25. SERRS spectra of purified cytochrome c
at a silver electrode as a function
of electrolyte concentration..... 172
26. Effects of sample purification on
SERRS spectra of cytochrome c
at a silver electrode..... 175
27. Schematic diagram for converting
optical intensity to absorbance..... 199
28. Molecular motions contributing to
the observed normal vibrational modes
of the ν_3 and ν_4 bands..... 221

LIST OF SYMBOLS

A_n	normalized absorbance
ΔA	difference absorbance response
A/D	analog-to-digital
ADP	adenosine diphosphate
ATP	adenosine triphosphate
ap	anomalously polarized
c°	bulk molar concentration of oxidized species
CD	circular dichroism
CDNP	4-carboxy-2,6-dinitrophenyl
CV	cyclic voltammetry
D_O	diffusion coefficient of oxidized species
dA/dE	derivative optical response
DCVA	derivative cyclic voltabsorptometry
dp	depolarized
E	electrode potential referenced to the normal hydrogen electrode
E°'	formal redox potential referenced to the normal hydrogen electrode
E_f	Fermi level
$E_{f,b}$	flat-band potential
$E_{p,a}$	anodic peak potential
$E_{p,c}$	cathodic peak potential
ΔE_p	peak potential separation
E_{step}	potential applied to the working electrode
EM	electromagnetic

LIST OF SYMBOLS (continued)

EPR	electron paramagnetic resonance
$I_{ }$	intensity of scattered radiation in the parallel mode
I_{\perp}	intensity of scattered radiation in the perpendicular mode
i_{ADS}	current due to adsorbed material
i_{DL}	current due to double layer charging
i_F	faradaic current due to species of interest
i_T	total current obtained in a CV experiment
$k_{b,h}$	back heterogeneous electron transfer rate constant (potential dependent)
k_{et}	unimolecular electron transfer rate constant
$k_{f,h}$	forward heterogeneous electron transfer rate constant (potential- dependent)
$k^{\circ}{}_{s,h}$	formal heterogeneous electron transfer rate constant (evaluated at $E = E^{\circ}$)
n	stoichiometric number of electrons transferred
NADH	nicotinamide adenine dinucleotide
NHE	normal hydrogen electrode
NMR	nuclear magnetic resonance
ORC	oxidation-reduction cycle
ox	oxidized species
p	polarized
ph_{pzc}	point of zero charge when no other electrolyte ions besides H^+ and OH^- are specifically adsorbed

LIST OF SYMBOLS (continued)

pzzp	point of zero zeta potential
red	reduced species
RR	resonance Raman
SERS	surface enhance Raman scattering
SERRS	surface enhanced resonance Raman scattering
SPS/CA	single potential step chronoabsorptometry
t	time in seconds
TNP	2,4,6-trinitrophenyl
Tris	tris(hydroxymethyl)aminoethane
UVR	ultraviolet resonance Raman
UQ	ubiquinone
α	reductive electrochemical transfer coefficient
ϵ	molar absorptivity
$\Delta\epsilon$	difference molar absorptivity between two forms of a molecule (typically $\epsilon_{red} - \epsilon_{ox}$)
η	charge transfer overpotential ($E_{step} - E^{\circ}$)
ρ	polarization ratio
$\Delta\nu$	Raman frequency shift
μM	micromolar
μC	microcoulombs

ABSTRACT

ELECTROCHEMICAL AND SURFACE ENHANCED RESONANCE RAMAN STUDY OF HEME PROTEINS AT BARE METAL ELECTRODES.

David E. Reed

Virginia Commonwealth University, 1988

Major Director: Dr. F. M. Hawkridge

Direct heterogeneous electron transfer reactions between horse heart cytochrome c and silver electrodes were investigated by electrochemical and spectroelectrochemical methods. The kinetics of these reactions were established as being quasi-reversible, with a formal heterogeneous rate constant ($k^{\circ}_{s,h}$) ranging between $0.18 - 1.5 \times 10^{-3}$ cm/s, for both polished and electrochemically roughened silver surfaces. Such reactions were stable and reproducible for over ten hours at room temperature. These results clearly demonstrate that neither electrode surface modification nor the inclusion of mediators is necessary to study electron transfer reactions of heme proteins at metal electrodes.

A crucial factor in obtaining the quasi-reversible heterogeneous electron transfer kinetics described above is the use of highly purified, never lyophilized, cytochrome c samples. When samples were lyophilized after purification, irreversible electron transfer kinetics were observed. These results show the profound negative impact that lyophilization has on the rates of electron transfer at bare metal

electrodes. The lyophilization process was indicated to produce small amounts of oligomeric material which rapidly and irreversibly adsorbs on the electrode surface preventing further solution cytochrome c molecules from reacting. This denatured form, along with other solution impurities, is believed to be the reason for the lack of stable facile responses towards metal electrodes.

Surface enhanced resonance Raman spectroscopy was used to monitor conformational changes associated with the direct electron transfer reactions of purified cytochrome c at silver electrodes. The results of this study indicated that cytochrome c exists in a penta-coordinate high spin configuration, with a formal potential ≈ 0.350 volts more negative than its corresponding bulk solution value when adsorbed. This suggests that cytochrome c is still capable of exchanging electrons in a quasi-reversible fashion even though there is strong irreversible adsorption of a denatured form on the electrode surface.

I. INTRODUCTION

A. Overview

Over the years there has been great interest in studying the thermodynamics, kinetics and mechanisms of direct heterogeneous electron transfer reactions of metalloproteins at various electrode surfaces. Interest in these studies is due to the possibility of gaining better insight into the interactive behavior of such proteins at biological interfaces. Physiologically, a number of metalloproteins are known to transfer their electrons in a heterogeneous fashion at an enzyme/cytoplasm interface. Although an electrode in solution is surely not as complicated as such interfaces, it can provide donor or acceptor capabilities to the active site in the protein much like its enzyme redox partner. Therefore, the advantage of direct heterogeneous electron transfer at electrodes is that it might provide a way of investigating and modeling some of the important features of in vivo electron transfer systems.

One important feature of in vivo electron transfer systems involves enzyme-metalloprotein redox intermediates formed prior to the electron transfer step (referred to as "precursor complexes"). These complexes occur during the collision process of the reaction partners and are formed by way of specific binding interactions for one another. Like-

wise, the pathway by which a diffusing metalloprotein can donate or accept electrons heterogeneously at an electrode/solution interface can be viewed as involving a similar type of intermediate. In this case, the intermediate will be between the electrode surface and the particular protein of interest and can be perceived as a specifically adsorbed intermediate. Indeed, protein adsorption on electrode surfaces seems to be a general phenomenon. Therefore, features such as proteins adsorbing at electrode surfaces might also be viewed as being analogous to their physiological binding interactions with either membrane or protein interfaces.

However, the role played by protein adsorption (binding) in heterogeneous electron transfer reactions of metalloproteins at electrode surfaces is not yet fully understood. Generally, it has been accepted that the strength of protein association (adsorption) and dissociation (desorption) might play a major part in the electron transfer process. The rate of electron transfer would then depend on the diffusing protein's ability to bind transiently (never irreversibly) to the electrode surface. However, the surface adsorption properties of proteins at electrodes are not always in agreement with the preceding concept. For example, an electron transfer heme protein like cytochrome c is known to react in a rapid diffusion controlled manner with a tin-doped indium oxide electrode in the presence of an

adsorbed layer of this protein on its surface (1). Film transfer experiments indeed indicated that this protein does not readily desorb from the electrode surface, suggesting that the presence of adsorbed protein at the electrode does not have an adverse effect on the electron transfer rate. The adsorption behavior observed was indicated as being due to high affinity binding sites resulting from surface defects (1), since later studies (2) indicated weak adsorption at such electrodes. In contrast, when adsorption of this same protein is present on various bare metal electrode surfaces such as silver (3) and gold (4), more sluggish electron transfer kinetics have been reported. These findings clearly indicate that other factors besides the necessity for reversible adsorption must be considered when modelling electrode reactions of diffusing proteins.

A factor that might have a critical effect on the electron transfer rate, is the extent of conformational changes attending adsorption of protein on the electrode surface. In fact, surface denaturation of cytochrome c has long been reported to occur at bare metal electrodes such as silver (3) and gold (4). This has been indicated by its large negative shift in formal potential when adsorbed on such surfaces. The fact that this same protein is in its native state when adsorbed on metal oxide electrodes (1), as indicated by the small negative shift (≈ 0.015 volts) in the formal potential relative to that in solution, might explain

its facile electron transfer reaction with such surfaces. Therefore, the nature of this adsorbed layer will be of interest in determining heterogeneous electron transfer properties of metalloproteins at various electrode surfaces.

Cytochrome c has been the most widely studied of all the metalloproteins, mostly because it can be easily isolated in a purified form, its structure and chemical reactivity are well characterized, and it is relatively stable under in vitro conditions. The present study was aimed at characterizing the interfacial behavior of cytochrome c at bare metal electrode surfaces, since they have been found to exhibit negligible responses with this protein in the past. As was mentioned above this is possibly due to the nature of the adsorbed layer and this is the focus of the present study.

In this work, conventional electrochemical techniques were coupled with a structure sensitive spectroscopic method, surface enhanced resonance Raman scattering (SERRS) spectroscopy, since this combination can give structural as well as thermodynamic and kinetic information on the reaction of proteins at an electrode/solution interface. Bare silver electrodes were used in this study since they have been shown to increase the Raman scattering cross sectional area of molecules adsorbed on their surface (5), thus giving rise to the enhancement observed in SERRS. Therefore, SERRS spectroscopy was used in this study as a

means for identifying and clarifying the various structural features of cytochrome c upon adsorption at such interfaces.

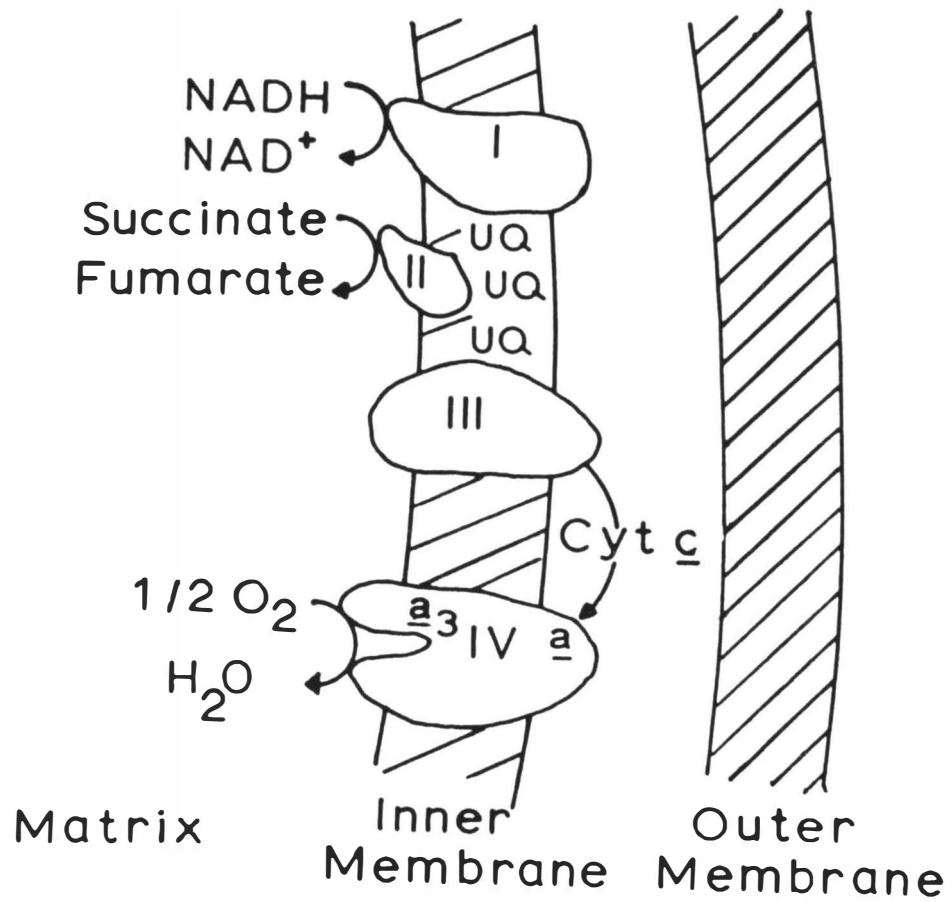
Before discussing the outcome of the present research a brief description of cytochrome c's role in the mitochondrion, its properties and reactions will be given in the remainder of this chapter.

B. Physiological Reactions of Cytochrome c

The mitochondrial respiratory chain consists of several biological components which ultimately catalyze the reduction of molecular oxygen to water. As Figure 1 illustrates, this electron transport chain is localized in the inner mitochondrial membrane. This membrane is believed to fix the associated biological substrates in a proper orientation for transporting electrons down the respiratory chain. By successively transferring electrons down this chain, the membrane bound substrates drive the phosphorylation of adenosine diphosphate (ADP) to adenosine triphosphate (ATP), producing a total of three ATP molecules for each pair of electrons transferred from nicotinamide adenine dinucleotide (NADH) to dioxygen.

In the electron transfer pathway along the inner mitochondrial membrane, illustrated in Figure 1, complexes I-IV represent a simplified view of more than a dozen individual electron carriers embedded in this membrane. Complex I and complex II in the first portion of this chain are known as

Figure 1. Schematic representation of the mitochondrial respiratory chain. In this figure complex I represents NADH dehydrogenase, complex II: succinate dehydrogenase, complex III: cytochrome bc₁, complex IV: cytochrome aa₃ and UQ: ubiquinone. (Adapted from Palmer, G. Pure & Appl. Chem. 1987, 59, 749-758).



NADH dehydrogenase and succinate dehydrogenase, respectively. In the latter portion of the chain, complex III is referred to as either cytochrome c reductase or cytochrome bc₁, while complex IV is referred to as cytochrome c oxidase or cytochrome aa₃. These last two complexes are involved in reactions with cytochrome c.

Ubiquinone (UQ) in this diagram is a lipophilic quinone with six 5-carbon isoprenoid units, which links complexes I and II to complex III (6). By oxidation of NADH and succinate on the matrix side, complexes I and II reduce the UQ pool in the inner mitochondrial membrane. Following reduction, the UQ molecules successively transfer their reducing equivalents to complex III. Controversy exists as to whether the quinone molecules are able to diffuse within the lipid membrane, or remain attached to the large multiprotein complexes. Based on studies which have directly measured the kinetic response of the quinone molecule with complexes in the inner membrane, Rich (6) suggests that they are able to move freely between the membrane associated components.

Complex III or cytochrome bc₁ is a transmembrane protein, tightly bound to the inner mitochondrial membrane, which functions in reducing oxidized cytochrome c. This complex is a multisubunit enzyme which contains three heme proteins, one c₁ and two b's (7). These redox centers are located on the cytosol side of complex III, between the inner and outer mitochondrial membranes. The cytochrome bc₁

complex also contains a UQ unit and an iron sulfur protein known as a Rieske cluster (8). The difficulty in isolating this complex in a relatively pure and stable form, has prompted investigators to examine each of the individual components separately. Bosshard et al. (9) have isolated cytochrome c₁ and cytochrome b of this complex and found that cytochrome c₁, unlike cytochrome b, binds with high affinity to cytochrome c. Erecińska et al. (10) using photoaffinity-labeled ¹²⁵I-cytochrome c showed that cytochrome bc₁ contains a binding site for cytochrome c. These two studies suggest that the interaction site of cytochrome c with complex III is located on cytochrome c₁.

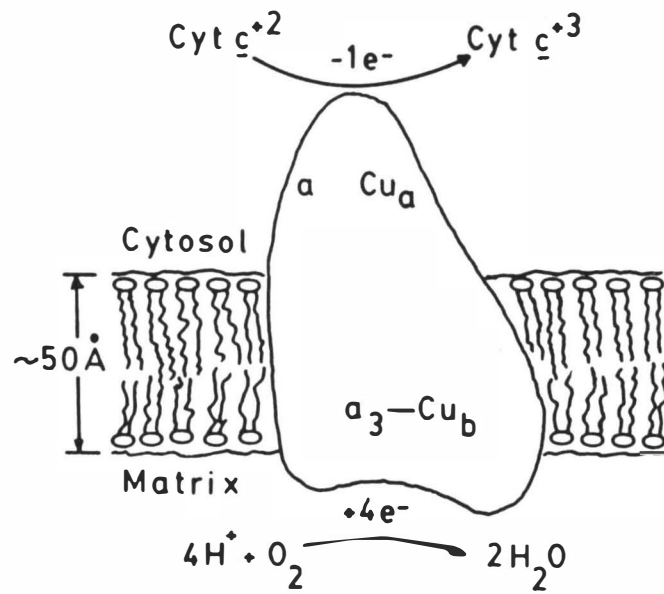
Complex IV or cytochrome aa₃ is also a transmembrane protein associated with the inner mitochondrial membrane in the terminal portion of the respiratory chain. Its physiological function is to catalyze the reduction of dioxygen to water on the matrix side of the membrane, while oxidizing reduced cytochrome c on the cytosol side. This complex contains between ten and thirteen subunits per monomer and four redox-active prosthetic groups (11). Two of these redox-active groups are iron containing hemes, while the other two are copper atom centers (12). The two redox-active heme groups in this enzyme are cytochrome a and cytochrome a₃. They differ only in their axial ligands and both contain the heme a prosthetic group. Both cytochrome a and a₃ are six-coordinate complexes, cytochrome a being a

low spin bis-imidazole complex (13) while the sixth ligand of cytochrome a₃ has yet to be identified.

The two copper prosthetic groups in this enzyme are referred to as Cu_a and Cu_b. Cu_b is magnetically undetectable when the enzyme is in the totally reduced or oxidized state, however an electron paramagnetic resonance (EPR) signal has been obtained during catalytic turnover (14,15). Although the exact distance between the metal centers of cytochrome a₃ and Cu_b has not been firmly established, it has been reported to range between 3-4 Å (16,17). A shared ligand between these two metal centers has long been suspected to mediate their magnetic interaction, thus giving rise to the undetectable copper center. Although the identity of this bridging ligand has not been firmly established, an imidazole nitrogen from a histidine residue (18), a cysteine sulfur (19), or an oxygen atom (20) have been proposed. Two other metals, zinc and magnesium, have recently been found in complex IV (21,22). Both zinc and magnesium have been determined to be tightly bound in a 1:1:1 stoichiometric ratio with cytochrome aa₃. The role of these two metals, in the functioning of the oxidase, has yet to be established.

The exact location of the four prosthetic groups of cytochrome aa₃ mentioned above is not known. However, Figure 2 illustrates the most accepted view of where these groups are located. Cytochrome a and Cu_a are located on the cytosol side of the inner mitochondrial membrane, whereas

Figure 2. Interaction of cytochrome aa₃ with cytochrome c and dioxygen. (Adapted from Colosimo, A.; Antonini, E. In "The Biology and Chemistry of Active Oxygen", Bannister, J.V.; Bannister, W.H., Eds.; Elsevier Science Publishing Co.: New York, 1984; Vol.26, Chapter 3, pp.45-67).



cytochrome a_3 and Cu_b reside on the matrix side of this membrane. As depicted in this figure, the subunits of the cytochrome aa_3 monomer give a "Y" shaped appearance, the base of the Y being on the cytosol side and the arms on the matrix side. The dimensions of this monomer are such that it spans the entire inner membrane, protruding approximately 55 Å on the cytosol side and 20 Å on the matrix side (23). As Figure 2 illustrates, reduced cytochrome c donates one equivalent per molecule to the cytochrome a and Cu_a sites located on the base side of the Y of complex IV. Also shown in this figure is the catalytic reduction of dioxygen to water by this complex. This reaction takes place within the area surrounded by the protruding arms of the cytochrome aa_3 monomer, on the matrix side of the inner membrane. A binuclear center is believed to be the catalytic site for this reaction which involves two of the redox-active prosthetic groups previously mentioned, cytochrome a_3 and Cu_b (12).

Whereas the exact positions of the four prosthetic groups in cytochrome aa_3 have not been well defined, the geometrical relationship between these redox centers has been established through various indirect methods of analysis. One of the methods that has proven to be more successful in this approach is that of EPR spectroscopy. The approximate distances of these redox centers from one another, obtained in several laboratories by means of EPR methodology, have been recently summarized by Palmer (24). Accord-

ing to this report, the calculated distance between the cytochrome a and Cu_a centers ranges between 8-13 Å. The distance separating cytochrome a and cytochrome a₃ is less than 15 Å while that between Cu_a and the binuclear center, formed by cytochrome a₃ and Cu_b, is less than 10 Å.

In considering the reaction scheme shown in Figure 2, a total of four reduced cytochrome c molecules are required to fully reduce one oxidized cytochrome aa₃ monomer. A concerted four electron/four proton catalytic reduction of a dioxygen molecule to two water molecules, then follows. In a complex sequence of events, the four electrons donated by the diffusing cytochrome c molecules are internally transferred from the cytosol side of cytochrome aa₃ to the oxygen binding site, located on the matrix side. The internal electron transfer, which occurs in the delivery pathway between the cytochrome c and dioxygen binding sites on the enzyme, is the rate limiting step in this catalytic reduction cycle. The initial electron from ferrocycytochrome c is believed to enter at the cytochrome a site of the enzyme, possibly being shared with the Cu_a site. The second electron is then accepted more slowly with the complete reduction of cytochrome a and Cu_a. The intramolecular electron transfer rate from the reduced cytochrome a to Cu_a site has been estimated to have $k_{et} \approx 40-100 \text{ s}^{-1}$ (25). Following the introduction of the second electron by ferrocycytochrome c, an intramolecular electron exchange

involving the cytochrome a₃-Cu_B center is believed to occur. The internal reduction process of cytochrome a₃ with the resting (i.e., the fully oxidized) enzyme was indicated to have $k_{et} \approx 0.5 \text{ s}^{-1}$ (26). Therefore, the complete reduction of the cytochrome aa₃ enzyme necessary to support the overall catalytic reduction of dioxygen to water, is limited by the final electron transfer to cytochrome a₃.

Although the intramolecular electron transfer rate between the electron accepting and donating sites of this complex have been shown to be quite slow, its reaction with ferrocycytochrome c is known to be very fast. The bimolecular rate constant for the reaction of cytochrome c with purified oxidized cytochrome aa₃ has been observed to vary from $10^6 \text{ M}^{-1} \text{ s}^{-1}$ (26) to greater than $2 \times 10^8 \text{ M}^{-1} \text{ s}^{-1}$ (27-30). Such bimolecular rates are close to the diffusion controlled rates, observed between reactants in which every collision leads to a reaction. Just as the reaction of cytochrome c with cytochrome aa₃ is shown to occur in a facile manner, the electron transfer of cytochrome aa₃ in the totally reduced state with the dioxygen molecule has also been shown to be very fast. In fact, the oxidation of ferrous cytochrome aa₃ by oxygen is complete within 20 μsec . in vitro (24).

A point of controversy in the physiological reactions of cytochrome aa₃, has been the incompatibility of the internal electron transfer rate with the turnover rates of

dioxygen and ferrocyclochrome c. As previously mentioned, the intramolecular electron exchange rate in the resting enzyme is several orders of magnitude slower than its reaction with either dioxygen or ferrocyclochrome c. Although this should lead to a rate limiting step in the overall reduction process of dioxygen to water by ferrocyclochrome c, it does not. Studies have suggested that cytochrome aa₃ goes into what is called a "pulsed state" upon reaction with ferrocyclochrome c and dioxygen (31-33). The pulsed state is believed to be an intermediate species formed immediately after reaction of the totally reduced cytochrome aa₃ enzyme with a dioxygen molecule. The issue here is that the four equivalents donated to the dioxygen molecule by the reduced enzyme should leave the enzyme in the totally oxidized "resting" state. However, studies have indicated that an intermediate or pulsed state, different from the resting state, exists just after the dioxygen reaction of this enzyme.

In the pulsed state of this enzyme an increase of 4-5 times in the rate of reduction of cytochrome a₃ over the resting enzyme has been indicated (34). This pulsed state results in a higher dioxygen turnover and has been shown to have a higher reactivity towards the oxidation of cytochrome c (23). Although details of the overall mechanism of the pulse state have not been clearly established, it is this state that is believed to provide cytochrome aa₃ with the

means for obtaining such high turnover rates of dioxygen and ferrocytochrome c under respiring conditions.

Along with electron transport cytochrome aa₃ has the capability of proton translocation. This capability allows cytochrome aa₃ to transport or pump protons from the matrix space to the cytosol side of the inner mitochondrial membrane. The exact mechanism by which cytochrome aa₃ pumps protons across the inner membrane is still not clear. Palmer (24) has suggested that proton pumping may be directly related to conformational changes in the enzyme during redox reactions. The importance of proton pumping has been related to the chemiosmotic hypothesis proposed by Mitchell (35). According to this hypothesis, the proton gradient across the inner mitochondrial membrane supplies the energy which drives the phosphorylation of ADP to ATP.

In considering the physiological reactions of cytochrome c with its membrane bound redox partners, cytochromes bc₁ and aa₃, it is generally accepted that rapid electron transfer between these two can occur by a diffusion mediated mechanism. It has been shown by Brown and Wüthrich (36), that cytochrome c is weakly associated with the negatively charged outer portion of the phospholipid membrane. As proposed by Roberts and Hess (37), this weak association allows cytochrome c to shuttle electrons between its two redox partners by two-dimensional lateral diffusion along the inner membrane's surface. The lateral diffusion coeffi-

coefficients of cytochrome c along the inner membrane have been determined to range between $(3.5 - 7.0) \times 10^{-10} \text{ cm}^2/\text{s}$ (38). From this study, it was estimated that cytochrome c's mobility is not sufficient to account for the random diffusion mediated mechanism observed under normal steady-state conditions in the mitochondria. Hochman et al. (38) have proposed a model, in accordance with these diffusion coefficients, in which more rapid rates can be achieved by physical association of cytochrome c between cytochromes bc₁ and aa₃. Such association was then indicated to restrict the movement of cytochrome c between its redox partners, thus making electron conductance more efficient in comparison to the random diffusion model.

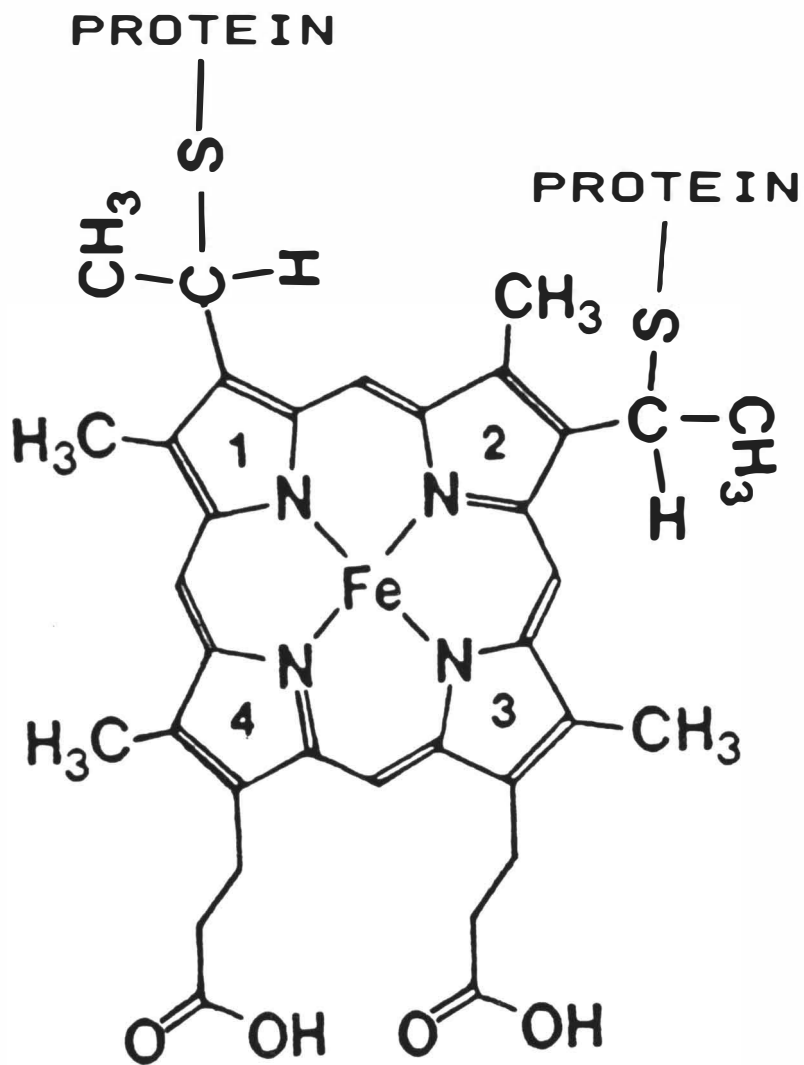
Cytochrome bc₁ and aa₃ are believed to have electrostatic groups which are complementary to those of cytochrome c. These complementary groups are thought to involve the negatively charged carboxyl residues (glutamic and aspartic acids) on cytochromes bc₁ and aa₃, and a number of positively charged lysine residues on cytochrome c's surface. Electrostatic interactions between these groups are believed to bind cytochrome c in a proper orientation for electron exchange with its physiological redox partners. These electrostatic properties have been indicated by the existence of high affinity binding sites ($K \leq 10^{-7}$) for cytochrome c on both cytochromes bc₁ (39) and aa₃ (40).

C. Structure of Cytochrome c

The primary structure (i.e., the complete amino acid residue sequence) of horse heart cytochrome c is shown to consist of a single polypeptide chain of 104 amino acids attached to a single heme iron unit (41). The molecular weight of the native protein was calculated and found to be $\approx 12,400$ (42). Figure 3 shows the heme group in this protein, heme c. This porphyrin is very similar to protoporphyrin IX found in several other iron porphyrin complexes (e.g., myoglobin, hemoglobin, catalase, and the peroxidases) with the exception that the vinyl groups are saturated in this particular protein. The only two cysteinyl residues in this molecule, cysteine residues 14 and 17, serve to covalently link the polypeptide to the heme. This occurs through thioether linkages to the two vinyl side chains of the porphyrin. This subsequently makes cytochrome c a more rigid structure when compared to the previously cited iron porphyrin complexes.

The iron atom is bonded to four pyrrole nitrogens in the plane of the porphyrin. There are two other points of attachment of the heme iron to the polypeptide (not shown in this diagram) which occur at the fifth and sixth coordinate positions at neutral pH. The compact folding of the globin portion of the molecule around the heme furnishes these two axial ligands. One of these coordination bonds is formed with an imidazole nitrogen of histidine 18 of the

Figure 3. Heme c.



polypeptide. The other heme iron coordination site is furnished by a sulfur atom of the methionine 80 residue.

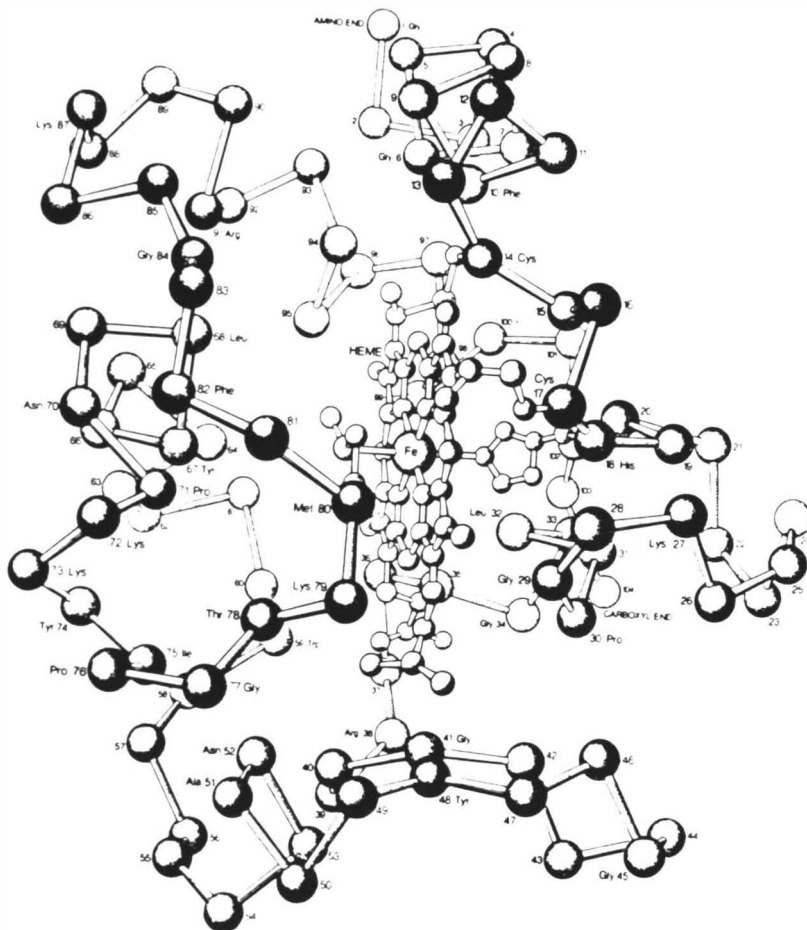
Most globin type proteins can give rise to a higher ordering of the amino acid sequence due to its frequent folding pattern. This higher ordering of the globin is known as the protein's secondary structure. The folding pattern of the polypeptide can create a helical configuration known as an α -helix. The α -helix configuration gives rise to a right-handed turning sequence of the polypeptide. In other cases the folding of the polypeptide will assume a rippled configuration instead of an α -helix and this configuration is known as a β -sheet. Since the polypeptide chain in horse heart cytochrome c is so tightly wrapped around the heme group there is very little room for α -helix or β -sheet configuration of the globin. In this regard horse heart cytochrome c was shown to contain only five short α -helical segments, residues 1-11, 49-55, 60-68, 70-75, and 89-101, which comprise $\approx 45\%$ of the total protein structure (43). This molecule was also shown not to have a β -sheet configuration. This is unlike some of the iron porphyrin complexes that were referred to earlier, such as myoglobin which contains $\approx 80\%$ α -helix configuration (44). Evidently, the globin structure in myoglobin needs this extra flexibility to allow insertion of oxygen during its physiological transportation in mammalian tissue. The α -helix content in both ferricytochrome c and ferrocycytochrome c were indicated as

being of about the same magnitude (45). Therefore, providing evidence of very little change in the secondary structure upon oxidation and reduction. However, there have been studies which provide some evidence of conformational changes upon electron transfer. This will be discussed later in this section.

The X-ray crystal structure of horse heart cytochrome c has been carried out to a resolution of 2.8 Å (45). Only the X-ray crystal structure of the oxidized or ferri-form of this particular protein has been performed, its α -carbon map is illustrated in Figure 4. Cytochrome c has been shown to be a prolate spheroid having dimensions of 30 x 34 x 34 Å. These dimensions include all the amino acid residues but exclude any solvent molecules which surround the protein. In Figure 4 each amino acid of the polypeptide chain, not involved in bonding to the heme, is represented by its α -carbon atom (circles). Only those amino acid groups attached directly to the heme are shown, all the amide linkages (-CO-NH-) are represented by a line between each α -carbon atom. A more detailed crystal structure of tuna cytochrome c has been obtained by Takano and Dickerson (46) at 1.5 and 1.8 Å resolution for both the reduced and oxidized states, respectively.

Due to the insufficient detail of the crystal structure, much of the conformational analysis of horse cytochrome c has been taken from the latest X-ray crystal

Figure 4. Molecular Structure of cytochrome c. This standard front view of horse heart cytochrome c, in the oxidized state, illustrates the solvent exposed heme edge in the center of the molecule facing towards the reader. Only those amino acids attached directly to the heme (met-80, his-18, cys-14, cys-17) are shown, all others are represented by circles depicting α -carbon atoms of the polypeptide backbone. All amide linkages are represented by a line between each α -carbon atom. The left and right sides of the molecule are as viewed. (Adapted from Dickerson, R.E. Sci. Amer. 1972, April, 58-72).



structures of tuna cytochrome c. Although the primary structures of the two protein species differ to some extent, their tertiary structures have been shown to be the same. The differences in primary structures between these two proteins involves only 12 residues. Evidently, the amino acid residues responsible for holding these two proteins together in their compact configuration have been conserved. This leads to the similar packing arrangement of the amino acid side chains around the heme in both proteins. Moore and Williams (47) have indicated that the denaturation temperature of horse cytochrome c is approximately 10 °C higher than that of tuna. This indicates a slight difference in secondary structure between the two species, possibly a higher α -helix content for horse cytochrome c.

As shown in Figure 4, the polypeptide chain folds around the heme group (represented by the dark circles in the center of the diagram) causing it to reside in a nearly hydrophobic environment, leaving only a small portion of the heme exposed to the more polar solvent. This exposed segment is located at the edge of the heme, which contains pyrrole rings II and III as shown in Figure 3. As shown in this figure, the thioether linkage at cysteine 17 attached to pyrrole ring II and the methyl group at pyrrole ring III are both exposed to the solvent. This region of the heme is the so-called solvent exposed heme edge. Based on the X-ray crystallographic structure of horse heart cytochrome c,

Stellwagen (48) calculated that the amount of surface area of the heme accessible to the solvent forms only $\approx 0.6\%$ of the total surface of the protein. Therefore, the micro-environment of the heme is such that it can be viewed as being almost entirely insulated from the surrounding solvent by this polypeptide layer.

One of the important features of this protein is that the only solvent accessible site occurs at the heme edge. Wüthrich (49) was the first to recognize this area of the protein as a possible site for electron transfer. It has been emphasized that facile electron transport to and from the iron center in cytochrome c can occur as a result of mixing of the t_{2g} -orbitals (i.e., d_{xy} , d_{yz} , d_{xz}) on the Fe cofactor with the π^* - orbitals of the porphyrin ring. Such mixing then effectively delocalizes some of the metal d-electron density to the outer peripheral portion of the heme. This delocalization is then believed to render cytochrome c more susceptible to peripheral electron transfer reactions. Using nuclear magnetic resonance (NMR) spectroscopy Keller and Wüthrich (50) were able to calculate the amount of charge delocalized over the porphyrin periphery of this protein. It was estimated that approximately 2% of the electron density of the Fe cofactor is delocalized on pyrrole rings II and IV, while only $\approx 0.5\%$ was found at pyrrole rings I and III. Therefore, it is suggested that the location of pyrrole ring II at the solvent exposed heme

edge along with the extra electron density found at this ring are important features in electron transfer reactions of this protein.

Attachment of the polypeptide to the heme (Figure 3) orients it in such a way that the thioether linkage at pyrrole ring I and the two propionate carboxylates at pyrrole rings III and IV are buried inside the hydrophobic heme pocket. According to Moore et al. (51), this feature is believed to be of physiological importance in preventing the propionates from ionizing over a neutral pH range. This structural feature is clearly evident from the NMR data of Gupta and Koenig (52) which shows that these groups do not ionize over the pH range 4.6 to ≈ 9 at 27 °C. The stabilizing effect of the hydrophobic interior of the protein is also in general agreement with the redox potential being considered pH-independent over much of this pH range (53).

The restricted propionate ionization may also be a crucial environmental factor for holding the protein together in its compact conformational state. The high resolution crystal structures (46) have revealed an extensive network of interactions of these unionized heme propionates with the various portions of the interior of the protein cavity. The interior propionic group on pyrrole ring IV was shown to be hydrogen bonded to tyrosine 48 and tryptophan 59 of the polypeptide backbone. The more exposed propionic group on pyrrole ring III was also shown to be

hydrogen bonded to tyrosine 48. Recently, Moore et al. (54) have proposed an intramolecular interaction between an arginine 38 residue and the inner propionate group of the heme. They claim that the internally located arginine 38 lies close enough to the inner propionate group to form either a hydrogen bond or possibly a salt bridge. This salt bridge is believed to result from the interaction between the positively charged arginine residue and the partially ionized inner propionate. This partially ionized inner propionate group is a result of the buried water molecule that has been found to reside in this region of the protein as determined from the crystal structures (46).

The view presented of cytochrome c in Figure 4 is that of a protein constituting two halves of a single polypeptide chain wrapped around the heme group. One half contains residues 1 to 47 to the right side and the other half contains residues 48 to 91 to the left. Residing between these two halves sits this heme group with its solvent exposed heme edge facing outward. Such submersion of the heme in the polypeptide gives rise to what is frequently referred to as the "heme crevice". This folding sequence around the heme therefore makes the heme crevice a hydrophobic pocket. Such appearance gives the protein a clam shape image which has led some researchers to address cytochrome c in this fashion. The remaining residues 92 to 104 form an α -helix configuration extending to the far back right side

of the protein.

The standard front view of cytochrome c, shown in Figure 4, indicates that the right side of the molecule is a more rigid structure when compared to that of the left. This analogy can be explained from the fact that the right side of the polypeptide is physically bonded to the heme by three points of attachment while the left is bonded by only one point. Cysteines 14 and 17 and histidine 18 attach the heme to the polypeptide on the right side of the heme crevice, while on the left it is only attached by methionine 80. The two axial bonds that make-up the left and right sides are also involved in hydrogen bonding to certain portions of the polypeptide chain which surrounds them. The δ -nitrogen atom of histidine 18 is hydrogen bonded to the carbonyl oxygen atom of proline 30. This bond is believed to stabilize the imidazole ring in a rigid conformation while the ϵ -nitrogen of the histidine can coordinate with the heme iron (45). A hydrogen bond is also formed between the hydroxyl groups of tyrosine 67 residue and the sulfur atom of the methionine 80 residue. This last bond is believed to help stabilize the left side of the heme crevice.

The native fold of cytochrome c is not only regulated by the bonds which form between the polypeptide and heme, but also by the intramolecular forces within the polypeptide itself. Horse heart cytochrome c contains no sulfhydryl

groups which could form an intramolecular covalent linkage (i.e., disulfide bonds) as seen in other globular protein structures. Therefore, the forces which hold this globular structure together are not due to covalent interactions. One such interaction would be the result of intramolecular electrostatic bonds between oppositely charged residues. These bonds would be stabilized in regions of high concentrations of hydrophobic groups where they would be partially shielded from the high dielectric solvent medium in which they reside. A good example of this type of electrostatic bond is seen at the top front face of the heme crevice. The positively charged ϵ -amino of lysine residue 13 has been shown to form a salt bridge with the negative charge on the γ -carboxyl of glutamine residue 90 in both the solid and the solution states (55,56). This particular electrostatic bond helps to stabilize the closed heme crevice region in the top front face of the molecule. The stability of the closed heme crevice structure is also maintained by a hydrogen bond that is formed in the lower region of the heme crevice. This hydrogen bond is formed between the ϵ -amino of lysine residue 79 and the α -carbonyl of threonine residue 47 (56).

The hydroxyl groups of the various threonine, serine, and tyrosine residues also appear to play an important role in maintaining the tertiary fold in this protein. These residues can potentially join and hold together certain regions of the molecule through an extensive network of

hydrogen bonds. One other force that holds the looped polypeptide in its package-like conformation involves the hydrophobic interactions that occur between the various residues along the chain. The hydrophobic residues (i.e., alanine, valine, leucine, isoleucine, phenylalanine, and methionine) are mostly found localized in clusters around the polypeptide chain. In order to avoid the more polar solvent (i.e., water) they have a tendency to associate towards the interior of the protein. In doing so, they are shielded from the solvent and are able to undergo hydrophobic-hydrophobic interactions with each other.

D. Properties of Cytochrome c

Cytochrome c is a highly basic water soluble protein with an isoelectric point of ≈ 10.0 (57). The basic character mainly stems from the relatively high lysine content in the molecule. Horse heart cytochrome c contains 19 of these positively charged basic residues (41). At neutral pH arginine residues contribute two more monopositive charges to the protein. Only a small amount of this overall positive charge on the molecule is compensated for by the negatively charged aspartic and glutamic acid residues. A maximum of 13 negatively charged groups can be accounted for: 3 aspartates, 9 glutamates, and the negative charge which resides on the carboxyl-terminal end of the protein (41). Allowing for the +1 charge on the heme in the oxidized state, horse ferricytochrome c has an overall net

charge of +9 at neutral pH when calculated from the amino acid sequence (42). Since the charge on the reduced heme is zero, ferrocyanochrome c should have an overall net charge of +8. However, it must be noted that the net charge on ferri- and ferrocyanochrome c can be effectively altered in the presence of binding anions and cations.

One of the striking features about cytochrome c is that the positive and negative charges are distinctly segregated on its surface. The basic residues are mainly located on either side of the heme crevice with only a small segment being concentrated towards the back right side, near the carboxyl-terminal end of the chain. The acidic residues on the other hand tend to be more concentrated towards the top left rear of the molecule. Therefore, it appears as though the basic residues are more homogeneously distributed over the surface of the protein than are the acidic residues.

Of special interest is the two basic patches that lie to the left and right side of the solvent exposed heme crevice region, where most of the positively charged lysine residues are clustered. One or both of these surface patches are believed to play a crucial role in recognition and binding of cytochrome c with its redox partners. However, it should be noted that most of the positive charge from the lysine residues lies to the left side of the heme crevice.

When viewing the α -carbon map of cytochrome c in Figure

4 it appears that the right side of the heme cleft is more open than the left side. Dickerson et al. (45) have called this opening a channel. This channel extends into the interior of the protein, however, since the channel contains a number of hydrophobic groups it is not accessible to the solvent. There is a second channel, not seen in the front face view of Figure 4, which extends from the top left portion of the molecule. The significance of these two channels is at the present time unknown. However, Dickerson et al. (45) have mentioned these channels could play a role in providing an alternate route for binding. They propose that a hydrophobic side chain of another macromolecule could slip into one of these channels and hold the molecule in a proper orientation for electron transfer.

The highly asymmetric distribution of charges over cytochrome c's surface leads to a calculated dipole moment of 312 and 300 debye for ferri- and ferrocycytochrome c, respectively (58). Koppenol et al. (59,60) have calculated that the positive end of this dipole lies approximately midway between lysine residues 12 and 13 located on the left front face of the molecule. This region is near the β -carbon of phenylalanine 82. The negative end of this dipole is near the β -carbon of phenylalanine 36. Although the left front face contains most of the positive charge, the major contribution to the dipole moment is related to the very high concentration of negative charges located at the back

left portion of the molecule. In this area is located a cluster of nine negatively charged acidic groups. The significance of this negative patch is unclear. However, the large contribution of this patch to the dipole moment indicates that it plays a role in the strength and direction of the dipole's positive end, near the interaction domain of the molecule.

The solvent exposed heme edge is surrounded by lysines 8,13,27,72,79,86, and 87. This is sometimes called the 72-87 loop and is conserved in all cytochrome c species. It has been proposed that electrostatic interactions of these charged lysine residues and the corresponding dipole are of physiological importance in reactions of cytochrome c with its redox partners (59,60). Koppenol et al. (59,60) have described a reaction mechanism scheme in which the positive end of the dipole of cytochrome c interacts with the electric fields generated by its redox partners. This is believed to guide the molecule into proper orientation for electron transfer and therefore increases the number of productive encounters. Once a productive encounter occurs, the surface complementary groups on either redox partner are believed to bind electrostatically with lysine residues surrounding the exposed heme edge. Formation of such precursor complexes is then suggested to minimize the distance between redox centers. In doing so, this lowers the activation energy required for electron transfer and

increases the rate of the reaction.

A multitude of studies have used inorganic complexes as probes for redox reactivity and as a means of assessing the sites for electron transfer in cytochrome c. Various charges, sizes, and surface properties of these reactants have been used to ascertain the nature of the redox site on this protein. By employing Marcus theory (61) it has been possible to calculate the self-exchange rate constant for cytochrome c from the corresponding crossreaction rates of a number of metal complexes. Wherland and Gray (62) calculated cytochrome c's self-exchange rate constant using a variety of inorganic reagents and found them to react in decreasing order according to $\text{Fe}(\text{CN})_6^{3-} > \text{Co}(\text{phen})_3^{3+} > \text{Ru}(\text{NH}_3)_6^{2+} > \text{Fe}(\text{EDTA})^{2-}$. This order was shown to directly correlate with the inorganic reagent's ability to be affected by the electrostatic, hydrophobic, and porphyrin π system upon penetration of cytochrome c's heme edge surface. When these electrostatic and nonelectrostatic contributions are accounted for the calculated self-exchange rates are seen to agree reasonably well with that observed directly by Gupta et al. (63,64) using NMR. Using this experimental approach Gupta et al. (63) have calculated from the diffusion limited self-exchange rate constant that $\approx 7 \text{ \AA}^2$ of cytochrome c's surface is available for self-exchange. This value is relative to a total accessible surface area of $5,307 \text{ \AA}^2$ (48) for this protein and is therefore in general

agreement with the amount of exposed heme area of 32 \AA^2 calculated by Stellwagen (48) from the X-ray crystal structure of cytochrome c. Therefore, from such studies cytochrome c appears to use the same electron transfer pathway with metal complexes as it does in its self-exchange reaction. Investigations with such inorganic probes support the hypothesis that electron transfer of cytochrome c takes place by an outer-sphere mechanism in close proximity to the partially exposed heme edge (65-67).

All of the above methods used NMR spectroscopy to map out the region in which the small inorganic reagents bind to cytochrome c. More recent studies with inorganic complexes have been conducted using rapid flow kinetics along with single site modification of lysine residues on cytochrome c (68-70). Arylation of lysine residues with CDNP (4-carboxy-2,6-dinitrophenyl) and TNP (2,4,6-trinitrophenyl) has been shown to be quite effective in mapping out cytochrome c's interaction surface. Modification of cytochrome c with CDNP changes the charge of the lysine residues from +1 to -1. This is due to the single negative charge located at the carboxylic acid group on CDNP. Modification with TNP changes the charge only from +1 to 0. Therefore, CDNP modifications have been used most frequently on cytochrome c since it decreases the net positive charge on the molecule by 2 units while being less bulkier and hydrophobic than the TNP modification.

It is generally assumed that the modified cytochrome c functions in the same intrinsic manner as the native protein. Although the redox potentials are very similar, Moore et al. (71) have questioned if one can interpret changes in observed rates after modification in terms of binding strength. This is due to the fact that some of the lysine residues are involved in stabilizing the protein structure, as mentioned earlier, with the top and bottom heme crevice bonds. In spite of this view it has been possible to identify which residues are involved in interactions with small inorganic complexes. For example, it was found that the negatively charged $[\text{Fe}(\text{CN})_6]^{3-}$ is most influenced by lysine 72 modification with CDNP, while on the contrary the positively charged $[\text{Co}(\text{phen})_3]^{3+}$ is most influenced by lysine 27 modification (70). As discussed earlier, most of the positive charge on cytochrome c lies to the left of the heme crevice. Lysine 72 is found on the left front face while lysine 27 is located toward the right of the heme crevice.

The methodology of independent single lysine modification has also enabled a detailed assessment of the sites involved on cytochrome c interacting with much larger reactants, such as cytochrome c oxidase and cytochrome c reductase. Using a variety of singly modified derivatives of cytochrome c (72-78), studies have shown that the ring of lysine residues surrounding the heme crevice is also involved in interactions with the protein's physiological

redox partners. A comparison of reaction rates and binding constants of these various modified forms with native cytochrome c supports the analogy that binding occurs with oxidase and reductase largely by an electrostatic mechanism (79). This type of mechanism is believed to involve the surface complementary carboxyl groups on oxidase and reductase in hydrogen bonding with certain lysine residues surrounding the heme crevice of cytochrome c. The particular lysine residues involved in binding with oxidase and reductase in all these studies have been defined as the following: lysines 8,13,27,72,79,86, and 87. These particular residues make up the so-called "active site" in this protein and are among those lysine residues which are clustered around the exposed edge of the heme crevice.

Modification studies have indicated that the interaction domain on cytochrome c for both redox partners is largely overlapping. The center of this domain is relatively close to the β -carbon of phenylalanine 82 which is precisely where the positive end of the dipole moment lies. These facts led Koppenol et al. (59,60) to suggest some kind of physiological importance to the dipole moment in reactions of cytochrome c with its two redox partners. However, overlapping binding domains on cytochrome c's surface for both oxidase and reductase does not per se describe the same sites for electron transfer. Both redox partners are very large in comparison with cytochrome c. Therefore it is

possible that both redox partners can bind in the same location while still being capable of donating or accepting electrons at different sites on cytochrome c's surface. Experiments using antibodies of cytochrome c (80) have indeed indicated that there are different and distinct sites on cytochrome c's surface for electron transfer with oxidase and reductase.

E. Conformational Changes of Cytochrome c with pH

Cytochrome c is known to undergo various conformational changes with pH. Five pH conformations have been shown to exist for ferricytochrome c and three for ferrocyclochrome c (81). The iron in both oxidation states remains low spin at neutral pH. Ferricytochrome c at neutral pH is referred to as the state III form. Recent investigations have particularly focussed on the transition neutral III to alkaline IV state where the sixth ligand of the heme iron, methionine 80, is replaced by another strong field ligand, probably lysine 79 or 72 (82). The pK of this alkaline isomerization can range from 9.35 to 7.8 depending on the presence of certain anions in solution (81,83-86). Anions such as phosphate and perchlorate are known to bind to cytochrome c in both the ferrous and ferric state (87). In the presence of such anions the pK for the state III to IV transition is shifted to lower pH values indicating stabilization of the former structure upon binding.

Controversy still exists as to lysine replacing methio-

nine as the sixth coordination site in the low spin complex of state IV. Bosshard (88) tested this proposition by measuring the relative rates of acetylation of various lysine residues at neutral and alkaline pH for the intact oxidized cytochrome c and the fragment 66-80 of this protein moiety. He observed no significant difference in acetylation rates between these two species in the pH range 7 to 11. According to Bosshard, this contradicts any involvement of lysine 79 or 72 during alkaline isomerization as the reactivity of these two residues should decrease dramatically upon entering the coordination sphere of the heme iron.

A more detailed description of the alkaline conformational change is believed to involve two of the three water molecules that have been revealed in the X-ray crystal structures of tuna cytochrome c (55). One of these water molecules has been shown to be buried deep inside the heme crevice, near methionine 80 to the left side of the heme. The other water molecule is located external to the heme crevice, between pyrrole rings 3 and 4 and the isoleucine 81 side chain of the polypeptide. The alkaline isomerization is first believed to involve weakening of the Fe-S bond formed by the methionine 80 residue upon deprotonation of the buried water molecule. The weakening of the heme crevice allows the second external water molecule, now in the OH⁻ form, to enter the heme crevice region. This second water molecule is then proposed to be electrostatically

attracted by the +1 charge on the ferriheme causing the now weakened Fe-S bond to break.

The above model might explain why methionine 80 remains the sixth ligand in reduced cytochrome c even up to pH 12 (81). Since the ferrous heme is neutral, there would not be a tendency for the external OH⁻ to be electrostatically attracted into the heme crevice region. This lack of electrostatic attraction could explain why the methionine-to-iron bond in the reduced form of cytochrome c is about 1000 fold stronger than in the oxidized state (81). Whether the hydroxyl group actually assists in the replacement of methionine by another strong field ligand remains unclear. Kinetic studies have indicated a transient form of ferri-cytochrome c just prior to breaking of the Fe-S bond (81). Myer et al. (89) have differentiated an intermediary form between the state III to state IV transition which they have labeled state III_b using resonance Raman (RR) spectroscopy. This study indicated a tightening of the outer domain of the pyrrole rings while the porphyrin core dimensions remained unchanged during this transition.

The stability of the closed heme crevice form of cytochrome c can be monitored by the absorption band at 695 nm. This absorption band is not due to a $\pi \rightarrow \pi^*$ transition as observed in other porphyrin type complexes. Rather, it results from a porphyrin $a_{2u}(\pi)$ to Fe $a_{1g}(dz^2)$ promotion. This type of promotion is referred to as a charge-transfer,

and is related to the sulfur atom of methionine 80 coordinating to the heme iron in oxidized cytochrome c (90,91). It is a relatively weak absorption band with a calculated $\Delta\epsilon_{695\text{nm}}$ (reduced minus oxidized) of $800 \text{ M}^{-1} \text{ cm}^{-1}$ (92).

The 695 nm band is related to the overall conformation of the protein moiety of ferricytochrome c and is absent for the reduced form. As a result it can and has been used as a sensitive indicator of the native structure of ferricytochrome c. When the conformation of the protein's heme crevice region is sufficiently disturbed so that this bond is broken, there is a concomitant loss of the 695 nm absorption band. This may be accomplished in ferricytochrome c by extremes of pH (82), high temperatures (51,93,94), and the addition of denaturants such as trichloroacetic acid (93), urea (95,96), guanidinium hydrochloride (97), and alcohols (98,99). This band is also absent in the dimer and higher oligomers of ferricytochrome c (100) and in complexes formed with ionic ligands such as CN^- and N_3^- (101,102). The closed heme crevice conformation of ferrocycytochrome c is less susceptible to changes in environmental conditions. Circular dichroism (CD) spectra of ferrocycytochrome c both with and without 9.0 M urea were in excellent agreement with one another (102). Such agreement in CD spectra indicates that the conformation of reduced cytochrome c in high concentrations of urea are indistinguishable from the native protein. In the same study, however, CD spectra of ferri-

cytochrome c indicated large conformational changes in the presence of urea, which are in direct correlation with the loss of the 695 nm absorption band. The stability of the ferrous state has been shown to exist under such extreme conditions as 95°C (51), pH 12.0 (81), and the addition of reagents such as CN^- , N_3^- and imidazole (81).

When the pH of ferricytochrome c is raised to 13 another low spin complex (state V) is produced with a pK of 12.76 (81). This state is believed to be considerably unfolded while still retaining the strong field ligand of state IV. Lowering the pH of the neutral form below ≈ 3 produces a high spin complex (state II) with a pK of 2.5 (81). This transition of ferricytochrome c from low spin (state III) to high spin (state II) upon acidification is believed to involve replacement of at least one of the axial ligands by a water molecule. From NMR relaxation experiments, Gupta and Koenig (52) confirmed that water molecules were rapidly exchanging with at least one of the axial ligands as the pH was lowered below ≈ 4 . Myer et al. (89), using RR spectroscopy to study the core size of the porphyrin, indicated that the iron lies in the heme plane in state II. Based on this investigation they concluded that the acidic state II form of ferricytochrome c consisted of a hexacoordinated high spin complex with two water molecules as the axial ligands. If only one water molecule was coordinated, a mixed configuration (one weak and one strong

field axial ligand) would have existed causing the iron atom to lie out of the heme plane. Therefore, RR spectroscopy has confirmed the coordination configuration water-Fe-water for ferricytochrome c at pH values below 3 as was first suggested by Harbury and Loach (104).

Both the far-ultraviolet absorption band at 190 nm and the ultraviolet resonance Raman (UV RR) spectra showed a hypochromic enhancement upon acidification of state III (105). This hypochromism was associated with disordering of the polypeptide backbone in going from state III to state II. However, the amide I frequency at 1650 cm^{-1} in the UV RR spectra remained unchanged between these two states (105). If substantial unfolding of the helices were to occur, this band would have been expected to shift to a higher frequency upon acidification. It thus appears that a major alteration of the heme iron spin state occurs with only minimal disruption of the protein's secondary and tertiary structure in this state III to II transition.

According to RR spectral analysis of Myer et al. (89) an additional conformational form occurs for ferricytochrome c prior to formation of state II. They have labeled this precursor to the acidic form as state III_a, having a pK of 3.6. Energetic changes in certain vibrational modes reflected that the low spin hexacoordinate structure of the native state III conformation was maintained with slight shrinking of the porphyrin core dimensions in the transition

III to III_a. Using RR analysis Myer et al. (89) calculated heme core dimensions for ferricytochrome c both with and without 4M urea added at pH 7.0. The former indicated a slight compression of the heme core of ≈ 0.01 Å while still retaining all other structural features of a low spin hexacoordinate heme c compound. Ferricytochrome c is known to undergo a slight loosening of the heme crevice region upon addition of 4 M urea (95,96). This led Myer et al. (89) to conclude that shrinking of the heme core upon going from state III to III_a was due to a disruption of protein-heme interactions caused by weakening of the heme crevice region. Likewise, this behavior was suggested by proton NMR studies in this same acidic pH range (106).

In contrast to the state III \rightarrow II transition further acidification of ferricytochrome c gives rise to a form (state I) that is totally denatured. The pK for the state II to I transition is ≈ 0.42 and results in another high-spin complex (81). The axial ligands in this state I form are presumably the same as those in state II, water molecules. In summarizing, Myer et al. (89) have established all of the various pH-dependent conformational states of ferricytochrome c at both limits of the pH scale. Following is a schematic representation of these conformational states:



By analyzing heme energetics, core size, planarity, and coordination configuration with the aid of RR spectroscopy Myer et al. (89) have elucidated two additional states over and above the five given by Dickerson and Timkovitch (81). RR spectroscopy has been shown to be a powerful probe for monitoring conformational and configurational transitions occurring in cytochrome c under various conditions.

F. Redox Conformational Changes of Cytochrome c

Intense activity has developed concerning any observable conformational changes that might exist between the oxidized and reduced states of cytochrome c. The idea of a drastic conformational change between the two redox states was believed to explain such indirect observations as the reduced state being more highly resistant to thermal denaturation (81) and trypsin digestion (107). Such evidence suggested that the reduced state was much more compact when compared with the oxidized state of this protein. With these and many other lines of evidence, it was proposed that such large state-dependent conformational changes might account for the different binding properties of this protein for its two redox partners (108).

The extent of these conformational changes was not known with certainty until 1980, when the first high resolution X-ray crystal structures of these two redox states were published for tuna cytochrome c (46). Surprisingly, the refined X-ray analysis indicated very little

structural difference between the two states. Functionally one would expect this to be the case, considering that any large energy consuming conformational change might impact on the rates at which cytochrome c donates and accepts electrons in vivo. More recently, Mayo et al. (109) have experimentally determined the energy required for internal reorganization of cytochrome c upon reduction. In a unique experimental approach, they used a modified ruthenated form of cytochrome c and determined the long-range intramolecular electron transfer rate between the surface bound ruthenium complex and the heme iron in cytochrome c. Such long-range intramolecular electron transfer rates were temperature independent, suggesting a relatively small (≈ 0.3 eV) reorganization energy between the two redox states.

Although the energetics between redox states indicated very little internal reorganization, small but significant conformational changes over large portions of the protein have been observed upon reduction. The occurrence of such small structural changes were seen in the X-ray crystal analysis involving the buried water molecule that is hydrogen bonded to different parts of the polypeptide (46). In the oxidized state, this water molecule was shown to be 1.0 Å closer to the heme with the heme itself moving 0.15 Å out of its heme crevice. Such motions cause a few of the residues, whose side chains are involved in hydrogen bonding with this water molecule and the heme, to undergo a slight

shift upon electron transfer. X-ray analysis showed that the hydrogen bond formed between the inner propionate group on the heme with tryptophan 59 and tyrosine 48 causes these residues to move towards the interior of the protein upon reduction. Another residue, tyrosine 67, was shown to be hydrogen bonded to this buried water molecule and it underwent a similar type of motion. The X-ray structures have also indicated a simultaneous downward movement of asparagine 52, which is located at the bottom left portion of the protein. The slight movement of tryptophan 59 between oxidation states has also been evident in studies of the fluorescence spectrum of this protein in solution (110,111). Fluorescence spectra obtained upon reduction indicated a movement of the tryptophan towards the heme by $0.7 \pm 0.3 \text{ \AA}$ (110).

Bosshar and Zürcher (112), using a differential chemical modification approach, compared the chemical reactivity of the various lysine residues between the reduced and oxidized forms of horse heart cytochrome c. When this comparison was made, only 3 of the 19 lysine residues reflected any major differences in acetylation rate with acetic anhydride. Lysine residues 53, 55, and 39 were all shown to be less reactive towards acetic anhydride for ferrocycytochrome c when compared to the ferri form. The rationale for such a decrease was based upon the increase of pK's of these particular lysine residues caused by them becoming more exposed to

the aqueous medium on reduction.

Lysine residues 53, 55 and 39 are all grouped together in the lower left portion of the molecule, just below the heme pocket. Studies in solution with NMR spectroscopy have also demonstrated that this region of the protein is very flexible upon oxidation state change, particularly around isoleucine 57 (113). In addition, NMR studies have also indicated that this flexibility extends to the surface of the protein in the region around phenylalanine 10.

Dickerson et al. (45) recognized the possible dynamic features of surface groups when using Kendrew models of cytochrome c derived from X-ray crystal structures for this protein. They demonstrated from such models, that it was possible to swing the phenylalanine 82 residue to the right side in such a way that it blocks the heme crevice opening. Such a local conformational change at that time was suggested to be instrumental in mediating electrons between the heme edge of cytochrome c and the electron transfer site of its redox partners. Recent computer modeling studies on docking of cytochrome c and cytochrome b_5 X-ray crystal structures have revealed insight to this motion (114). In these molecular dynamics simulations phenylalanine 82 was shown to be quite flexible, sampling many regions before bridging between the two heme groups in this precursor complex. What significance this bridging has on electron transfer reactions of cytochrome c with its physiological

redox partners remains unclear. However, as pointed out by Wendoloski et al. (114) it could be of importance in coupling the heme electronic systems or displacing solvent at the molecular interface. Indeed, from the resulting gain in entropy on precursor complex formation between cytochrome c and cytochrome c oxidase, water is believed to be expelled within the interaction domain (78).

More recently, Liang et al. (115) have indicated the biological significance of the evolutionarily conserved phenylalanine 82 residue by replacing it with a nonaromatic amino acid. In comparison with the native protein, replacement of this group led to a 10^4 decrease in the intramolecular electron transfer rate of the complex formed between cytochrome c and zinc-substituted cytochrome c peroxidase. At this time it can only be speculated that such differences are not caused by the disruption of the protein structure upon replacement of this residue. From these and other studies (51), the most dynamic changes are seen to occur at the surface of the molecule where exposed mobile residues are not limited by the packing constraints that exist in the interior of the protein structure.

Surface flexibility has been proposed for some time to be necessary for protein-protein recognition and binding between cytochrome c and its two membrane bound reaction partners. Lysine residues surrounding the heme edge are quite flexible, thus allowing them to bind more effectively

with the various carboxylates of cytochrome c's redox partners. Changes in the binding affinity of cytochrome c towards its redox partners upon oxidation-reduction have been indicated through graphical docking experiments (116). This study suggested a large movement ($\approx 0.5 \text{ \AA}$) of lysine 27 away from the binding face of its redox partner upon oxidation. According to Rackovsky and Goldstein (116), this motion leads to a change in binding affinity which provides a dissociation signal to the cytochrome c-redox partner complex.

G. Electrode Reactions of Heme Proteins

Although the means of determining thermodynamics, kinetics, and mechanisms of heterogeneous electron transfer have been known for quite some time, it wasn't until after the mid 1970's that the use of these techniques began to gain popularity for large biological molecules. The reason for this slow development was the inherent lack of communication between biological molecules and electrode substrates. Such lack of communication led to slow and often negligible rates of direct electron transfer, thus preventing the use of conventional electrochemical techniques involving current measurements, in their characterization.

Slow and irreversible heterogeneous electron transfer rates were attributed to the insulating properties of the protein surrounding the molecule's active site, making this site inaccessible to the electrode. However, in 1977 three

groups reported more well defined electrochemistry of two redox proteins, cytochrome c (117,118) and ferredoxin (119). Since then, a substantial amount of knowledge has been gathered concerning the interfacial behavior of heme proteins at various electrode surfaces.

A property viewed as necessary in order to achieve well behaved diffusion controlled rates, is the reversible binding and dissociation of the electrode surface towards heme proteins (120). Functional groups at the electrode solution interface that are capable of binding directly or indirectly with the protein are therefore believed to be necessary for the above conditions to be met. Electrodes with such characteristics were first used by Yeh and Kuwana (117) in experiments involving horse heart cytochrome c at a tin-doped indium oxide electrode. Such electrodes contain oxide groups which can potentially bind with the protein, thus placing the molecule in a preferred orientation for electron transfer.

At the same time that tin-doped indium oxide electrodes were being used, work on gold electrodes was being carried out by two separate groups. Landrum et al. (119) reported that a polymeric form of methyl viologen adsorbed on a gold minigrid electrode was capable of direct heterogeneous electron transfer with ferredoxin at rates faster than previously reported for this protein. Eddowes and Hill (118) were likewise able to enhance the electron transfer

rate of cytochrome c at a gold electrode substrate, by the addition of 4,4'-bipyridine to the solution. Such compounds were different from the electroactive organic molecules used before this time, called "mediators", whose formal potential had to be within the same range as the biological molecule of interest (121, 122). The 4,4'-bipyridyl compound, when added to solution, was one of the first molecules known to accelerate the electron transfer rate of redox proteins while being electroinactive in the potential window of the molecule being studied. Based on the structure and the voltammetric responses of such compounds Hill et al. (123) have suggested that this molecule is perpendicularly oriented towards the electrode, having a nitrogen atom of one pyridyl ring adsorbing onto the electrode surface while the other ring is directed out into solution. Therefore according Hill et al. (123), this so-called "surface promoter" type electrode contains weakly basic pyridyl groups which are believed to be capable of binding with cytochrome c. However, the exact orientation of this promoter on the electrode surface is still not certain and is currently an area of intense investigation.

The opinions regarding the mechanism by which surface promoters might function are divided. As mentioned earlier, Albery et al. (120) believe such promoters increase rates through their specific binding interactions with the protein in solution at the electrode interface. According to Chao

et al. (124), promoters might also play a role in preventing electrode fouling by irreversible adsorption of protein. Indeed, throughout the literature adsorption of proteins onto electrode surfaces seems to be a general phenomenon. However, these two concepts of protein electron exchange are contradicted in the case of cytochrome c₃, a polyheme-type protein similar to the monoheme cytochrome c. In this protein, fast electron exchange rates are known to occur at gold electrodes in the absence of such promoters, even though strong irreversible surface adsorption has been indicated (4). Such bare electrode surfaces lack the functional groups that are necessary, according to the model proposed by Albery et al. (120), for protein binding interactions. However, Bianco and Haladjian (125) have more recently proposed that electron exchange in this molecule might occur due to the interactions between oppositely charged sites of adsorbed and free cytochrome c₃ molecules in solution. This type of mechanism would support the original model for protein binding interactions proposed by Albery et al. (120). Therefore, the action of these modifiers is still unclear.

Modifying electrode surfaces with an electron promoter opened up a new area in electrochemistry, by providing a convenient way of investigating direct heterogeneous electron transfer reactions of heme proteins. Since the initial report by Eddows and Hill (118) many effective

promoters have now been found which can enhance the electron transfer reactions of large biological molecules at a variety of different electrode surfaces. Taniguchi et al. (126) were the first to report the use of a pre-adsorbed promoter, bis(4-pyridyl) disulphide, which exhibited a well defined quasi-reversible rate of electron transfer for cytochrome c at a gold electrode, without the need for any promoter in solution.

Allen et al. (123) have more recently defined the necessary structure-function relationship of various promoter molecules that will facilitate the transport of electrons between electrode and redox systems. After investigating some fifty-four electron transfer promoters, they have proposed that in order to achieve a successful modification, a bifunctional molecule of the X \backslash Y type is necessary. In such a molecule, X represents a functional group which adsorbs or binds to the metal surface, while Y represents a functional group positioned away from the electrode surface, out into solution. The surface active end, X, must be an electron pair donor group having either a nitrogen, phosphorous, or sulfur atom. The functional end, Y, on the other hand must be an ionic or weakly basic group capable of forming a salt bridge and/or hydrogen bond to positively charged lysine residues on cytochrome c's surface. Bifunctional promoters containing weakly basic pyridyl and aniline-like nitrogen groups were shown to be capable of hydrogen bonding to ly-

sine residues. While promoters containing groups like carboxylate, sulfonate, and phosphate were found capable of forming salt bridges with such residues.

Allen et al. (123) have also indicated in their study that promoters should maintain limited conformational flexibility in order to react more effectively with cytochrome c molecules in solution. Such flexibility must be limited in order to prevent the Y end of the promoter from adsorbing onto the electrode surface. The consequences of extreme conformational flexibility were demonstrated with 1,2-bis(4-pyridyl)ethane (123). This molecule was shown to be able to flip over and adsorb both of the pyridyl nitrogens onto the metal electrode surface. Such a conformational change prevented the Y groups from providing an electrode/solution interface capable of protein binding interactions, thus giving no observed electrochemistry for cytochrome c. However, 1,2-bis(4-pyridyl)ethylene, a more rigid molecule due to its double bond character, was shown to promote direct heterogeneous electron transfer for this protein. Therefore the observed electrochemistry of these two surface adsorbers towards cytochrome c, supports the necessity for limited conformational flexibility and rigidity of the promoter.

Parallel to the development of modified electrodes has been the rapid growth in interest towards unmodified electrode systems. Such interest sprang from the early report

of Yeh and Kuwana (117) describing the direct electrochemistry of horse heart cytochrome c at tin-doped indium oxide and fluorine-doped tin oxide semiconductor electrodes in the absence of surface modifiers. The electrode reaction of cytochrome c at tin-doped indium oxide was a well behaved quasi-reversible reaction while that of tin oxide was of a lower degree of reversibility. Upon further investigation (127-129) of these two electrode systems, electron transfer reactions were found to proceed in a well behaved diffusion controlled manner but with slower rates than had been originally reported. Not only were the kinetics much slower, but the electrode reactions were also found not to obey Butler-Volmer theory (130-132) for a simple one electron transfer system. This difference was later attributed to the impurity of cytochrome c samples used in the latter studies (133).

The electrochemistry of cytochrome c at metal oxide semiconductors has more recently been found to be strongly dependent upon electrode pretreatment procedures (1). In the case of tin-doped indium oxide semiconductors, highly reversible voltammetric responses ($k^{\circ}_{s,h} > 10^{-1}$ cm/s) were observed for cytochrome c. Such responses were obtained when the electrode was subjected to a standard pretreatment procedure, i.e., sonication in ethanolic detergent mixtures and then highly purified deionized water, followed by pre-equilibration in a buffer solution containing tris/cacody-

late, pH 7.0. The electrode reaction was indicated to be highly reproducible even in the presence of an adsorbed layer of cytochrome c (ca. 10% of a monolayer).

In contrast with the indium oxide electrode, fluorine-doped tin oxide electrodes subjected to the same standard pretreatment procedure gave electrochemical responses for cytochrome c that were much less reversible, yielding considerably lower rate constants ($k'_{s,h} < 1.0 \times 10^{-3}$ cm/s) (1). The temporal dependence of the heterogeneous kinetics for cytochrome c at the tin oxide electrode was interpreted as being due to non-equilibrium surface conditions of the electrode when subjected only to the standard pretreatment procedure. Voltammetric cycling of the electrode allowed equilibrium to occur as the responses became more reproducible, though with poorer kinetics than the first few cycles. This study therefore indicated that the hydration state of the oxide surface may play an important role in obtaining stable rates of heterogeneous electron transfer towards heme proteins.

Electrostatic interactions between the surface of the metal oxide electrode and heme protein are also believed to be important in controlling rates of heterogeneous electron transfer (1). Metal oxide electrodes contain a high concentration of surface oxygen species which can be either protonated, neutral, or negatively charged depending on the particular metal oxide used and the pH of the solution that

it is in. Such acid-base equilibria can control coulombic and hydrogen bonding interactions between the protein molecule and the metal oxide surface, much like that required in protein-protein interactions. The surface charge for a particular metal oxide electrode is related to what is called the point of zero zeta potential (pzzp). The pzzp is the pH at which adsorbed H^+ and OH^- are equal on the electrode surface. The pzzp is also referred to as the point of zero charge (pH_{pzc}) when no other electrolyte ions, besides H^+ and OH^- , are specifically adsorbed. Therefore, the charge on the electrode surface would depend on its particular pzzp, being either attractive or repulsive with respect to this value for a particular charged protein.

Another factor that can presumably affect surface charge on semiconductor type electrode surfaces is the flat-band potential (E_{fb}) (1). Excess charge in a semiconductor is distributed in the space charge region, unlike that of a pure metal in which excess charge resides on the surface or so-called Helmholtz layer. As the potential of a pure semiconductor is changed, excess charge in this region along with that residing at the electrode solution interface, causes band bending in the semiconductor. The semiconductor bands are bent upwards, towards the solution interface, when the charge on the semiconductor is positive with respect to that in solution. The electrode potential at which the bands are not bent is the E_{fb} . With the high doping levels

used in the semiconductor type electrodes described here, the electrode will have both semiconductor and metal type characteristics. Therefore, using such highly doped electrodes might offset or reverse the sign of a particular semiconductor if its E_{fb} is very much different from that of its pzzp. This last point has been used to explain the apparent positive surface charge observed for the quasi-reversible rates of cytochrome c at the fluorine-doped tin oxide semiconductor (1).

The availability of different kinds of metal oxide surfaces has now made these electrodes attractive for studying heterogeneous electron transfer reactions of a variety of biological molecules. Harmer and Hill (134) have found direct quasi-reversible electrochemistry for cytochrome c, ferredoxin and rubredoxin at ruthenium dioxide and iridium dioxide electrodes. Tin-doped indium oxide electrodes have now been successfully used to obtain quasi-reversible rates for proteins like myoglobin (135) and cytochrome c₅₅₃ (136). Therefore, the hydrophilic and near neutral acid-base properties of these kinds of interfaces appear to be compatible with a variety of different proteins.

Non-metal electrodes such as carbon have also shown direct electron transfer with cytochrome c as well as other proteins (137,138). Differences between cleaved, polished and edge oriented pyrolytic graphite have been described

(137). Electrochemistry of cytochrome c at a freshly cleaved basal plane graphite electrode was rather poor. The fact that such surfaces were indicated to be hydrophobic could probably explain such results. However, upon polishing with alumina slurry more productive electrochemistry was achieved for this protein. The fastest of the pyrolytic graphite results was with an edge oriented electrode. Such an electrode was shown to give quasi-reversible rates for cytochrome c. The rate enhancement in going from cleaved to edge oriented graphite was shown to be due to the formation of (C-O) functional groups on the carbon electrode's surface. The principle of cutting the graphite across the aromatic rings in the edge oriented case was believed to rupture C-C bonds which could then possibly recombine with oxygen to form C-O. The same principle was believed to occur upon polishing. The various (C-O) functionalities therefore constitute reversible and productive binding domains similar to the metal oxide and modified type electrodes.

Bare (unmodified) metal and mercury electrodes, unlike the electrodes mentioned above, have shown very little success in obtaining direct and near reversible rates of heterogeneous electron transfer with most heme proteins. An exception here is noted in the case of cytochrome c₃, which is known to exchange electrons in a reversible manner with both mercury and bare solid electrodes (4,125). Cytochrome

c₃ is a protein with the same dimensions as cytochrome c but unlike this molecule, cytochrome c₃ contains four heme groups. Even though an exact mechanism for this protein is still rather vague, a possible explanation for the reactivity of cytochrome c₃ might be based on the relative position of the heme groups in relation to the protein's surface. Since the heme groups in cytochrome c₃ are closer to the molecular surface, when compared to the position of cytochrome c's heme group, the probability of electron exchange is expected to be higher for cytochrome c₃ due to shorter distance between the hemes and the electrode.

Polarographic studies of cytochrome c at mercury, indicated that the reduction of this protein occurs through an irreversibly adsorbed layer (139). Later studies with cytochrome c at mercury indicated the strong effect adsorption played on the electron transfer rate. Serre et al. (140), among others, demonstrated that cytochrome c's reduction can be polarographically reversible if its concentration is kept below 30 μM . However, with higher concentrations adsorption became evident by the increasing irreversibly and negative shifts in the polarographic half-wave potential. Strong adsorption effects were also indicated in the calculation of diffusion coefficients for this protein at mercury. In this regard, polarographic currents were shown to be diffusion-controlled while the diffusion coefficients calculated from them were shown to be far less ($< 1/2$) than by hydrodynamic

methods.

Several models have developed over the years to explain the sluggish electron transfer process for the reduction of cytochrome c on mercury. In the Kuznetsov (141) model, native cytochrome c molecules are believed to be capable of exchanging electrons with the electrode in the pores of an irreversibly adsorbed monolayer of flattened and denatured molecules on the electrode surface. In this type of model, increases in electrode overpotential were shown to be directly correlated with the energy spent in pore expansion as the native cytochrome c molecules squeezed into the pores of the flattened monolayer of protein. It was indicated that film pressures in the monolayer increase with concentration making it more difficult for the native molecules to squeeze into the pores, thus increasing the distance of electron transfer to the electrode surface. Therefore, rates of electron transfer abruptly slow down as the bulk concentration of cytochrome c is raised due to this distance effect. Higher overpotentials are then needed in order to compensate for the slower rates of electron transfer.

Scheller (142) proposed a model in which at low concentrations a native conformation exists for the adsorbed cytochrome c molecules. When the concentration is increased electron transport is then believed to occur by two simultaneous pathways. One involving an exchange type mechanism with already reduced molecules on the electrode surface and

the other by way of a hopping mechanism through the adsorbed layer of molecules. A similar, but somewhat different, mechanism was proposed by Haladjian et al. (143). In their model a highly flattened and denatured adsorbed layer is believed to exist on the mercury electrode surface, similar to the Kuznetsov model mentioned earlier. However, electron transfer in this model is believed to proceed by way of an exchange between the denatured adsorbed layer and the native cytochrome c molecules in solution. In such a case, an elementary electrochemical model would be of the type: electrode / adsorbed denatured protein / protein in solution. That adsorbed cytochrome c was actually denatured could be demonstrated by Haladjian et al. (143) using film transfer experiments in both the presence and absence of oxygen. The adsorbed layer in that study was indicated to be easily oxidized by oxygen. However, in the case of native cytochrome c this is known not to happen. The extent of this denaturation is still a point of controversy and is part of the work that will be reported in this dissertation using silver electrodes.

In the case of bare metal electrodes, studies of direct heterogeneous electron transfer of heme proteins have been even slower to develop. Kôno and Nakamura (144) in 1958 were the first to demonstrate direct reduction of cytochrome c at solid bare metal electrodes when using platinum. However, large overpotentials ($\eta > 0.5$ volts) were necessary in

order to drive the reduction process. Even larger overpotentials ($\eta > 1.2$ volts) have been reported for both gold and platinum electrodes for the oxidation process of cytochrome c (145). Such irreversible electrode responses for cytochrome c were also noted for bare metal substrates such as nickel (146) and silver (3,147). Lack of voltammetric redox peaks at such bare metal electrode surfaces have therefore limited their use in determining direct heterogeneous electron transfer parameters for heme proteins.

The general lack of hydrophilic chemical functional groups (148) and strong irreversible surface adsorption of protein and/or solution impurities (1,124) are thought to be the main reason for negligible responses of metal electrodes towards heme proteins. The requirements for a clean hydrophilic bare electrode surface have been substantiated in the work reported by Bowden et al. (1). With a special pretreatment procedure on a gold electrode, i.e., exposing the metal to a soft hydrogen flame prior to study, they were able to achieve nearly reversible heterogeneous rates ($k^{\circ}_{s,h} > 8.0 \times 10^{-2}$ cm/s) of electron transfer with cytochrome c. Such pretreatment was reported to remove organic contaminants, which made the electrode surface hydrophobic, resulting a more hydrophilic type surface. Although their responses did not last very long, calculated diffusion coefficients were consistent with known hydrodynamic values, unlike those of mercury mentioned earlier.

The temporal dependence of the voltammetric responses cited above were believed to be due to slow contamination of the gold surface by irreversible adsorption of solution impurities or protein. Cytochrome c samples used in that work were chromatographically purified and then lyophilized. In a more recent report from our laboratory (149), which will be elaborated on later in this dissertation, it is clear that lyophilization has a dramatic effect on both the rate and stability of direct heterogeneous electron transfer of cytochrome c at bare metal electrodes. Lyophilization denatures some of the cytochrome c sample, which then irreversibly adsorbs onto the electrode surface causing electrode fouling with time. This possibly explains the lack of temporal stability for cytochrome c at gold cited by Bowden et al. (1).

H. Resonance Raman Spectroscopy of Heme Proteins

In the present section a simple introduction will be given to the field of resonance Raman (RR) scattering spectroscopy. Since the basis of the work presented has been with heme containing proteins, the discussion of the technique of RR will be limited to this area. This section is not meant to be comprehensive but rather it is designed to establish a starting point from which the reader may proceed in understanding some of the points to be made later under the section entitled surface enhanced resonance Raman scattering (SERRS) spectroscopy.

By employing RR spectroscopy it is possible to obtain structural information from deep within very complex biological molecules. The nature of the RR effect is such that only vibrational modes associated with the chromophoric group, i.e., the heme in this case, of the molecule are enhanced (150). The consequences of this effect are very important since the remainder of the vibrational modes associated with the heme protein are not enhanced and therefore do not complicate the spectra. This is relevant from a physiological standpoint since the technique is both a highly selective and extremely sensitive probe of the chromophoric group, which is often the site of biological activity.

A Raman spectrum can be obtained when incident photons, usually from a visible light source such as a laser, are inelastically scattered from a sample. Various molecular transitions of the sample cause these scattered photons to gain or lose a quantum of energy. Those photons which gain a quantum of energy are referred to as anti-Stokes scattering, while those which lose a quantum of energy are known as Stokes scattering. While both types of Raman scattering provide the same information, Stokes scattering is the one most often used due to its higher intensity. The molecular transitions often observed in the Raman scattering process can be of translational, rotational, vibrational, or electronic origin. For large biological molecules the

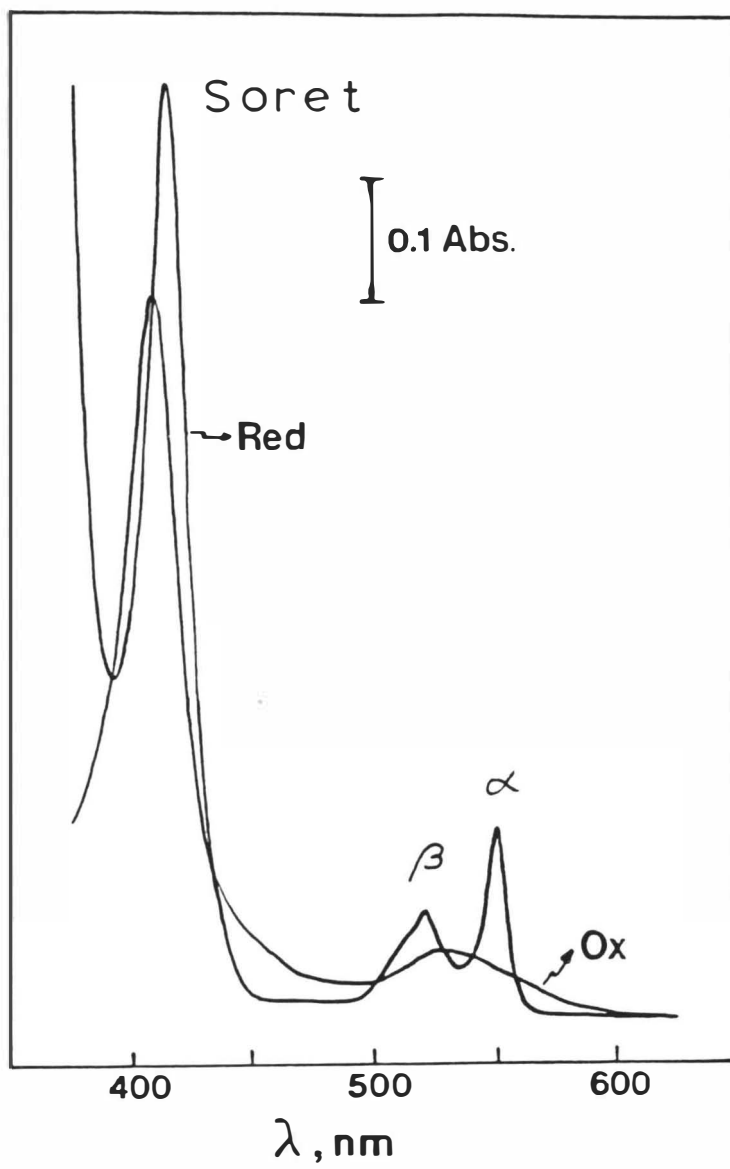
transition of greatest interest is vibrational. Such a vibrational spectrum in Raman spectroscopy will be displayed as a frequency shift ($\Delta\nu$) between the incident and scattered radiation. This frequency shift corresponds to the energy transferred between molecules and photons upon scattering. Its measurement reflects the characteristic vibrations of the molecule. For heme proteins, these characteristic Raman vibrational bands will undergo specific changes in both frequency and intensity when the chromophoric unit of the molecule is altered.

Polarization properties of the molecular light scattering process can also be used as a diagnostic tool in Raman spectroscopy of heme proteins. By measuring the intensity of the scattered radiation in the parallel ($I_{||}$) and perpendicular (I_{\perp}) modes, estimates of the polarization ratios $\rho = I_{\perp}/I_{||}$ can be made. These ratios are useful in structural studies of heme proteins since the symmetry of a particular vibrational mode can be determined from them. Vibrational bands with polarization ratios of 0.75 ± 0.1 are designated as depolarized (dp), those with polarization ratios lower than 0.75 as polarized (p), and those with ratios greater than 0.75 as anomalously polarized (ap) (151). Using these established polarization ratios porphyrin ring modes can be assigned in the Raman spectrum. Totally symmetric vibrations give rise to polarized bands which are assigned to A_{1g} modes. The B_{1g} and B_{2g} modes are

assigned to non-totally-symmetric vibrations producing depolarized Raman bands. Anti-symmetric vibrations of the porphyrin ring are assigned to A_{2g} modes. These last modes are only active in resonance Raman scattering and give rise to anomalous polarization.

In addition to polarization properties, resonance Raman scattering can also provide insight into the normal modes of vibration. Resonance Raman scattering will occur when the exciting laser line is tuned into an electronic absorption band. Upon resonance with an electronic absorption transition some of the Raman bands will be greatly enhanced. Figure 5 illustrates the most prominent optical absorption bands for cytochrome c. In the case of reduced cytochrome c, two absorption transitions are observed in the visible region (α and β), and one in the near ultraviolet (Soret). In this figure, the Soret band appears at 416 nm while the α and β bands occur at 550 and 520 nm, respectively. For a heme protein such as cytochrome c, the non-totally-symmetric (B_{1g} , B_{2g}) and anti-symmetric (A_{2g}) modes are enhanced upon resonance of the laser line with either the α or β electronic absorption bands (152,153). On the other hand, when the laser line is in resonance with the Soret band polarized scattering from totally symmetric A_{1g} modes are the most predominant vibrations in the spectrum. Therefore, the fact that only certain Raman vibrational bands are enhanced

Figure 5. Visible absorption spectra of reduced (red) and oxidized (ox) forms of cytochrome c. (0.1 cm path; 60 μ M solutions; pH 7.0).



imparts a selectivity to the resonance Raman effect.

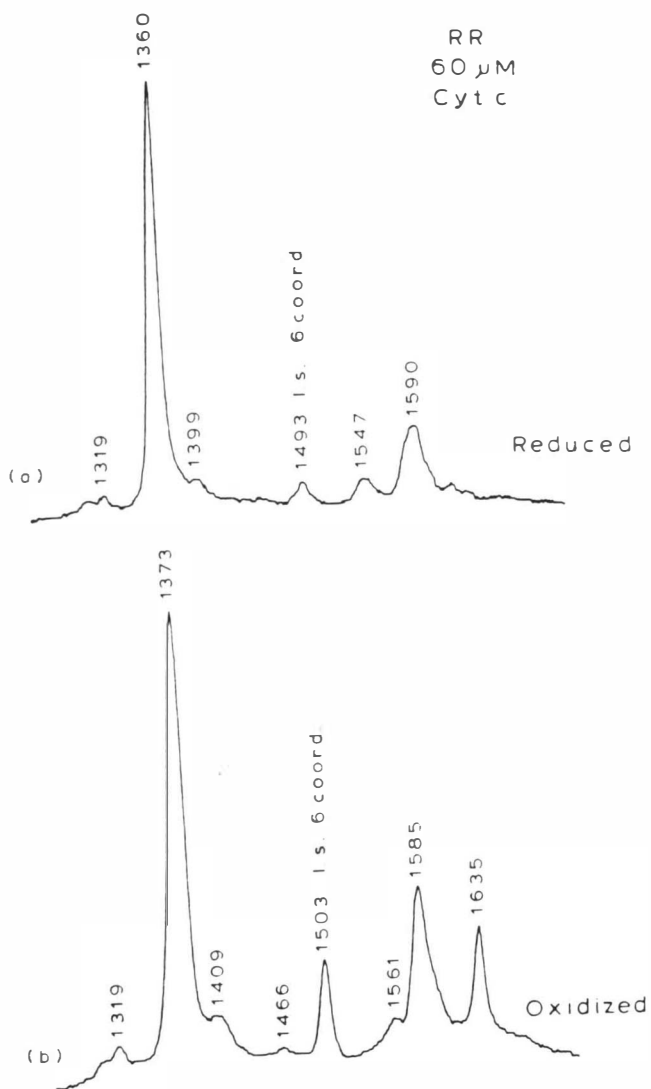
Another distinct feature of RR spectra obtained under either Soret or α,β -band excitation is the magnitude of the enhancement effect. Under Soret excitation, enhancement is greater since its electronic transition is approximately ten times stronger and much narrower than either the α or β absorption bands. Such strong enhancement allows both lower concentrations and lower incident laser powers under Soret excitation. More importantly, in relation to the present work, is that the main oxidation state marker band (ν_4) is a polarized mode which is strongly enhanced under Soret excitation (154). Enhancement of the ν_4 band therefore allows one to monitor changes in the oxidation state of heme proteins. Another Raman band of importance in the present discussion involves the spin-state marker band ν_3 (154). This is also a polarized band and it is strongly enhanced during Soret excitation, thus it provides a means of monitoring changes in the spin state of heme proteins. For principal molecular motions contributing to the observed normal vibrational modes of the RR indicator bands (ν_3 and ν_4) see Appendix II. Further assignments of heme protein vibrational Raman bands are available in the literature (154,155).

The following discussion concentrates on two of the primary RR indicator bands (ν_3 and ν_4). The first is ν_4 , an oxidation state marker mode whose frequency is sensitive to

electron density in porphyrin π^* -orbitals. This band is sensitive to both the oxidation state of the metal ion, and the presence of axial ligands having π -acid character (156). Figure 6 illustrates shifts in frequency corresponding to changes in cytochrome c's oxidation state. In particular, the ν_4 band shifts from 1360 cm^{-1} in the reduced state to 1373 cm^{-1} in the oxidized state. This has been interpreted in terms of π back donation from the Fe $e_g(d_\pi)$ orbitals to the porphyrin $e_g(\pi^*)$ orbitals (154). In the oxidized state, π back donation is diminished due to the lowering of the Fe $e_g(d_\pi)$ energy level. This causes an increase in the force constants of porphyrin stretching modes, thus leading to the observed upward shift in frequencies.

Whereas the ν_4 band is only dependent on oxidation state, the ν_3 band is sensitive to changes in oxidation state, spin-state, and coordination of the heme iron. This polarized mode, found in the region of $1480\text{-}1510\text{ cm}^{-1}$, is a common feature in Soret excitation Raman spectra of heme proteins. As illustrated in Figure 6, for a six-coordinate low spin heme protein such as cytochrome c, the ν_3 frequency is found at 1493 cm^{-1} in the reduced state and 1503 cm^{-1} in the oxidized state. This change in frequency of the ν_3 band can be interpreted in a similar fashion to the frequency shift of the ν_4 band. This is due to the fact that both the coordination and the spin state of the heme iron remain the same. However, in cases where the spin-state and coordina-

Figure 6. Resonance Raman spectra of cytochrome c: (a): reduced form, (b): oxidized form. (413.1 nm excitation wavelength; 60 μ M solutions; pH 7.0).



tion of the heme iron change, somewhat different frequency shifts occur. In the case of a six-coordinate high-spin complex in the oxidized state, ν_3 occurs at 1482 cm^{-1} and shifts to $1492\text{-}1496\text{ cm}^{-1}$ for a five-coordinate high-spin species (154,157). According to Spiro and Strekas (154) these frequency shifts of the ν_3 band are due to structural changes of the heme protein, with possible doming and ruffling of the porphyrin ring. In such a case, frequency shifts are believed to arise from alterations in the π -bond order due to less effective overlap of porphyrin π orbitals (158).

I. Surface Enhanced Resonance Raman Spectroscopy

In this section some very basic background will be presented for the technique of surface enhanced resonance Raman scattering (SERRS) spectroscopy of heme proteins. SERRS is similar to the technique of resonance Raman (RR) scattering mentioned in the previous section. However, in the case of SERRS spectroscopy, a higher enhancement factor is observed in the Raman scattering cross-section from molecules adsorbed on or placed near rough metal surfaces such as copper, gold and silver (159). Not only can intense signals be obtained at rough metal surfaces, but also at such metal structures as gratings, lithographically produced metal spheroids, island films, and colloidal particles. Of these surfaces, silver has been observed to give a greater spectral enhancement ($\approx 10^6$) and is therefore the surface

used in the present study. However, the main concern of this study will be with SERRS at electrode interfaces. This large enhancement factor provides the means for obtaining high resolution vibrational spectra of heme proteins adsorbed on these particular metal surfaces. Such spectra, like RR, enable one to characterize in situ the interfacial and conformational behavior of a heme protein such as cytochrome c at an electrode surface.

Although both SERRS and RR spectroscopy give similar Raman spectra, there are some differences between them. One experimental anomaly observed in SERRS is the complete depolarization of all vibrational modes. This effect is presumably due to multiple scattering effects at the roughened surface (160). Whereas ρ values are approximately zero for symmetric vibrations in RR, this value lies in the range of 0.60 to 0.75 for all SERRS bands. Since all bands are essentially depolarized, it is not possible to use polarization measurements to determine mode symmetries of vibrational bands. Instead, bands must be correlated with previously assigned RR bands whose normal mode symmetry has been well established. The extensive literature on heme protein RR spectra provides a means for making structural inferences from the SERRS spectra of such proteins. The fact that all SERRS bands are depolarized is a good criterion for proving that the observed spectra are indeed surface enhanced.

Another feature in the surface enhanced mechanism is the departure from ν^4 intensity dependence which applies to normal but not resonance Raman scattering (160,161). The surface enhanced mechanism is instead dependent on the particular surface and the state or roughness of that surface. This mechanism's intensity profile has been shown to follow the excitation of local surface plasmon resonances from surface protrusions (162). These protrusions give the surface its roughness, a crucial factor for the adsorbate's enhancement from the substrate. Formation of silver microstructures, known as adatom complexes, on the scale larger than 250-500 Å are deemed necessary in order to observe significant enhancement. These adatom complexes can be formed on a silver electrode surface by a typical oxidation/reduction cycle (ORC) (explained in the Experimental section). This submicroscopic scale roughness is believed to be involved in the long-range enhancement effects predicted by electromagnetic (EM) theories (163).

Although the final mechanism of the enhancement is still undetermined, most groups now operate with the working hypothesis that coupling of surface plasmon waves in the metal and the adsorbed species by way of an EM mechanism, is responsible at least to a large measure for the effect. Simultaneously with the EM mechanism a short range enhancement mechanism (164), based on chemical theory, is believed to occur. In this mechanism direct contact between the

adsorbate and special surface sites on the metal, referred to as "SERRS active sites", are believed to be necessary for the short range enhancement. This chemical mechanism gives rise to estimated enhancement factors of ca. 2 orders of magnitude (164). Watanabe et al. (165) have indicated these sites to consist of Ag^+ complexes which occupy a rather small fraction (<10%) of the entire surface, at the end of electrode ORC pretreatment. Calculations by Roy and Furtak (166,167) have more firmly established the nature of these active sites by suggesting a pyramidal Ag_4^+ cluster.

In the chemical enhancement mechanism a weak chemical bond is formed between the positively charged Ag_4^+ cluster and the lone pair of the adsorbate. This bond might also be formed by either a bridging anion, a specifically adsorbed anion (ion pair), or a π bond interaction between the adsorbate and the active site. A chemical enhancement mechanism was first envisioned by Otto (164) using a charge-transfer excitation process between the surface Ag^+ complex and the adsorbate. In the charge-transfer process the incident photon is believed to promote an electron from the silver Fermi level (E_f) to the excited state of the chemisorbed molecule leaving a hole in the metal. The electron then charge transfers back into the metal and radiatively recombines with the hole while the adsorbed molecule is left in the excited vibrational state. Therefore the charge-transfer process resembles a RR process in which the photon

directly excites the electron from the ground state of the molecule into the first excited electronic state. This transition can also occur in a reverse manner in which the electron is charge transferred from the ground state of the chemisorbed molecule into the E_f of the metal. The energy alignment between E_f and the molecular states of the adsorbed molecule is a function of chemisorption and of the applied potential at the electrode/electrolyte interface. This type of mechanism has reasonably accounted for the observed potential dependence of the surface enhancement, since changes in potential will shift the relative position of the silver E_f against the vacant level of the adsorbed molecule.

Another important property of SERRS in relation to RR spectroscopy involves fluorescence. It has been found that the metal surface can effectively quench the fluorescence of adsorbed molecules (168). This is especially important when one is dealing with chromophoric systems since most are highly fluorescent. The presence of even a small amount of fluorescence or phosphorescence contaminant could easily wipe out the spectrum. This is due to the fact that RR scattering is several orders of magnitude weaker relative to either the fluorescence or phosphorescence and is therefore consistently plagued with signal to noise difficulties. However, in the case of SERRS the signal to noise is much higher since fluorescence is effectively quenched.

The preceding paragraphs were directed towards presenting the fundamental mechanisms of surface enhancement. The multiplicity of effects and the difficulties in distinguishing between them, have not led to the establishment of a mechanism which explains all the experimental observations. However, even without knowledge of its precise mechanism, SERRS can be applied to the elucidation of many important interfacial phenomena. The conformation of biological molecules in the adsorbed state is just one of its promising areas.

CHAPTER II - EXPERIMENTAL

In a previous report from our laboratory (133) attention has been drawn to the effects of sample purity on the voltammetric response of cytochrome c at solid metal oxide electrodes. In that report it was clear that impurities found in high quality commercial samples of cytochrome c could affect the heterogeneous electron transfer kinetics at electrodes. These impurities were recognized by Brautigan et al. (169) when commercial samples of cytochrome c were applied to a CM-cellulose ion exchange chromatography column. Impurities preceding the native band were referred to as deamidated and those after as polymeric (oligomeric) forms. Only the central band is the native form of cytochrome c since the other two fractions have been shown to react with both CO and O₂ (170). In addition, the oligomeric form of cytochrome c has been shown to be enzymatically inactive with the cytochrome c oxidase system (171,172). As can be seen cytochrome c can exist in multiple forms only one of which, native cytochrome c, occurs in vivo. Therefore, in order to model in vivo electron transfer reactions it is necessary to avoid contamination of the sample by deamidated and oligomeric forms.

Cytochrome c from commercial sources arrives in lyophilized (dried) form. Both magnetic susceptibility (173) and EPR (174) type measurements have detected a high-spin denatured component in lyophilized ferricytochrome c. This component, however, has been indicated to disappear (in ≈ 20 sec.) upon redissolving dehydrated ferricytochrome c into aqueous media (175). This observation that denaturation of cytochrome c upon drying is a reversible process has therefore led most laboratories to use lyophilization of cytochrome c as a convenient means of storing this protein for long periods of time after chromatographic purification. However, a more recent report (2) has indicated that a small amount of this denatured ferricytochrome c does not return to its native state when reintroduced into aqueous media. Upon repurification, three chromatographic bands were observed for samples lyophilized after purification but only one band was observed for non-lyophilized purified samples. The three bands observed in samples lyophilized after purification eluted in a similar fashion to that reported by Brautigan et al. (169) in non-purified commercial samples. Therefore, the process of lyophilization generates various amounts of deamidated and oligomeric forms of cytochrome c which do not return to their native form when redissolved. Although the amount of these impurities has not been quantified, chromatographic observations indicate that it is certainly less than 0.1 % of the native material. Even

though this quantity of impurities may seem small, it can have dramatic effects on the heterogeneous electron transfer of native cytochrome c at silver electrodes, as will be shown later in this study.

In the present study, horse heart cytochrome c (type VI from Sigma Chemical Company) was chromatographically purified as previously described (133,169) using a carboxymethylcellulose (CM-52, Whatman) column. Approximately 100 milligrams of this cytochrome c sample were dissolved in 4 mL of 40 mM phosphate buffer, pH 7.0. This solution was then carefully pipeted onto a 50 mL buret containing 40 mL of carboxymethylcellulose equilibrated with the same 40 mM phosphate buffer. After the sample was loaded on the column, separation was begun by eluting with 90 mM phosphate buffer, pH 7.0. The entire purification process was carried out in a refrigerator at 4 °C. The eluent was collected in 5 mL aliquants by a fraction collector (Redirac model #2112). The central chromatographic band was pooled and then concentrated using an Amicon ultrafiltration cell with a YM5 filter. Phosphate ions were removed from this portion of the purified cytochrome c sample by chromatography on a desalting column (Bio-Rad #P-6DG) with water as the eluent. A fraction of this purified desalted cytochrome c was then lyophilized and stored at -4 °C for use in later experiments. Solutions of cytochrome c in 0.05 M Na₂SO₄ and in 0.05 M Tris/cacodylic acid buffer pH 7.0 were prepared by

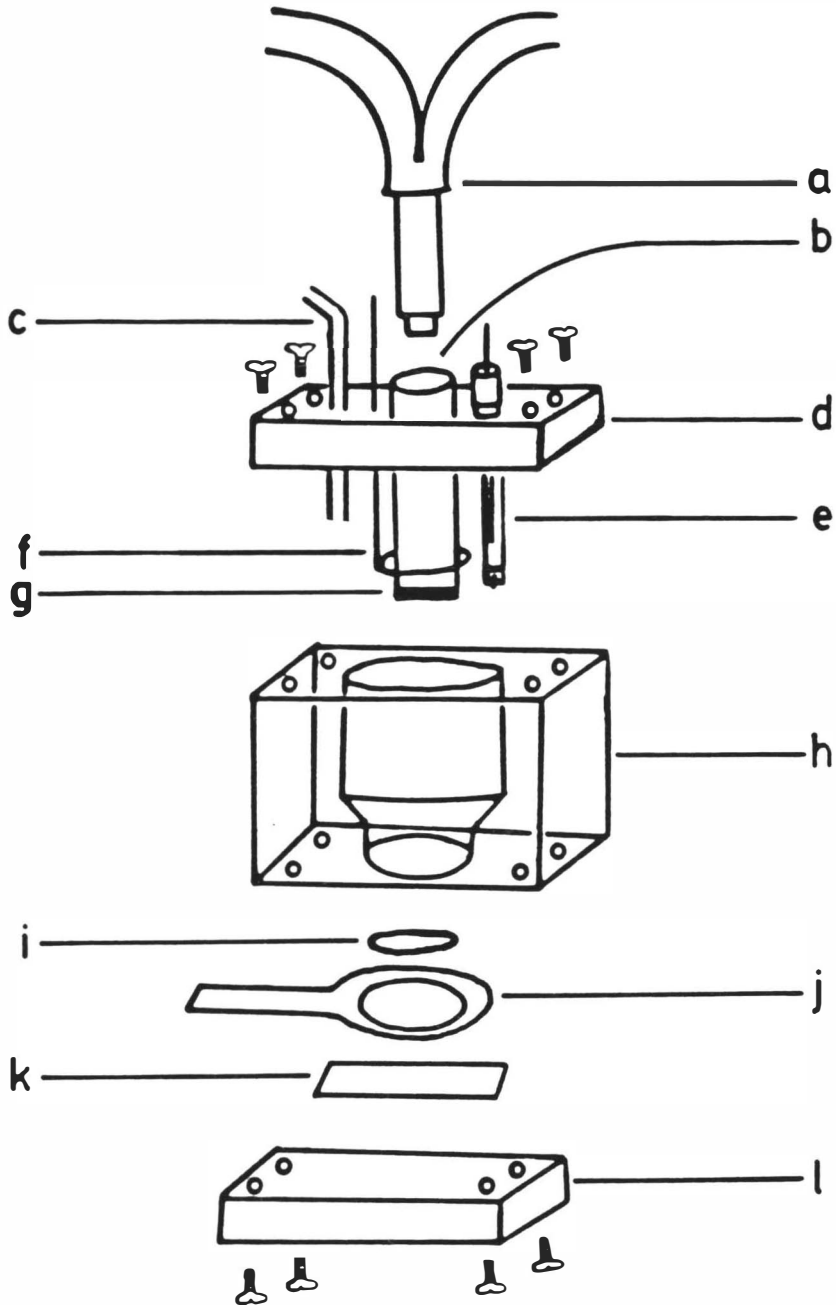
adding an appropriate amount of the corresponding electrolyte to the non-lyophilized aqueous purified cytochrome c solution. Similar solutions were made by adding appropriate amounts of the lyophilized material to the electrolyte solutions. All Na_2SO_4 solutions used in this work had a measured pH of 6.3. In this study, best results were obtained when cytochrome c samples were used within a short period of time after chromatographic purification. This was found to be particularly important in cases where cytochrome c is in solution with either Na_2SO_4 or phosphate buffer solutions since these samples are easily contaminated by bacteria within 3 or 4 days after purification. However, samples of cytochrome c in Tris/cacodylic acid were found to give good results after a longer period of time (\approx 2 weeks). This is probably due to the effect cacodylic acid has in inhibiting bacterial growth thus limiting the amount of contamination in such samples with time. Cytochrome c concentrations were determined using a Beckman Acta MVII spectrophotometer at 550 nm using a reduced minus oxidized difference molar absorptivity, $\Delta\epsilon = 21,100 \text{ M}^{-1} \text{ cm}^{-1}$ (176). Absorbance spectra were recorded for fully reduced cytochrome c by addition of solid sodium dithionite (ACS grade) to the aqueous purified ferricytochrome c sample.

Tris(hydroxymethyl)aminomethane (Sigma Chemical Company, Trizma Base, reagent grade) and sodium sulfate (Fisher Scientific Corp., ACS grade) were used as received.

Cacodylic acid (Sigma Chemical Company, 98% pure) was recrystallized twice from isopropanol. All solutions were prepared in water purified with a Milli-RO-4/Milli-Q system (Millipore Corp.) which exhibited a resistivity of 18 M Ω on delivery. Samples were deoxygenated prior to use by passing water-saturated nitrogen over the surface of the solution while stirring gently over night at 4°C in a sealed serum bottle. Nitrogen used in each experiment was deoxygenated prior to water saturation by passage over hot copper turnings (ca. 500°C).

The spectroelectrochemical cell used, similar to the design of Pyun and Park (177), is shown in Figure 7. Specular reflectance from the silver electrode surface was obtained with a glass fiber optic bundle (Bifurcated, 12 inch, Catalog No. 22-0285, Ealing Optical Co.). The combined end of the parallel pair of the fiber optic bundle was inserted inside a quartz tube which had been sealed at one end by a flat quartz disc. This prevented the contamination that would result from liquid seepage between the glass fibers. The open end of the quartz tube was epoxyed to the top of the cell cover plate so that the sealed flat end of the tube was positioned ca. 0.6 mm above the silver electrode surface. This maintained a distance which ensured that semi-infinite linear diffusion conditions would exist during each experiment. Wrapping Teflon tape around the combined end of

Figure 7. Spectroelectrochemical cell design (a): bifurcated fiber optic light guide, (b): quartz tube, (c) nitrogen blanket purge tube, (d): cell cover plate, (e): reference electrode, (f): platinum auxiliary electrode, (g): quartz disc window, (h): plastic cell body, (i): O-ring, (j): brass shim, (k): silver working electrode, (l): retainer plate.



the fiber optic bundle allowed the ferruled end to fit snugly inside the quartz tube and firmly against the sealed quartz window at the end of the tube. This arrangement made it easy to remove the fiber optic bundle from the cell for safe storage between experiments. The silver electrode was mounted on the bottom of the cell using a retainer plate. Connection to the working electrode was made by a brass shim isolated from the solution by an O-ring seal. The geometric area of the working electrode, determined by the inside diameter of the O-ring, was ca. 1.23 cm². The cell cover plate also contained a nitrogen blanket/purge tube, a sample injection port, a reference electrode and a platinum auxiliary electrode. The reference electrode probe tip was positioned ca. 2 mm above the working electrode. All potentials in this dissertation are reported versus the normal hydrogen electrode (NHE) and were obtained with a Ag/AgCl (1.0 M KCl) reference electrode calibrated against saturated quinhydrone (Eastman) solutions of known pH (178) and found to be 0.229(±0.005) V vs. NHE. All experiments in this work were carried out at room temperature, 22(±2) °C.

Polycrystalline silver foil, 1.0 mm thick (Alfa, 99.999%), was used as the working electrode in cyclic voltammetry (CV) (179,180), derivative cyclic voltabsorptometry (DCVA) (127,128,133,181), and single potential step chronabsorptometry (SPS/CA) (182,183) experiments. Prior to each experiment the silver electrode was polished to a

mirror finish using successively finer grades of alumina: Fisher 0.3, 0.1, and 0.05 μm . The electrode was then sonicated in copious amounts of Milli-Q water. Immediately after sonication, the silver electrode was preconditioned by continuous voltammetric cycling from +0.380 to +0.100 V vs. NHE in deaerated electrolyte for ca. 30 minutes at a scan rate of 20 mV/s. After preconditioning of the electrode, background CV and SPS/CA responses were acquired for electrolyte alone under the same experimental conditions that would later be employed for the cytochrome c sample at that same electrode in a given electrolyte. Solutions of cytochrome c were transferred by a glass syringe from the sealed serum bottle to the cell anaerobically. The cell was kept deoxygenated after sample injection and during experiments by a blanket of nitrogen.

Optical monitoring in the spectroelectrochemical experiments (DCVA and SPS/CA) was performed with a single-beam spectrometer configuration (184). The spectrometer's configuration consisted of a quartz-halogen source, a Heath monochromator, a photomultiplier tube and a Heath photomultiplier module. After passing through the monochromator, the source image was focused onto one arm of the fiber optic bundle by a 63 mm focal length lens. The other arm of the fiber optic bundle was positioned directly in front of a photomultiplier tube. The current from the photomultiplier tube was converted to a voltage signal by a current-to-

voltage converter using a Philbrick 1026 operational amplifier. A series of additional operational amplifiers were used to amplify and offset this signal to fall within the 0.0-1.0 volt range of the analog-to-digital (A/D) converter. The electrode potential was controlled with a locally constructed potentiostat of conventional three-electrode design (185). The potentiostat and spectrometer signals were both transferred to an integrating 16-bit A/D converter interfaced to a dedicated UNC ZM80 based microcomputer (186). As it will be explained in the Appendix, the data acquisition, instrument control and subsequent data processing were directed by a UNC microcomputer with programs written in BASIC. All calculations were performed with this system.

For a number of reasons, the 550 nm absorbance maximum for ferrocyclochrome c was monitored instead of the more robust maximum at 416 nm. Absorption by the metal surface (187), the sharp drop-off in the transmittance of the glass fiber optics used in this work, and the weaker source intensity at 416 nm were considered. Moreover, a wider slit width can be used at the broader 550 nm absorption maximum compared with the sharp maximum at 416 nm. Special concern for the signal-to-noise ratio is belabored here because of the signal corruption that occurs upon taking a derivative of the optical signal in DCVA (127,128,133,181). Although the 416 nm difference molar absorptivity, $\Delta\epsilon = 57,000 \text{ M}^{-1} \text{ cm}^{-1}$ (176), is almost three times larger than the difference

molar absorptivity at 550 nm, the latter has been used here for the reasons given above.

The diffusion coefficient (D_0) of cytochrome c used in all digital simulations and kinetic analyses was 1.1×10^{-6} cm^2/s (188). The formal potential ($E^{\circ'}$) used in each calculation was determined from the midpoint between the forward and reverse peak potentials taken from slow scan DCVA experiments for each experimental condition. Formal heterogeneous electron transfer rate constants ($k^{\circ'}_{s,h}$) were calculated from DCVA and CV peak potential separations after the method of Nicholson (179). The electrochemical transfer coefficients (α) were determined from ($E_{p/2} - E_p$) values taken from the forward potential scans of DCVA and CV experiments (189). For comparison, these kinetic parameters were also determined from SPS/CA experiments (183). The formal heterogeneous electron transfer rate constants in the SPS/CA experiments were calculated from the intercept of a plot of $\log k_{f,h}$ vs. overpotential (η) and the electrochemical transfer coefficient was calculated from the slope of these plots.

Digital simulation algorithms for CV, DCVA and SPS/CA responses have been previously reported (128,181-183). These simulations are based on a simple one electron transfer Butler-Volmer system (130-132). A comparison between the simulated and experimental responses was carried out for each experiment using the system parameters (α , $k^{\circ'}_{s,h}$, $E^{\circ'}$)

mentioned above. For the CV digital simulation program refer to reference 190. This program was modified for DCVA simulation by converting the current, i , of the simulated CV into a derivative of absorbance with respect to potential, dA/dE . This conversion was carried out by using the following equation (derived from reference 181):

$$(dA/dE) = 2 \times i(10^3 \Delta \epsilon / nFAv) \quad (1)$$

where n is the number of electrons transferred, F is the Faraday constant, A is the electrode area in cm^2 , and v is the voltammetric scan rate in mV/s . Everything else is as usual. The factor 2 in equation 1 is due to the $2 / \sin \theta$ dependence of the optical response as it transverses the diffusion layer. In this correction factor to the optical response, θ is the angle between the incident light beam and the electrode surface. The dA/dE response is multiplied by two in this study since the optical light beam is fixed at a 90° angle by the fiber optic waveguides. This configuration allows the optical beam to traverse twice through the diffusion layer. Therefore, contrary to transmission experiments at optically transparent electrodes, where the light beam traverses only once through the diffusion layer, the response obtained by reflectance spectroscopy is increased by a factor of two. For the SPS/CA and DCVA data acquisition programs refer to the Appendix.

In order to convert the DCVA response (dA/dE) to its corresponding current analog (i), the dA/dE file was divided

by the factor $(2 \times 10^3 \Delta \epsilon / nFA\nu)$ in equation 1. Such a dA/dE file would correspond only to the current due to the faradaic process, unlike that in CV where both faradaic and non-faradaic processes occur at the same time during a potential scan. Therefore by acquiring CV's and DCVA's simultaneously it was possible to subtract the faradaic response while the sample was in solution, leaving only the non-faradaic component of the total current. By comparing the background of electrolyte potential scan with this non-faradaic component, derived from the CV/DCVA subtraction technique, it was possible to determine effects of the electroactive species on the double layer capacitance.

Electrochemical roughening of the silver electrode surface followed a previously described procedure (3). It consisted of an oxidation reduction cycle (ORC) pretreatment with a double potential step waveform from -0.370 V to +0.680 V in 0.1 M Na_2SO_4 . The current passed in the oxidation step was digitally integrated using the computer and then the potential was returned to -0.370 V after ca. 25 mCoul/cm² of anodization charge had passed (\approx 5 sec). The cell was then rinsed and a degassed cytochrome c solution was injected into the cell with a glass syringe as described earlier in this section.

Silver sols were made according to the preparation reported by Suh et al. (191). A silver nitrate (MCB) solution (22 mL of 1.0 mM) was added dropwise to a stirring

sodium borohydride (Alfa Inorganic) solution (60 mL of 2.0 mM); both solutions were chilled to ice temperature. Such solutions produced a yellow colloid suspension which changed to blue upon addition of cytochrome c. The quantity of cytochrome c added was calculated so as to give an overall solution concentration of 10^{-7} M. SERRS measurements of this cytochrome c colloid solution were made in a spinning quartz cylindrical cell.

The electrochemical cell used for SERRS in this work has been described by Birke et al. (159). The electrode used for these experiments was a thick silver wire (2 mm in diameter) inserted into an insulating teflon rod which was then cut at a 45° angle. This teflon rod was inserted in the cell from the bottom. With this configuration the laser beam was focused on the silver electrode from the top of the cell with the scattered radiation being collected at a 90° angle to the incident radiation. Both the top and the side of the cell were made with an optically flat quartz window. The reference electrode was a Ag/AgCl (1.0 M KCl) electrode which was isolated from the cell by an agar gel saturated in 1.0 M Na₂SO₄ solution. This isolation prevented chloride from contaminating the silver electrode due to leakage from the Ag/AgCl reference electrode. The auxiliary electrode used was a platinum wire. The electrode polishing and roughening (ORC) procedures were carried out as previously described.

The excitation source used in both SERRS and RR experiments was a krypton ion laser (Spectra Physics model 171) equipped with an ultra-high-field magnet. The excitation wavelength used in all experiments was 413.1 nm to observe Soret enhancement. Scattered light was collected at 90° by a Canon f/1.2 50 mm lens and focused onto the slit of a 0.5 m spectrograph (Spex model 1870) equipped with an 1800 groove/mm grating. Glass filters (Corning or Schott) were used when necessary to attenuate scattered laser light. The detection system was an optical multichannel analyzer (Princeton Applied Research Corp. Model 1215/1216) with a Model 1224 silicon-intensified vidicon detector head in a cooled (-50 °C) housing. All samples were excited at low (< 5 milliwatts) laser power as measured by a power meter (Liconi Model 45 PM). The beam waist at the sample was 100 μm . All spectra were calibrated with the known frequencies of indene (192). The resolution was 2 cm^{-1} and band frequencies are accurate to $\pm 1 \text{ cm}^{-1}$ for strong isolated bands. No smoothing was performed on any of the spectra shown in this dissertation.

A. Interfering Faradaic and Non-Faradaic Reactions at Silver Electrodes.

Cyclic voltammetry (CV) has been one of the most powerful and widely used voltammetric techniques for obtaining thermodynamic, kinetic and mechanistic information attendant to an electron transfer reaction at an electrode (179). The shape of the current voltage curves obtained from CV experiments can be used as a diagnostic criterion for the electron transfer reaction of a species. The voltammogram of a simple heterogeneous electron transfer reaction, one with no complications such as adsorption or homogeneous reactions preceding or following the charge transfer process, will give rise to two voltammetric peaks or waves. One on the forward (cathodic) scan, which occurs at some potential $E_{p,c}$, and another on the reverse (anodic) scan, at some value $E_{p,a}$. The peak potential separation, ΔE_p , (where $\Delta E_p = E_{p,a} - E_{p,c}$) can be one of the most prominent features for classifying the mechanism of the reaction, as well as obtaining electrochemical and chemical parameters of the system. By measuring ΔE_p for a given sweep rate of the potential it is possible to calculate the rate constant, $k^{\circ}_{s,h}$, of the electron transfer reaction in terms of theoretical values of ΔE_p given by Nicholson (179). Large

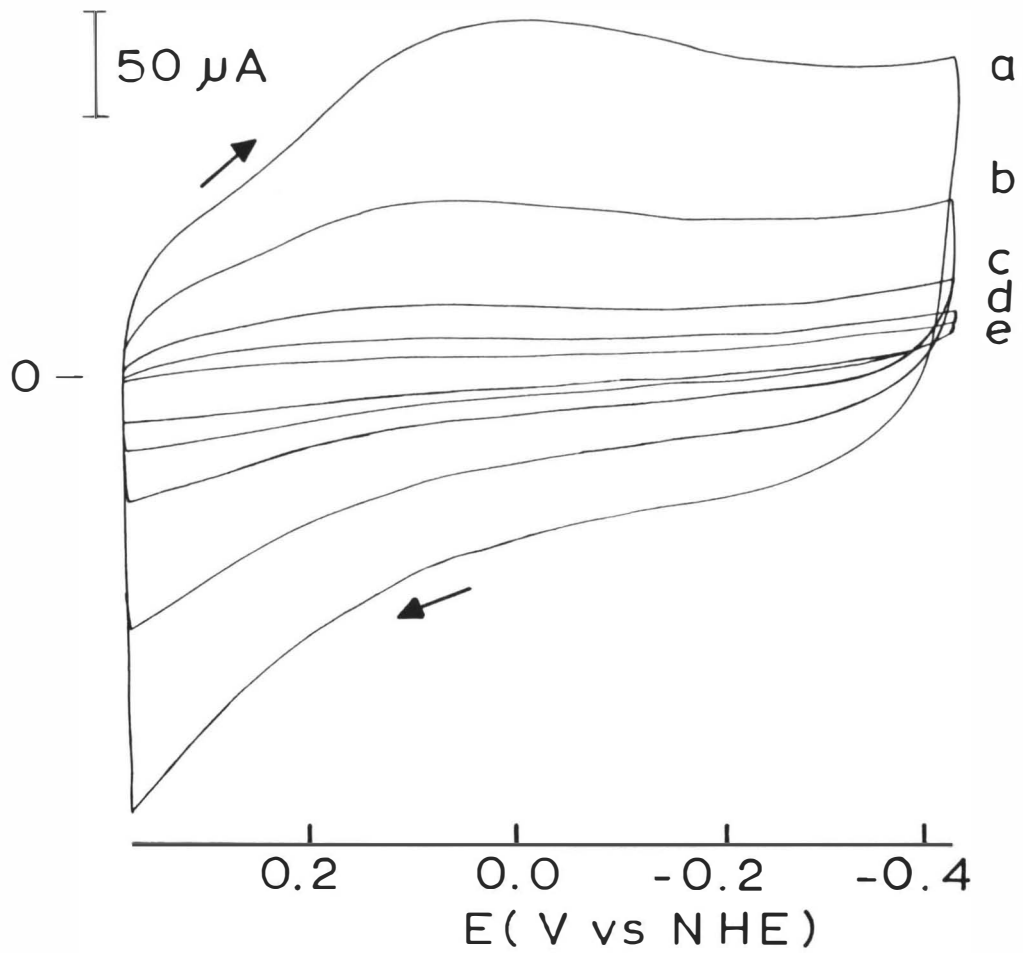
values of ΔE_p indicate a charge transfer process which is irreversible on the time scale of the experiment. In this case the charge transfer process is slow in comparison to the rate of diffusion of the species to the electrode, thus becoming the rate limiting step in the electrode reaction. The simplicity of varying the potential scan rate in CV's makes it possible to study the electrochemical system under different time scales in an experiment.

Therefore, the power of CV experiments is that almost any electrochemical rate constant can be obtained by simply varying the potential sweep rate of the cyclic voltammetric scan. Although it is theoretically possible to obtain a wide range of rate constants, experimentally it is not so straightforward. Certain experimental constraints can limit the ability to extract and interpret information from direct heterogeneous electron transfer reactions when using cyclic voltammetry. An experimental constraint related to the present investigation is the ability to discriminate between the faradaic current due to the electron transfer reaction of the species of interest and any other current responses observed during a cyclic scan of a CV. Complications arise when the difference between these voltammetric current responses are small. In such a case it is difficult to separate the purely faradaic current, due to a charge transfer process involving solution redox species, from that of the other components of the current. In the limiting

case of slow electron transfer kinetics there is greater difficulty in obtaining this separation since the faradaic component is only a small fraction of the total current. Therefore, before discussing the outcome of the present investigation it is appropriate to first consider the different current components obtained without the electroactive species present in solution. From these current voltage curves, inferences can be made as to whether it will be possible to observe the voltammetric response due exclusively to charge transfer of the electroactive species.

Figure 8 represents a typical set of cyclic voltammograms for a smooth silver electrode in a degassed 0.05 M Na_2SO_4 solution. The lower potential limit (+0.380 volts) was chosen to minimize the dissolution of silver which takes place at the more positive potentials. These oxidation-reduction cycles are typical background electrolyte scans for both smooth and roughened silver electrode surfaces. The current arising from such voltammograms is a result of two components. One is a faradaic component, which results from the partial oxidation and reduction of the silver electrode surface and possibly an oxide layer. The other is a non-faradaic component which results from the change of the electrostatic charge on the metal and the corresponding charge in the solution (i.e., ions and molecules at the electrode / solution interface). This last component is

Figure 8. Cyclic voltammetry of a smooth silver electrode in degassed 0.05 M Na₂SO₄ electrolyte. Electrode area = 1.23 cm². Potential scan rates in mV/s are as follows: (a) 100; (b) 50; (c) 20; (d) 10; (e) 5.



analogous to that of the charging current of a capacitor and is known as the double layer charging current. Such current is observed with or without an electroactive species present in solution. The detailed shape and the magnitude of the double layer charging current depends on numerous experimental variables, among them are: solvent, temperature, pH, electrolyte composition, adsorption, type of electrode used, electrode area and the scan rate of the potential excursion. Na_2SO_4 is the primary electrolyte in this investigation and was used to obtain the results in Figure 8, since it is the most commonly utilized electrolyte in SERRS spectroscopy experiments of cytochrome c at this metal surface (3,147,193).

The narrow range of positive potentials for this electrode severely restricts its use in electrooxidation reactions. This would certainly be the case when the formal potential, E°' , of the electroactive species lies close to that of the silver dissolution potential. In such case, the anodic current for the electroactive species on the positive (anodic) scan of a CV would be severely masked by the very large anodic current obtained from the silver electrode dissolution. This situation would be further aggravated when elevated rates of potential scan are initiated, since the current for the silver dissolution increases linearly with the scan rate while that of the electroactive diffusing species increases by the square-root of the scan rate. Another component of the current which increases linearly

with the scan rate is the non-faradaic capacity current (i.e., double layer charging current), which as previously mentioned results from the charging of the electrical double layer at the electrode/solution interface. The magnitude of this component will therefore be another major factor in the ability to discriminate the faradaic current for the species from that of the total current.

Hence in considering the current voltage curves at a silver electrode for a molecule such as cytochrome c, the faradaic current for the charge transfer process could be severely obscured by the additional current components in a cyclic voltammetric scan. It is important to note that the formal potential, E° , of cytochrome c is +0.260 volts (194). Therefore, the close association of this potential with the region of silver dissolution will limit how much information can be obtained from cyclic voltammetry. This is just one of the difficulties which had to be overcome in the early part of this investigation. Other problems such as the low concentrations of cytochrome c normally utilized in voltammetric experiments along with the slow kinetics observed in the past (1,2) at this electrode, made the faradaic current due to a charge transfer process by cytochrome c not clearly distinguishable from the background voltammetric responses.

In order to evaluate the kinetics of this system it is necessary to correct the experimentally obtained CV peak

current responses for the effects of these interfering faradaic and nonfaradaic processes. Usually these currents can be eliminated by acquiring CV's using only supporting electrolyte and subtracting this current from that obtained in the presence of cytochrome c. Under these conditions the shape of the current voltage curve will be due to only the faradaic charge transfer current of this protein. This experimental approach assumes that addition of cytochrome c to the electrolyte solution does not alter the current response that would be obtained in its absence. In cases where it does affect the background subtracted CV responses severe distortions such as broadening and lowering of the voltammetric peaks can occur. This last issue is of concern since such an impact makes it difficult to determine the exact peak potentials that will be used in the determination of kinetic parameters of the system.

The species selectivity and the freedom from interferences due to nonfaradaic and other faradaic reactions are widely recognized advantages of spectroelectrochemistry (195). A spectroelectrochemical technique known as derivative cyclic voltabsorptometry (DCVA) (127,128,133,181) provides response morphologies exactly identical to those of cyclic voltammetry and can be used in kinetic analysis of heterogeneous electron transfer reactions. The same methodology used in determining kinetic parameters from CV's (179,189) can be used in DCVA experiments. One of the main

advantages of the DCVA technique is that it is unnecessary to correct for the background contributions since the optical probe is insensitive to such processes. Therefore, the DCVA technique is more specific to the faradaic reaction of interest than its counter part CV. Another aspect of the DCVA technique is that the optical peak responses, $(dA/dE)_p$, increase by the inverse square root of scan rate, thus the responses become larger as the scan rate is decreased (181). This behavior is unlike that observed for CV responses for the diffusing electroactive species where the peak currents are directly proportional to the square root of the scan rate for reversible systems. For quasi-reversible and irreversible systems, DCVA has an important analytical advantage over CV. For such systems the advantage of trying to obtain larger current responses by using faster scan rates in CV experiments will not be realized.

B. Effects of Lyophilization on the Electron Transfer Kinetics of Cytochrome c

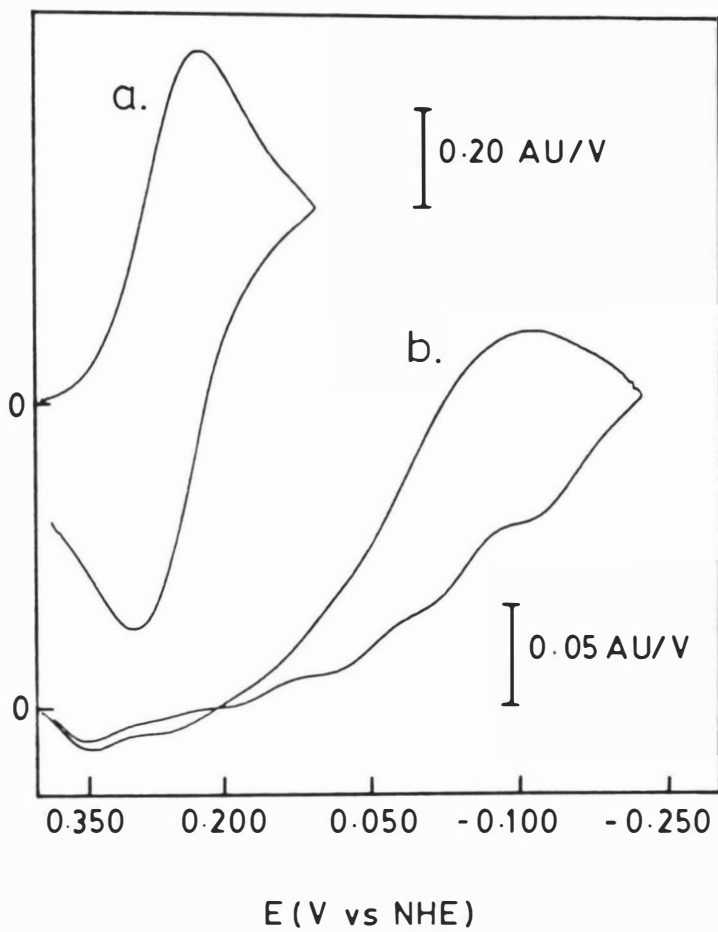
1. Evidence of a Contaminating Component After Lyophilization.

At the beginning of this investigation very little information had been obtained from direct heterogeneous electron transfer reactions of cytochrome c at bare metal electrodes (3,4,144-147). These electrode reactions were seen to proceed slowly and irreversibly with voltammetric currents not much different from that obtained from background

responses. An exception was noted in the case of gold where under certain experimental conditions (i.e., hydrogen flaming of the gold electrode) reversible voltammetric (CV) responses for cytochrome c were obtained (1). However, these responses were only transitory leading to more irreversible behavior with each succeeding cyclic scan of the potential. Therefore, facilitating stable and nearly reversible responses for cytochrome c at bare metal electrodes had not been successfully achieved until this study. Such conditions can be accomplished by using cytochrome c samples that have been chromatographically purified, but not lyophilized, prior to the voltammetric study (149). The following is a report of how lyophilization can effect the heterogeneous electron transfer reactions of cytochrome c at silver electrodes.

Figure 9 shows first scan DCVA responses at 1.04 mV/s for two differently prepared ferricytochrome c samples in 0.05 M Na₂SO₄ at a smooth polycrystalline silver electrode. The DCVA response for chromatographically purified samples, Figure 9a, is highly reproducible and profoundly different from the response obtained for samples that have been lyophilized after chromatographic purification, Figure 9b. The DCVA response shown in Figure 9a was reproducible for periods of time exceeding twelve hours, with $k^{\circ}_{s,h} = 1.5(\pm 0.4) \times 10^{-3}$ cm/s, a nearly reversible rate constant.

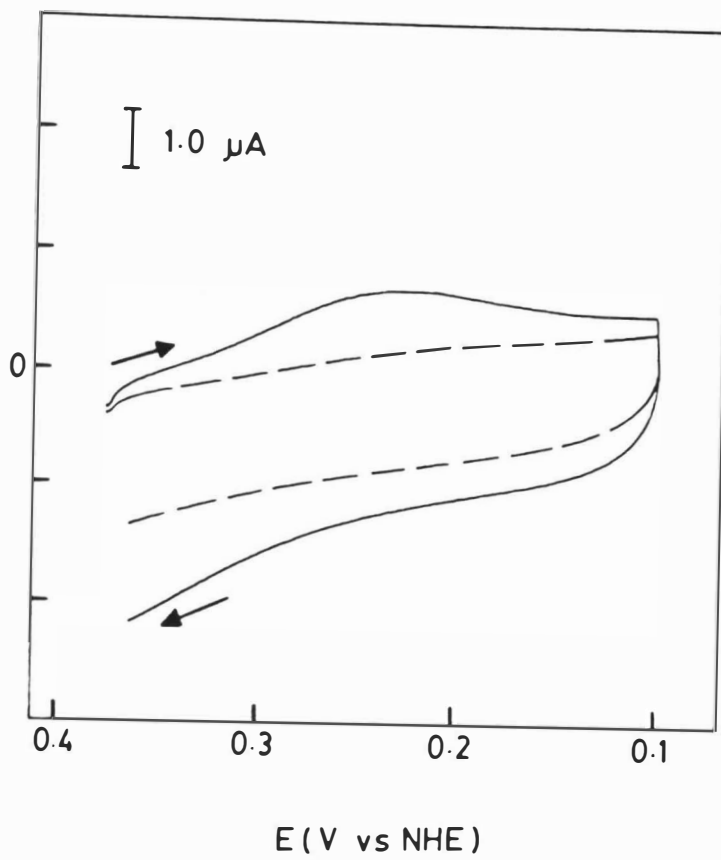
Figure 9. Derivative cyclic voltabsorptometry of cytochrome c at a smooth silver electrode in 0.05 M Na₂SO₄. (a): 199 μM chromatographically purified cytochrome c, (b): 98 μM chromatographically purified and then lyophilized cytochrome c sample. Electrode area = 1.23 cm². Potential scan rate for both: 1.04 mV/s, using 550 nm single wavelength monitoring.



However, the DCVA responses for the purified and then lyophilized sample, shown in Figure 9b, decayed with time leading to no observable response after ca. 30 minutes.

The results from this study clearly show that direct electron transfer between cytochrome c and silver electrodes can occur at facile (quasi-reversible) rates when samples are highly purified and never lyophilized. Irreversible electron transfer occurs with lyophilized samples, indicating fouling of the electrode surface by irreversible adsorption of a denatured form(s) of cytochrome c caused by the lyophilization process. This is consistent with a report (2) which stated that lyophilization of chromatographically purified ferricytochrome c gave a small amount of denatured material. New bands were evident about the native band when lyophilized samples were redissolved and subjected to ion exchange chromatography. Especially convincing evidence for the irreversible adsorption of a denatured form of cytochrome c on a smooth silver electrode is shown in Figure 10 with background CV's at 10.4 mV/s. Figure 10a shows the CV response obtained for a freshly cleaned silver electrode that had been cycled in deaerated electrolyte for ca. 30 minutes. Figure 10b indicates the CV response obtained for that exact same silver electrode and electrolyte system after performing 10 cyclic scans with a lyophilized sample of cytochrome c followed by thoroughly rinsing the cell and

Figure 10. Cyclic voltammetry of a smooth silver electrode in degassed 0.05 M Na₂SO₄ electrolyte. (a): Background cyclic scan of electrolyte before adding cytochrome c (solid line). (b): Background cyclic scan of electrolyte alone after adding 200 μM of purified/lyophilized cytochrome c, performing 10 scans, followed by rinsing cell and adding the degassed electrolyte (dashed line). Electrode area = 1.23 cm². Potential scan rate for both: 10.4 mV/s.

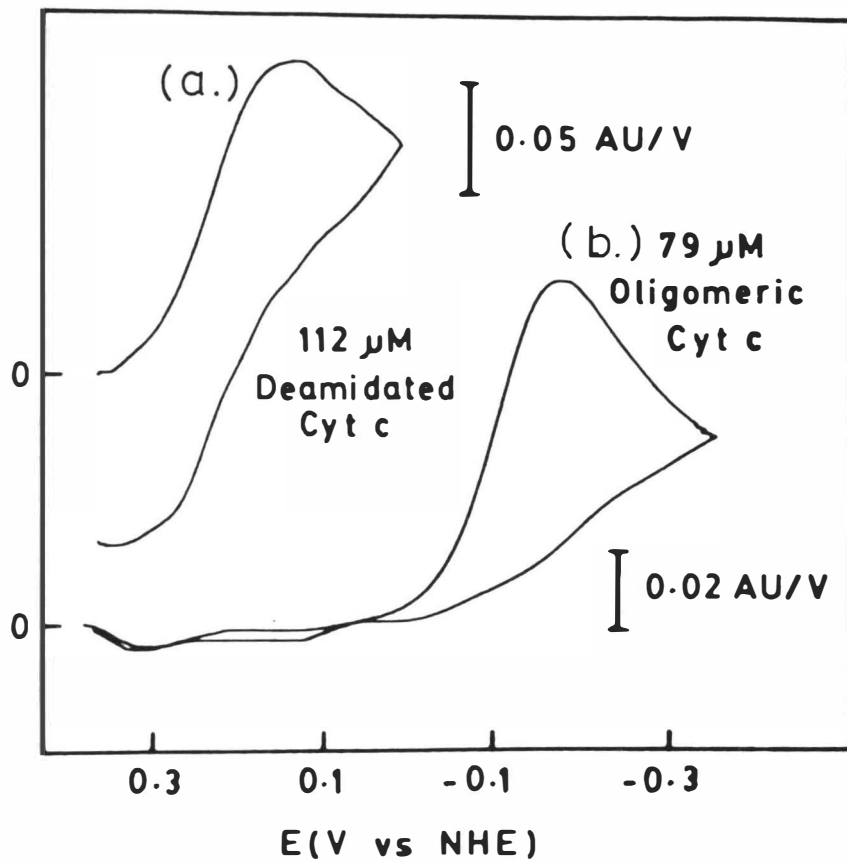


adding the same deaerated electrolyte. The dramatic reduction in the capacitive charging current after addition of the lyophilized cytochrome c, Figure 10b, suggests irreversible adsorption of a contaminating component generated by the lyophilization procedure on the electrode surface. This behavior is absent for cytochrome c samples that are studied immediately following chromatographic purification.

2. Identity of the Contaminating Component

The identity of the contaminating component, caused by the lyophilization step, is not known. However, ion exchange chromatography (169) of lyophilized samples that had been previously purified shows three bands (2) that are similar to bands observed in initial purification procedures. These bands have been ascribed to deamidated and oligomeric forms of cytochrome c (169). The deamidated forms have shorter retention times while oligomeric forms have very long retention times. Figure 11 shows that the oligomeric forms cause the decreased electron transfer rate for lyophilized cytochrome c samples. These DCVA's were obtained at 2.06 mV/s after polishing and cleaning the same smooth silver electrode used in Figure 9. The DCVA response obtained for the 112 μ M deamidated form of cytochrome c, Figure 11a, is quite similar to that obtained for the purified (native) form shown earlier in Figure 9a. The only difference between these two results is the slightly larger separation observed between forward and reverse peaks of the

Figure 11. Derivative cyclic voltabsorptometry of denatured forms of cytochrome c at a smooth silver electrode in 0.05 M Na_2SO_4 . (a): 112 μM deamidated cytochrome c, (b): 79 μM oligomeric cytochrome c. Electrode area = 1.23 cm^2 . Potential scan rate for both: 2.06 mV/s, using 550 nm single wavelength monitoring.



DCVA in the deamidated form of cytochrome c, Figure 11a. This larger separation is due to the slower kinetics of this system, $k^{\circ}_{s,h} = 2.8(\pm 0.6) \times 10^{-4}$ cm/s. However, it should be noted that the DCVA response presented in Figure 9a is the best situation obtained for the native form of cytochrome c at this electrode. Therefore, slightly slower kinetics resulting in larger peak separations in the deamidated case, Figure 11a, represents no distinction between the native and deamidated forms of cytochrome c.

Whereas the native and deamidated forms of cytochrome c give rise to rapid and near reversible responses at a clean smooth silver electrode, the response of the oligomeric form is highly irreversible and non-reproducible. Figure 11b illustrates the first scan DCVA response obtained for a 79 μ M oligomeric form of cytochrome c. With continuous voltammetric cycling over this potential range the cathodic peak obtained in this figure shifts to more negative potentials. This type of response is similar to that obtained earlier in Figure 9b for the lyophilized cytochrome c sample. A similar situation occurs when the oligomeric form is added to a solution of purified cytochrome c. In this case, the electron transfer kinetics rapidly decay giving similar responses to those of Figure 9b. On the other hand, upon addition of the deamidated form there is no observable effect on the electron transfer kinetics.

The preceding study indicates that the oligomeric form

of cytochrome c leads to slow heterogeneous electron transfer at metal electrodes. This form is very strongly adsorbed onto the electrode surface. Although the amount of this denatured material is quite small after the lyophilization process, less than 0.1% from chromatographic purification, it definitely has a drastic effect on the electron transfer rate. This was clearly illustrated in Figure 9 with the DCVA differences between the purified and lyophilized cytochrome c samples.

3. Mechanism for Decreased Electron Transfer After Lyophilization.

The slow irreversible kinetics observed for cytochrome c after lyophilization may now be explained by the previous information given about this system. One obvious interpretation is that the irreversible adsorption of the oligomeric form on the electrode surface might prevent the native cytochrome c molecules in solution from directly interacting with the electrode. The oligomeric form would block access to the electrode causing large electron transfer distances. The decreased rate of electron transfer can then be explained based on the Hopfield (196) equation which predicts that this rate varies exponentially with the separation distance. This requires a high surface coverage of the oligomeric form.

The surface coverage of adsorbed oligomeric cytochrome c could not be determined due to the high background cur-

rents observed for this electrode system. However, a maximum limit of 12% can be assumed based on SERRS adsorption isotherm measurements by Hildebrandt et al. (193) using commercial cytochrome c samples in silver hydrosols. Even though the amount of oligomeric form is greater in commercial than in lyophilized samples, surface coverage by the oligomeric form at the silver electrode should remain approximately the same in the concentration range used in Figure 9 (98 μM). This is due to specific adsorption sites which have been indicated, by measurements of Hildebrandt et al. (193), to be saturated at concentrations of commercial cytochrome c samples lower than 10 μM . Under such conditions, it can be estimated that the amount of oligomeric cytochrome c adsorbed on the electrode surface in lyophilized samples, Figure 9b, is also minimal (\approx 12% of the total surface area). Consequently, the low concentration of oligomeric form present on the electrode surface in the lyophilized samples would leave a large portion of the electrode surface free to react with native cytochrome c molecules in solution. Therefore, the model of surface blockage seems highly unlikely in explaining the electron transfer rates of the different sample preparations obtained in this work.

Another possible explanation for the decrease in kinetics after lyophilization could be related to the hydrophobic/hydrophilic character of the electrode/solution

interface upon adsorption of the oligomeric form. Chemisorbed water molecules at clean hydrophilic surfaces are expected to have preferential orientation in relation to the bulk water molecules (197). The interfacial water molecules are aligned so that the oxygen atom is directed towards the electrode surface. Hydrogen bonding within this first layer, as well as the first few layers of water molecules, creates an immobile interfacial zone of oxygen atoms at the electrode. Since cytochrome c's lysine residues are believed to hydrogen bond to the oxygen atom of the water molecules in the hydration layer (1), disruption of this layer by strong adsorption of the oligomeric form could limit the reversible binding interaction of cytochrome c towards the water molecules at the electrode/solution interface. However in order for this model to be operative it is necessary to consider if a surface coverage of 12% by the oligomeric form will disrupt this water layer (i.e., inner hydration layer). In other words, does such a low surface coverage make a large difference in the hydrophilic character of the electrode/solution interface in comparison to a clean silver surface? In order to answer this question, it is necessary to study the wettability of the electrode both with or without the oligomeric form present in order to further clarify the hydrophilic/hydrophobic properties of the silver interface.

A third possible reason for the decreased electron

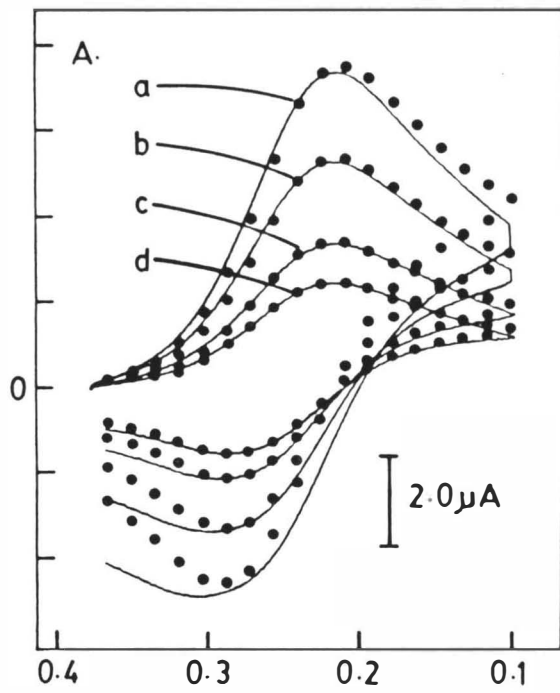
transfer in the presence of the oligomeric form can be attributed to an electrostatic effect. The oligomeric form has a very high positive charge, as evidenced by its slow chromatographic mobility in relation to the other forms of cytochrome c. Due to this high charge there will be an electrostatic repulsion interaction between adsorbed oligomeric and the positively charged cytochrome c molecules diffusing towards the electrode surface. Such repulsion will therefore limit the distance at which a diffusing cytochrome c molecule can approach the electrode surface, resulting in lower electron transfer kinetics.

C. Determination of Heterogeneous Electron Transfer Kinetic Parameters for Purified Cytochrome c.

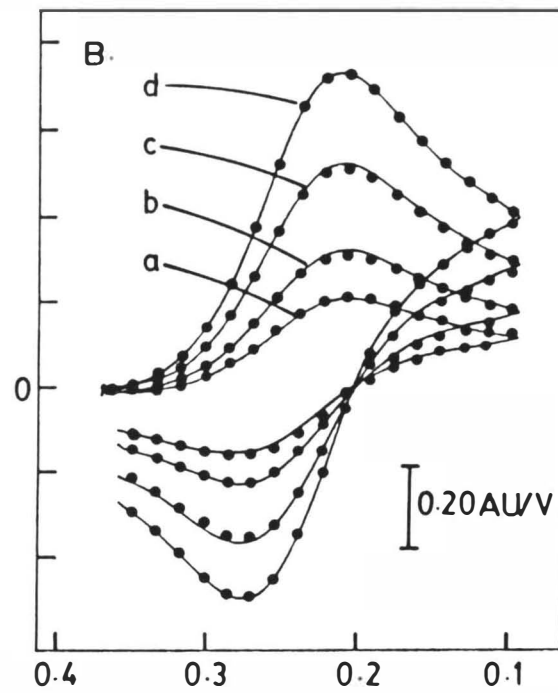
1. DCVA and Background Subtracted CV Responses of Purified Cytochrome c at Smooth Silver Electrodes.

Upon establishing conditions that provided reproducible electrochemical responses between bare silver electrodes and purified cytochrome c samples, heterogeneous electron transfer kinetic parameters, $k^{\circ}_{s,h}$ and α , were determined for this system. Figure 12 illustrates CV and DCVA responses obtained for a 199 μM cytochrome c sample using a smooth silver electrode in degassed 0.05 M Na_2SO_4 solution. These

- Figure 12. A. Background subtracted cyclic voltammetry of 199 μM purified cytochrome c in 0.05 M Na_2SO_4 at a smooth silver electrode. Electrode area = 1.23 cm^2 . Circles indicate simulated CV responses with $E^\circ' = 0.250$ volts, $n = 1.0$, diffusion coefficient (D_0) = $1.1 \times 10^{-6} \text{ cm}^2/\text{s}$, $k^\circ'_{s,h} = 1.5 \times 10^{-9} \text{ cm/s}$, $\alpha = 0.55$. Potential scan rates in mV/s are as follows: (a) 10.40; (b) 5.20; (c) 2.04; (d) 1.04.
- B. Derivative cyclic voltabsorptometry of purified cytochrome c. Same electrode and solution conditions as described in Figure 12A. Circles indicate simulated DCVA responses with difference molar absorptivity ($\Delta\epsilon$) at 550 nm = $21,100 \text{ M}^{-1}\text{cm}^{-1}$; other parameters same as given in Figure 12A.



E (V vs NHE)



E (V vs NHE)

results are for scan rates ranging from 1.04 to 10.4 mV/s and represent typical CV and DCVA responses for this system. Broadening of the background subtracted anodic CV peak current responses with faster scan rates, shown in Figure 12A, made it difficult to obtain electron transfer kinetics from these responses by the conventional method of using ΔE_p values. However, as shown in Figure 12B this broadening was not observed in DCVA responses. Therefore these derivative optical peak responses, $(dA/dE)_p$, were used to determine the kinetics of this system and then subsequently used to simulate both DCVA and CV responses.

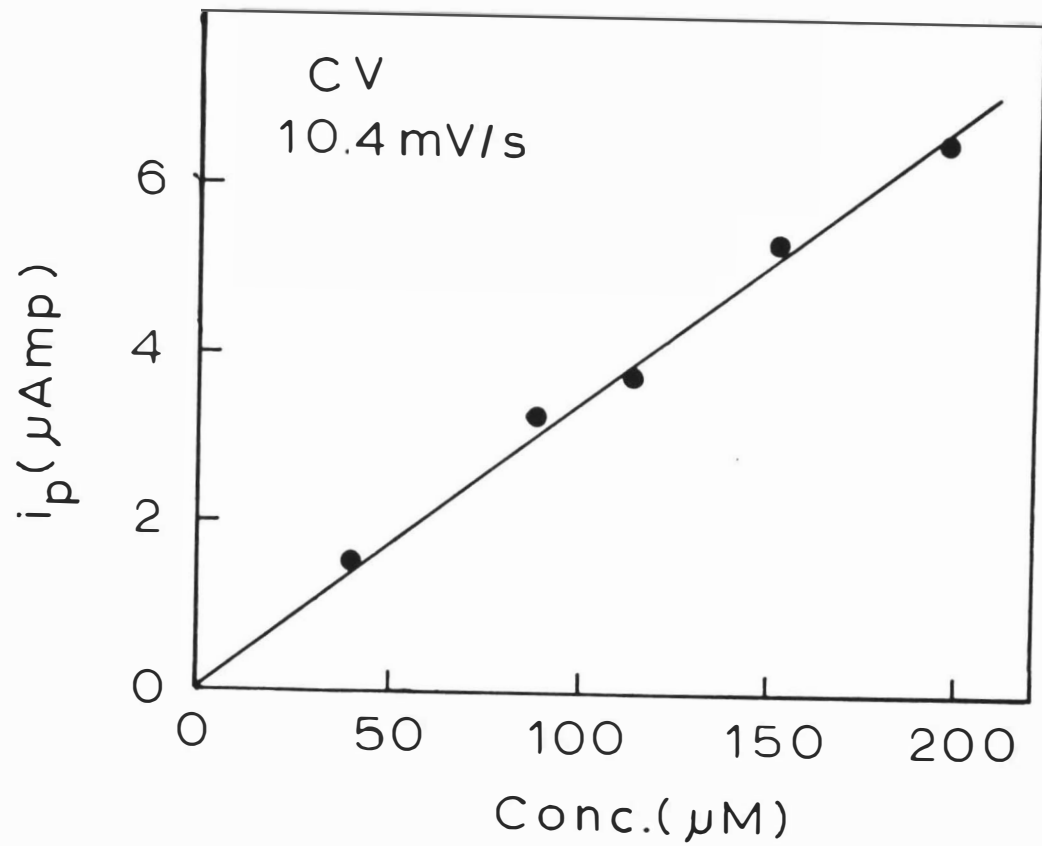
The circles in Figure 12 represent these simulated responses which are based on Butler-Volmer theory (130-132). They were obtained using a diffusion coefficient (D_O) of 1.1×10^{-6} cm²/s (188), an electrode area of 1.23 cm² and a mid-point potential value (E°') of +0.250 volts. This latter value was determined from the DCVA's using the formula $E^\circ' = (E_{p,a} + E_{p,c})/2$. The value of E°' obtained is in close agreement with the literature value of +0.260 volts (194), indicating a fairly symmetrical response for the DCVA's. The formal heterogeneous electron transfer rate constant ($k^\circ'_{s,h}$), determined from the scan rate dependence of the DCVA- ΔE_p responses in Figure 12B, was calculated to be $1.5(\pm 0.4) \times 10^{-3}$ cm/s from the method of Nicholson (179). The electrochemical transfer coefficient (α) was calculated to be 0.55(± 0.05) using the method of Matsuda and Ayabe

(189) from the forward potential scans of the DCVA responses. Therefore, the reaction of cytochrome c at this polycrystalline silver electrode is defined as quasi-reversible based on the criteria of Matsuda and Ayabe (189).

Theoretically the peak currents obtained in cyclic voltammetry under both a diffusion controlled or a kinetic controlled process, are directly proportional to concentration and the square root of scan rate. For quasi-reversible systems, however, this linear relationship only holds at relatively slow scan rates (< 200 mV/s). Unlike the processes mentioned above, adsorption currents are directly proportional to scan rate (along with the amount of adsorbed material). Therefore, an experimental plot of the peak current against these variables (square root of scan rate and concentration) will be of importance in defining the characteristics of the charge transfer process. In this investigation cathodic peak currents, shown in Figure 12A, increased linearly with the square root of scan rate in the range up to 10 mV/s. At higher scan rates however, a deviation in linearity was observed. This deviation was indicated by the lower current responses observed in relation to the simulated responses of this system. This lowering of the current at faster scan rates could possibly be due to kinetic effects. However, a more plausible reason for this deviation may be related to the inability to accurately subtract, from the cathodic peak currents, the large background

currents observed at this electrode (shown in Figure 8). Therefore, such behavior severely limits the ability to accurately assess the dependence of current on scan rate. However, by comparing the experimental and simulated peak current responses for the cathodic wave, the magnitude of the experimental response was always lower at scan rates higher than 10 mV/s. If substantial adsorption were present at the electrode, higher currents than in the simulated case would be expected, due to the direct dependence of the experimental response on scan rate. Since adsorption currents are generally more pronounced at larger scan rates, the lower experimental currents observed in these studies do not indicate adsorption of this protein in this potential range. Of equal importance is the dependence of this cathodic peak current on the concentration of cytochrome c. Figure 13 shows the background subtracted peak currents obtained for various concentrations of purified cytochrome c at 10.4 mV/s. The straight line in this diagram represents the simulated cathodic peak current responses obtained for the kinetic parameters given in Figure 12. The linear relationship between peak current and concentration is clearly evident. The diagnostic significance of these plots is that the reduction process appears to be totally controlled by diffusion of this protein to the electrode surface.

Figure 13. Plot of background subtracted cyclic voltammetry cathodic peak currents (i_p) versus concentration of purified cytochrome c at a smooth silver electrode. Scan rate was held constant at 10.4 mV/s as the concentration was increased. Solid line represents simulated responses using the parameters given in Figure 12A.



However, it must be noted that both adsorption and diffusion components of the current could be occurring simultaneously at this slow scan rate, with the adsorption process not being observed due to its small contribution.

The lack of agreement between experiments and simulated responses on the reverse anodic sweep in Figure 12A is probably due to errors caused by shifts in the silver oxidation process. The useful limit of voltammetry due to dissolution of silver from the electrode surface is approximately 50 mV more positive than the formal potential ($E^{\circ'}$) for cytochrome c. Therefore, small changes in the dissolution current with potential for the silver electrode in the presence of cytochrome c can cause errors in background subtracted CV's in the anodic region. Since the anodic dissolution of silver is a surface process, errors at anodic potentials are expected to be more pronounced at higher scan rates when cytochrome c is added. This effect is more evident in the CV's at the higher scan rates as shown in Figure 12A.

As illustrated in Figure 12B the DCVA's are not affected by the dissolution of the silver electrode surface, at least within this particular potential excursion. This is an important advantage of DCVA compared with CV (Figure 12A). No interference of the silver dissolution is evident in the DCVA's in Figure 12B, unlike the CV's obtained with this system (Figure 12A). However, with increasing applied positive potential ($> +0.380$ volts) it should be noted that

the dissolution becomes quite evident in the optical response and therefore restricts the anodic potential limit for this particular electrode. Again, the DCVA peak response increases as the scan rate is decreased, the opposite of that which is observed in CV (181). This linear dependence was observed for scan rates up to 50 mV/s under the conditions specified in Figure 12B. At higher scan rates it became more difficult to distinguish the DCVA peak responses from the noise of the system. This latter behavior is a consequence of the smaller diffusion layer (i.e., the concentration gradient of the electroactive species) developed at the electrode at higher scan rates and is compounded by the derivative required of the optical response in DCVA.

2. Reductive SPS/CA Responses of Purified Cytochrome c at Smooth Silver Electrodes.

The heterogeneous electron transfer kinetic parameters for the reaction of cytochrome c at silver electrodes have also been determined by single potential step chronoabsorptometry (SPS/CA) (182,183). This method is directly analogous to chronocoulometry (198) but again the advantage of species selectivity is provided by the optical probe. The SPS/CA technique is similar to DCVA experiments with the exception that the potential perturbations applied to the working electrode are of step fashion as opposed to being linearly scan in DCVA. SPS/CA methods for the determination

of heterogeneous electron transfer kinetic parameters have been reported for irreversible (182) and quasi-reversible (183) cases. From the analysis of the temporal dependence of the absorbance versus time response for each overpotential (η), where $\eta = (E_{\text{step}} - E^{\circ})$, it is possible to obtain kinetic results by using the method of Blount et al. (183) for a quasi-reversible system.

The SPS/CA technique can be understood by considering the following electrode reaction



where $k_{f,h}$ and $k_{b,h}$ are the forward and back heterogeneous electron transfer rate constants, respectively. The oxidized species in this equation is represented by Ox and the reduced form by Red. Using Butler-Volmer formulation (130-132), $k_{f,h}$ and $k_{b,h}$ can be related to the formal heterogeneous rate constant, $k^{\circ}'_{s,h}$, by the equations

$$k_{f,h} = k^{\circ}'_{s,h} \exp[-\alpha n F \eta / RT] \quad (3)$$

and

$$k_{b,h} = k^{\circ}'_{s,h} \exp[(1-\alpha)n F \eta / RT] \quad (4)$$

where η is the overpotential applied to the working electrode (E_{step}), and α is the electrochemical transfer coefficient

cient. Everything else is as usual. At the formal potential, $E^{\circ'}$, of the system $k_{f,h} = k_{b,h} = k^{\circ'}_{s,h}$. Both $k_{f,h}$ and $k_{b,h}$ vary with electrode potential, whereas $k^{\circ'}_{s,h}$ is potential independent and is the rate constant used to describe the electrode kinetics of the system.

As can be seen in equations 3 and 4, at large negative η -values (negative E_{step}) $k_{f,h}$ will increase and $k_{b,h}$ will decrease. In cases where the electrode kinetics of the reaction in equation 2 are irreversible (small $k^{\circ'}_{s,h}$), the flux of oxidized material arriving at the electrode under large negative η -values will be essentially independent of $k_{b,h}$. Under such conditions the back reaction of this electron transfer process can be neglected in the determination of the electron transfer kinetic parameters. The extraction of $k_{f,h}$ with η can be facilitated by using a single working curve that has been developed for the irreversible case (182). The relationship of the forward Butler-Volmer equation, equation 3, can then be used to determine the formal heterogeneous rate constant, $k^{\circ'}_{s,h}$, and the electrochemical transfer coefficient, α , of this system. However, in cases where the electrode reaction is quasi-reversible (moderate $k^{\circ'}_{s,h}$) the impact of $k_{b,h}$ on the evaluation of $k^{\circ'}_{s,h}$ and α from such a working curve is inaccurate. Working curves which consider the back reaction are available (183). A theoretical plot of such working curves is shown in Figure 14 for the normalized absorbance, A_N , versus $\log(k_{f,h}t^{1/2})$

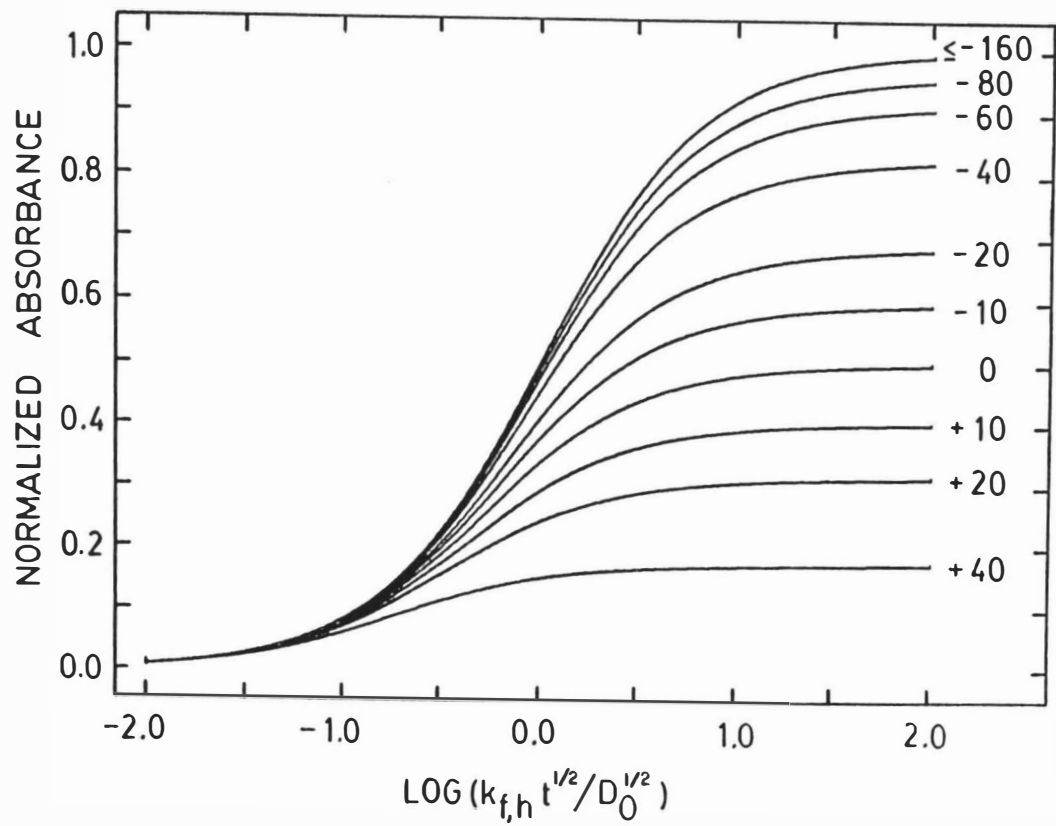
$/D_0^{1/2}$) using various η -values. These curves accurately describe systems which exhibit any degree of reversibility, unlike those for the irreversible case (182).

Using these working curves the optical responses which are kinetically controlled are normalized to the diffusion-controlled optical absorbance response. The diffusion-controlled optical response is obtained when the absorbance versus time dependence no longer increases as the potential is stepped to higher η -values. This absorbance response, ΔA , is given by the following equation (122)

$$\Delta A = \frac{2}{\pi^{1/2}} c^\circ \Delta \epsilon D_0^{1/2} t^{1/2} \quad (5)$$

where c° is the bulk molar concentration of the oxidized electroactive species and t is the time in seconds. Everything else is as previously defined. The value of $k_{f,h}$ is obtained for each experimental absorbance versus time transient by fitting the normalized absorbance versus $\log(t/D_0)^{1/2}$ response to the working curves shown in Figure 14. The value of $k_{f,h}$ is then calculated from the difference in abscissa \log values ($\log k_{f,h} = \log(k_{f,h} t^{1/2}/D_0^{1/2}) - \log(t/D_0)^{1/2}$). Kinetic parameters can then be obtained by plotting $\log k_{f,h}$ versus η following the rearranged form of equation 3

Figure 14. Normalized absorbance versus $\log [k_{f,h}(t/D_0)^{1/2}]$ working curves for SPS/CA experiments. Numerical values on the far right hand side of this figure correspond to the overpotential (η) expressed in mV. (Reprinted from Bancroft, E.E.; Blount, H.N.; Hawkrige, F.M., Anal. Chem., 1981, 53, 1862-1866; with permission from the American Chemical Society).

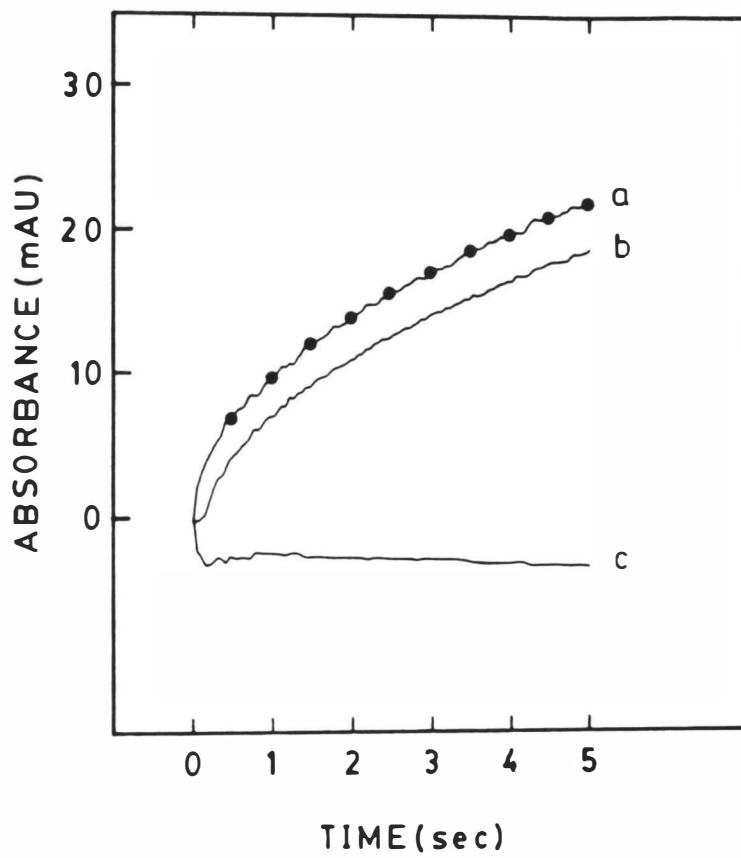


$$\log k_{f,h} = \log k^{\circ}_{s,h} - (2.303anF\eta/RT) \quad (6)$$

The slope of this plot will embody α and the intercept yields $k^{\circ}_{s,h}$. This is a more sensitive way of obtaining α than either the DCVA or CV techniques. The peak potential separations, ΔE_p , are almost totally invariant with respect to α ($0.3 < \alpha < 0.7$) in DCVA and CV for quasi-reversible and reversible systems.

Figure 15 shows the initial SPS/CA results obtained for a 199 μM purified cytochrome c sample at a smooth silver electrode in 0.05 M Na_2SO_4 electrolyte solution. The circles are the calculated diffusion controlled SPS/CA responses from equation 5. Equation 5 was multiplied by two to take into account the fact that the optical beam passes through the diffusion layer twice in normal reflectance experiments. Figure 15b indicates what should be a diffusion controlled SPS/CA response for this protein. However as this figure illustrates, the results for this step do not agree with the simulated response. Figure 15c shows the response for only the electrolyte and explains this lack of agreement. Changes in the reflectivity of the silver metal-electrolyte interface were shown to occur when potential step perturbations were applied to the electrode yielding an initial decrease in absorbance. These changes were most

Figure 15. Absorbance versus time response for a single potential step (SPS/CA) reduction of purified cytochrome c at a smooth silver electrode. Sample conditions and electrode are the same as those in Figure 12. Circles indicate a calculated diffusion controlled absorbance versus time response for a 199μ cytochrome c sample with $D_O = 1.1 \times 10^{-6}$, $n = 1.0$, and $\Delta\epsilon$ at 550 nm = $21,100 \text{ M}^{-1}\text{cm}^{-1}$. The initial potential, in volts, was stepped from +0.380 to -0.370. (a): represents a background subtracted cytochrome c response; (b): represents the cytochrome c response before background subtraction; (c): represents the response for the electrolyte alone.



dramatic as the potential step perturbation (η) increased. At potential steps, E_{step} , less positive than +0.150 volts this background reflectance change was not observed. McCreery *et al.* (199) have reported a similar effect when using an external reflection geometry at a platinum fiber electrode. This effect has been attributed to changes in electroreflectance (200,201) in combination with the reduction of a surface oxide film when the electrode is stepped to more negative potentials. Therefore, background corrected SPS/CA results were obtained by taking the difference between SPS/CA results acquired for the cytochrome c solution, Figure 15b, and the electrolyte alone, Figure 15c. The usefulness of this subtraction technique is clearly demonstrated by the close agreement between the background subtracted file, Figure 15a, and the simulated response. Therefore this subtraction technique was applied to all the SPS/CA results presented in this work. Such background corrected files were then used to determine heterogeneous electron transfer kinetic parameters.

Figure 16 shows a series of SPS/CA results obtained on the same cytochrome c sample and electrode used to obtain the CV and DCVA results shown in Figure 12. Figure 17 shows the dependence of the experimentally determined $\log k_{f,h}$ values on their corresponding overpotentials, η . As can be seen in Figure 17, a linear relationship is obtained with a

Figure 16. Background subtracted single potential step chronoabsorptometry (SPS/CA) responses, for the reduction of purified cytochrome c at a smooth silver electrode. Sample conditions and electrode are the same as those in Figure 12. Circles indicate simulated responses with $D_O = 1.1 \times 10^{-6}$, $n = 1.0$, $\Delta\epsilon$ at 550 nm = 21,100 M⁻¹ cm⁻¹, $k_{s,h}' = 9.1 \times 10^{-4}$ cm/s, and $\alpha = 0.52$. The initial potential before each step was +380 mV. Step potentials in mV are as follows: (a)-370; (b) +155; (c) +181; (d) +215; (e) +240; (f) +260.

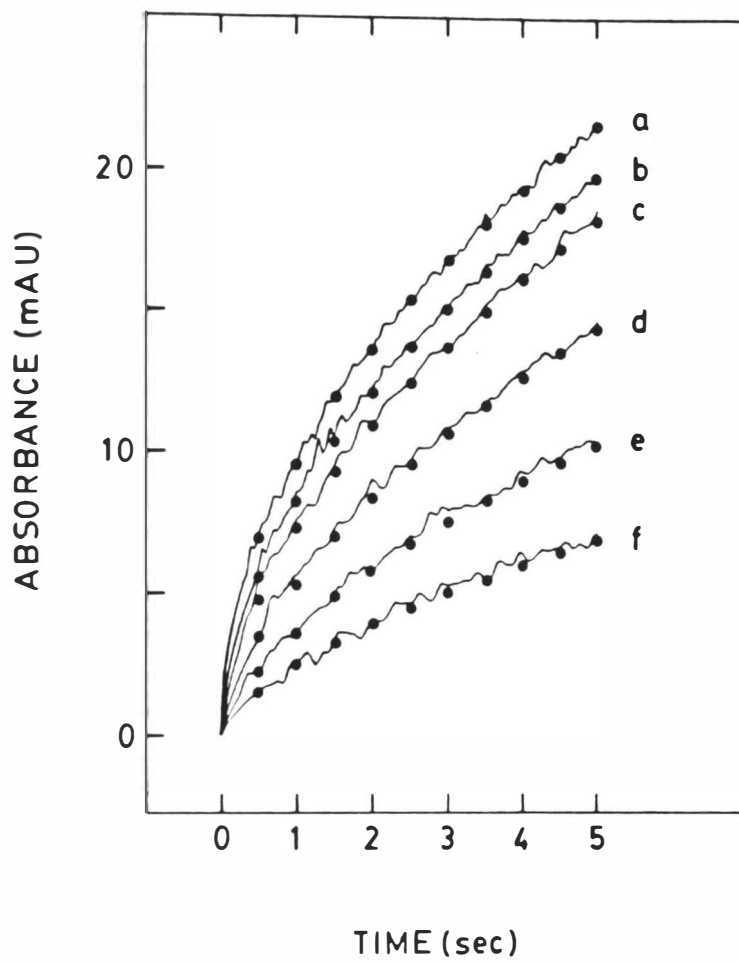
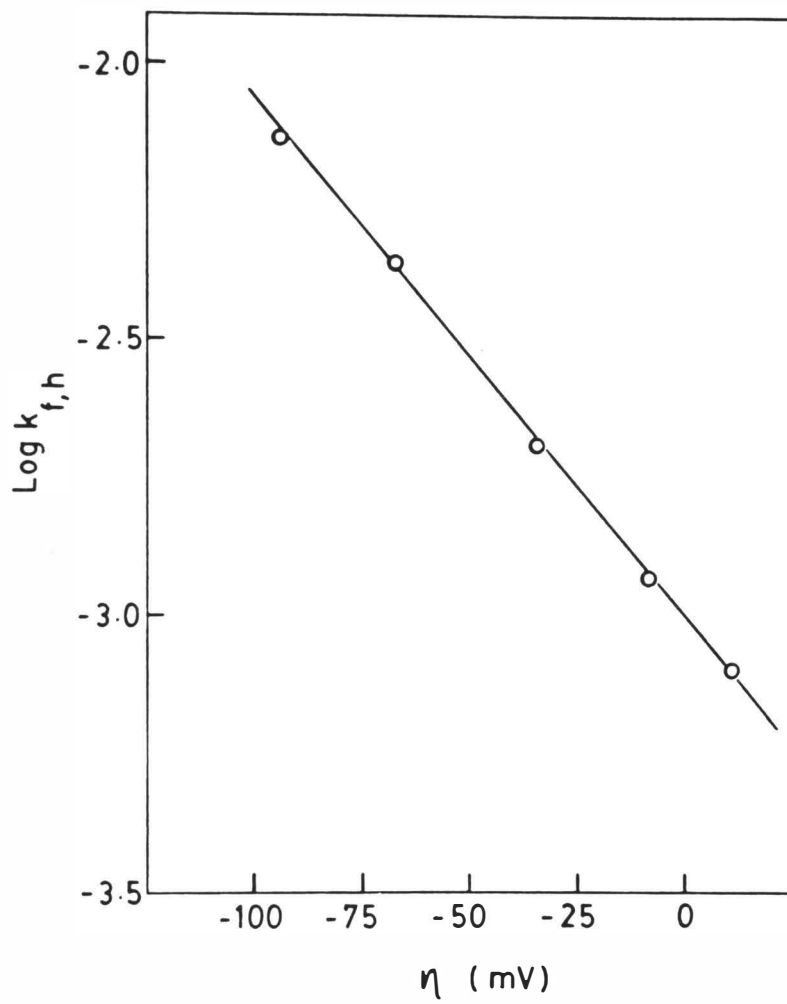


Figure 17. Dependence of $\log k_{f,h}$ on overpotential (η) for SPS/CA experiments shown in Figure 16. Circles represent $\log k_{f,h}$ values evaluated from the working curves in Figure 14. $E^{\circ} = 250$ mV, $n = 1.0$, $D_O = 1.1 \times 10^{-6}$ cm²/s, $\Delta\epsilon$ at 550 nm = 21,100 M⁻¹cm⁻¹. Corresponding overpotentials and $\log k_{f,h}$ values are as follows: $\eta = -95$ mV, $\log k_{f,h} = -2.14(\pm 0.07)$; $\eta = -69$ mV, $\log k_{f,h} = -2.36(\pm 0.06)$; $\eta = -35$ mV, $\log k_{f,h} = -2.69(\pm 0.05)$; $\eta = -10$ mV, $\log k_{f,h} = -2.94(\pm 0.03)$; $\eta = +10$ mV, $\log k_{f,h} = -3.09(\pm 0.04)$. From these values equation 6 was used to calculate $k^{\circ}_{s,h} = 9.1(\pm 0.4) \times 10^{-4}$ cm/s and $\alpha = 0.52(\pm 0.02)$.



formal heterogeneous electron transfer rate constant determined at $\eta = 0$ (+0.250 volts) of $k^{\circ}_{s,h} = 9.1(\pm 0.4) \times 10^{-4}$ cm/s. The transfer coefficient, α , from the slope of this plot was calculated to be $0.52(\pm 0.02)$. These values were then used to simulate the SPS/CA responses shown in Figure 16 (circles) and the agreement with experimental responses is good.

Table I summarizes the heterogeneous electron transfer kinetic parameters determined for the reaction of different purified cytochrome c samples at freshly polished silver electrode surfaces. All of the kinetic parameters reported for the various concentrations of cytochrome c in both Na_2SO_4 electrolyte and Tris/cacodylic acid buffer conform to the criteria set forth by Matsuda and Ayabe (189) for quasi-reversible electron transfer systems. As indicated in Table I the agreement between DCVA and SPS/CA experiments is good. Reproducible results were obtained for more than twelve hours with very little difference in electron transfer kinetics between experiments. The differences in kinetic parameters that are evident in this table are probably due to the use of a newly polished silver electrode surface in each experiment and new sample solutions.

Table I. Heterogeneous electron transfer kinetic parameters for chromatographically purified cytochrome c at a smooth silver electrode.

Cytochrome <u>c</u> (μM)	$k^{\circ},_{S,h}$ (cm/sec)	α	Technique
199 ^a	$1.5(\pm 0.4)^{\text{c}} \times 10^{-3}$	$0.55(\pm 0.02)^{\text{c}}$	DCVA ^d
199 ^a	$9.1(\pm 0.4) \times 10^{-4}$	$0.52(\pm 0.02)$	SPS/CA ^e
91 ^a	$6.0(\pm 0.4) \times 10^{-4}$	$0.52(\pm 0.03)$	DCVA
91 ^a	$4.7(\pm 0.2) \times 10^{-4}$	$0.52(\pm 0.02)$	SPS/CA
181 ^b	$2.8(\pm 0.4) \times 10^{-4}$	$0.69(\pm 0.02)$	DCVA
181 ^b	$3.7(\pm 0.1) \times 10^{-4}$	$0.65(\pm 0.01)$	SPS/CA
98 ^b	$1.6(\pm 0.4) \times 10^{-3}$	$0.67(\pm 0.07)$	DCVA
98 ^b	$1.6(\pm 0.4) \times 10^{-3}$	$0.67(\pm 0.12)$	SPS/CA
51 ^b	$2.2(\pm 0.6) \times 10^{-3}$	$0.71(\pm 0.08)$	DCVA

(a) solutions prepared in 0.05 M Na_2SO_4 .

(b) solutions prepared in 0.05 M Tris/cacodylic acid buffer, pH = 7.0.

(c) Parentheses contain standard deviations based on 4-5 different scan rates or potential step values for the same sample.

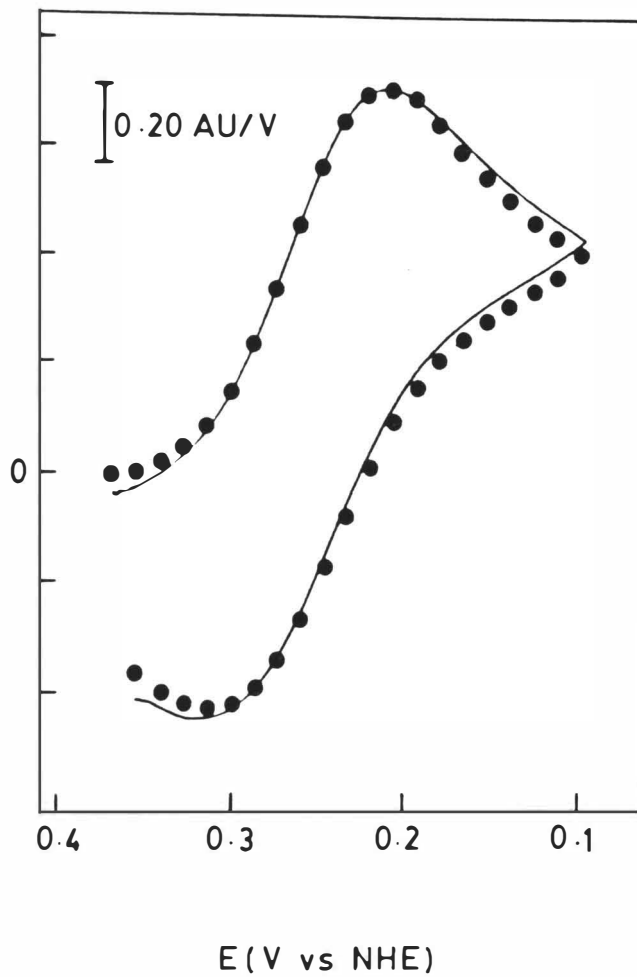
(d) Derivative cyclic voltabsorptometry.

(e) Single potential step chronoabsorptometry.

3. DCVA Response of Purified Cytochrome c at a Rough Silver Electrode.

The work presented to this point has dealt with smooth silver electrode surfaces. The original reason for using silver as an electrode is that it is one of the surfaces which can increase the Raman scattering cross section by some six orders of magnitude for molecules adsorbed on or near its surface (159). This technique, surface enhanced resonance Raman scattering (SERRS) spectroscopy, has been extensively used to study adsorbed cytochrome c (3,147,193, 202,203). In order to obtain such large enhancement effects, the silver surface must be roughened. DCVA was used in order to establish the effects of this roughening on heterogeneous electron transfer kinetic parameters. Figure 18 shows DCVA results obtained for a purified cytochrome c solution at a silver electrode roughened by a typical oxidation reduction cycle (ORC) pretreatment. A scan rate of 1.10 mV/s and a concentration of 284 μ M were used due to the low reflective properties of the roughened electrode surface. Although this surface is not very reflective good DCVA responses were still observed. A midpoint potential value of +0.262 volts was determined for this electrode reaction. The circles in this figure represent simulated responses with a $k^{\circ}_{s,h}$ of 1.8×10^{-4} cm/s and an α of 0.65. As can be seen in this figure, the experimental results are in close agreement with the simulated response. These

Figure 18. Derivative cyclic voltabsorptometry of 284 μM purified cytochrome c at a roughened silver electrode in 0.05M Tris/cacodylic acid buffer, pH = 7.0. Circles indicate simulated DCVA responses for 284 μM cytochrome c, $E^{\circ'} = 0.262$ volts, $n = 1.0$, $\Delta\epsilon$ at 550 nm = $21,100 \text{ M}^{-1}\text{cm}^{-1}$, $k^{\circ'}_{s,h} = 1.8 \times 10^{-4} \text{ cm/s}$, $\alpha = 0.65$. Scan rate = 1.10 mV/s .



results also indicate a quasi-reversible reaction based on the criteria of Matsuda and Ayabe (189). Therefore, the roughened silver surface provides a set of conditions necessary for facile electron transfer similar to that obtained for a smooth silver electrode surface. Following this study it has been possible to use SERRS to study direct electron transfer reactions of cytochrome c at silver electrodes.

D. Adsorption Effects of Purified Cytochrome c at a Smooth Silver Electrode.

Another advantage of the DCVA technique with regard to this study lies in the evaluation of the background contribution of the current after cytochrome c is added to solution (190,204). By simultaneously acquiring CV's and DCVA's of cytochrome c, a subtraction technique can be used to obtain a background response of the electrolyte solution in the presence of this protein. This can then be compared to the original background responses obtained for the electrolyte in the absence of cytochrome c. This technique can provide a convenient and qualitative method for determining the precise state of the electrode/solution interface and the impact of cytochrome c on it.

Equation 7 represents the total current, i_T , that can be obtained for a CV experiment.

$$i_T = i_F + i_{ADS} + i_{DL} \quad (7)$$

In this equation, i_F is the faradaic current due to the species of interest; i_{ADS} , is current due to adsorbed material; and i_{DL} , is current due to double layer charging (i.e., current due to the electrolyte alone). A relationship for the faradaic response, i_F , can be obtained from DCVA experiments by rearranging equation 1 in the experimental section to give the following:

$$i_F = \frac{2nFAv}{10^3 \Delta \epsilon} \cdot \frac{dA}{dE} \quad (8)$$

The (dA/dE) response can be converted into a purely faradaic current response, i_F , since the other parameters in this equation are constant during an experiment. Therefore, from the relationship of equations 7 and 8 the following equation can be derived:

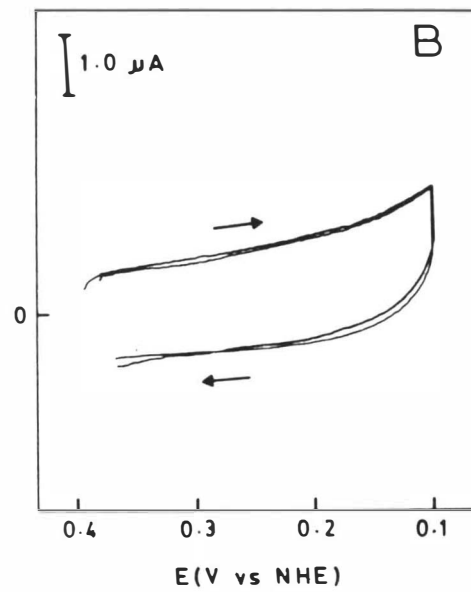
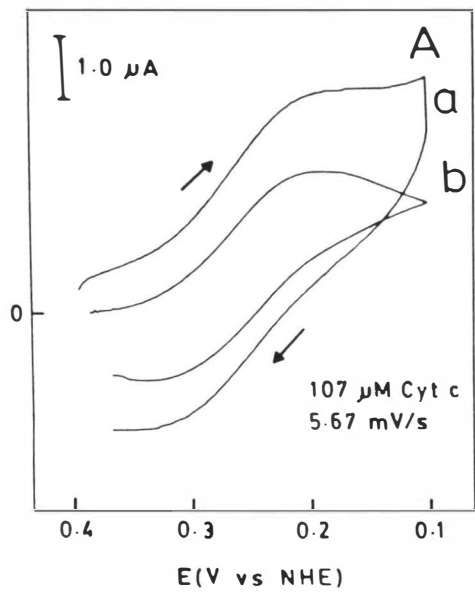
$$i_{ADS} + i_{DL} = i_T - \frac{2nFAv}{10^3 \Delta \epsilon} \cdot \frac{dA}{dE} \quad (9)$$

The double layer charging current, i_{DL} , can be determined when the DCVA response, dA/dE , is subtracted from the simultaneously acquired current, i_T , of a CV. In cases where there is weak or at least minimal adsorption, i_{ADS} will approach zero. In these cases the experimental i_{DL}

from equation 9 will equal the double layer charging current obtained in the absence of the electroactive species. If strong irreversible adsorption were to occur, alterations in the double layer structure at the electrode/solution interface would be observed by a lack of agreement between i_{DL} and the background current.

Figure 19 illustrates the application of this background subtracting technique for a 107 μM sample of purified cytochrome c at a smooth silver electrode using a scan rate of 5.67 mV/s. Figure 19A represents the DCVA response which has been converted to a current response using equation 8. This figure also illustrates a simultaneously acquired CV response which has not been corrected for background currents (double layer charging current). Figure 19B compares the original background current obtained in the absence of electroactive species to the current obtained when the two responses in Figure 19A are subtracted. In Figure 19B the agreement between the original and subtracted backgrounds clearly illustrates the small impact that purified cytochrome c has on the double layer at this electrode. The small difference observed on the anodic scan of this figure is most likely due to the silver dissolution problem discussed earlier in this chapter (Figure 12A). It can be concluded that adsorption of purified cytochrome c at a smooth silver electrode surface is minimal.

- Figure 19. A. Derivative cyclic voltabsorptometry and cyclic voltammetry of 107 μM purified cytochrome c at a smooth silver electrode in degassed Na_2SO_4 solution. Potential scan rate for both: 5.67 mV/s. $\Delta\epsilon$ at 550 nm = 21,100 $\text{M}^{-1}\text{cm}^{-1}$, electrode area = 1.23 cm^2 , $n = 1.0$. Using these parameters in equation 8, the DCVA was converted to a current response. (a): represents the CV without background subtraction; (b): represents the current converted DCVA.
- B. DCVA subtracted from CV in Figure 19A. Sample conditions and electrode are the same as Figure 19A. This corrected response is overlaid on the background response of electrolyte alone, Figure 19B.



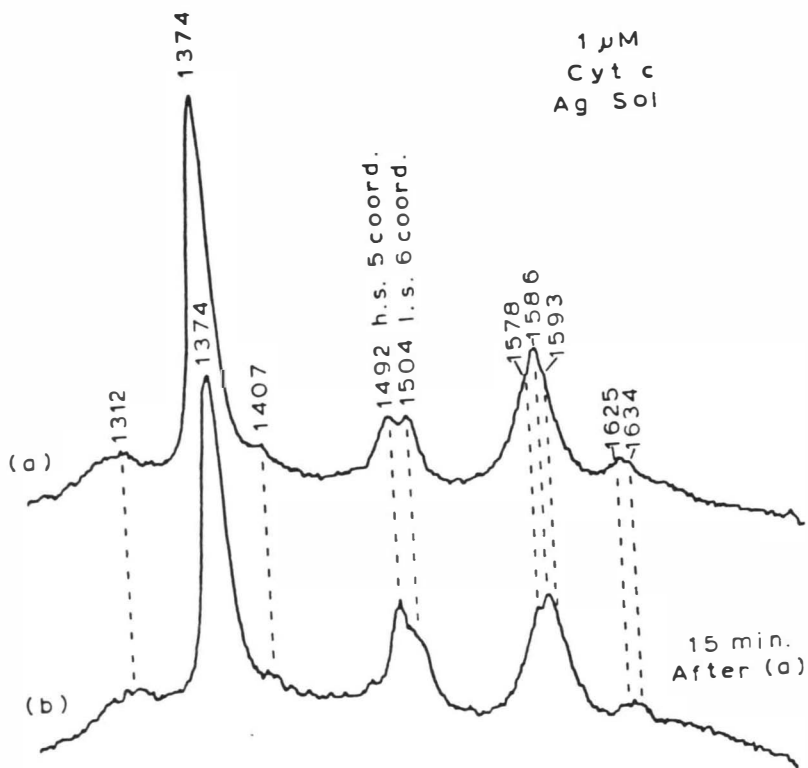
E. Surface Enhanced Resonance Raman Spectroscopy of Cytochrome c

1. Studies at Silver Sols Suspensions for Purified Cytochrome c.

This investigation next examined the conformations associated with the oxidation/reduction reaction of cytochrome c using SERRS spectroscopy. Information which complements the thermodynamic and kinetic descriptions previously determined for this protein using classical electrochemical techniques was sought. Surface enhanced resonance Raman scattering (SERRS) spectroscopy was used since it has been shown (3,147,193,202,203) to be a good tool for examining structural alterations of cytochrome c adsorbed on silver surfaces. The results described in this section are for purified cytochrome c samples and confirm the SERRS spectroscopy findings of previous studies (3,147,193,202, 203) with non-purified cytochrome c.

Figure 20 shows SERRS spectra of a 1 μM purified ferricytochrome c sample, in a silver sol solution, taken with 413.1 nm laser excitation. The spectrum in Figure 20a was taken within 2 minutes after addition of ferricytochrome c to the silver sol solution. This spectrum is similar to that previously reported by Smulevich and Spiro (203) for this protein with 406.7 nm laser excitation. Of particular interest in this figure is the band at 1492 cm^{-1} , assigned

Figure 20. SERRS spectra of purified 1 μM ferricytochrome c adsorbed on silver sol at 413.1 nm excitation wavelength. (a): Initial spectrum, taken 2 minutes after addition of cytochrome c to silver sol. (b): Spectrum taken 15 minutes after initial spectrum.



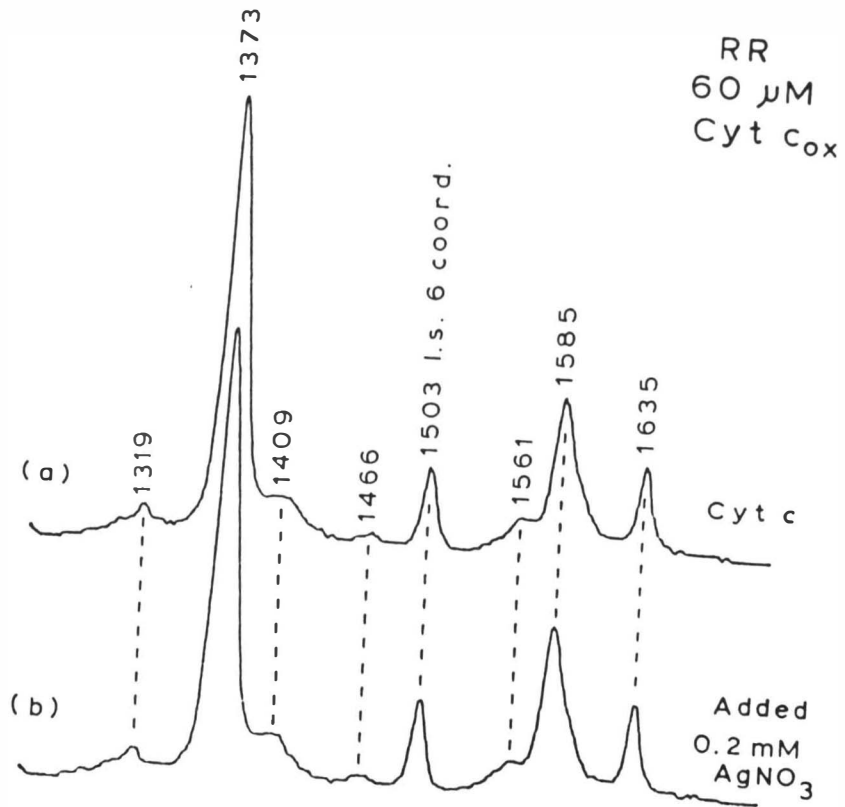
to the porphyrin skeletal mode ν_3 . The frequency at which this band appears is characteristic of high-spin penta-coordinate ferriheme complexes (154,157). Native cytochrome c on the other hand is a low-spin hexa-coordinate heme protein in both the oxidized and reduced states. The resonance Raman (RR) spectrum of the native ferricytochrome c, Figure 6b in Chapter I, shows a band at 1503 cm^{-1} also assigned to the ν_3 porphyrin skeletal mode. This frequency, characteristic of a low spin hexa-coordinate ferriheme complex, is present in the SERRS spectra of Figure 20a. Therefore the SERRS spectrum in Figure 20a indicate multiple forms of cytochrome c upon addition to the silver sol solution.

According to Smulevich and Spiro (203) the high-spin ferriheme signal at 1492 cm^{-1} is due to surface-bonded μ -oxo bridged iron porphyrin dimers, formed when the thioether links in cytochrome c are hydrolyzed by the Ag^+ ions coating the silver sol. This disruption of cytochrome c's heme-binding pocket is believed to cause the release of the heme groups, leading to the μ -oxo dimer formation on the silver surface. This analogy was based on observations by Paul (205) where under mild conditions silver salts promoted splitting of the thioether bond of cytochrome c, resulting in the liberation of the heme group from the protein part. However it must be noted that Paul's observations were carried out in an acid medium, pH 4, using an acid acetone

solution. Therefore a comparative study was necessary in order to determine if the interaction of the Ag^+ ions with this protein leads to the formation of the μ -oxo dimers. The results of such study are shown in the RR spectra of Figure 21, in which 0.2 mM AgNO_3 was added to a 60 μM ferricytochrome c solution. As can be seen in this figure the addition of Ag^+ ions did not have an effect on the cytochrome c solution, indicating that the high-spin ν_3 frequency at 1492 cm^{-1} is not a result of μ -oxo dimer formation. Therefore, from the preceding study the possibility must be considered that structural alterations of this protein upon absorption onto the silver surface must be due to effects other than just a chemical interaction. Electrostatic surface forces at the silver/solution interface, rather than chemical interaction, is now a more appropriate model to explain the drastic differences between solution RR and SERRS spectra of this protein (193).

The reproducibility of SERRS spectra at silver sols was very poor. An indication of this behavior is shown in Figure 20, where the same cytochrome c/sol mixture was monitored with time. Figure 20b shows the spectrum obtained 15 minutes after the initial spectrum in Figure 20a. The temporal dependence of the ν_3 band indicated that the native hexa-coordinate low spin form of cytochrome c (1504 cm^{-1} band) decreased in relation to the penta-coordinate high spin form (1492 cm^{-1} band). The higher intensity of the

Figure 21. Effect of Ag^+ ions on the resonance Raman spectra of $60 \mu\text{M}$ purified ferricytochrome c at 413.1 nm excitation wavelength. (a): Spectrum of cytochrome c alone. (b): Spectrum of cytochrome c upon addition of 0.2 mM AgNO_3 .



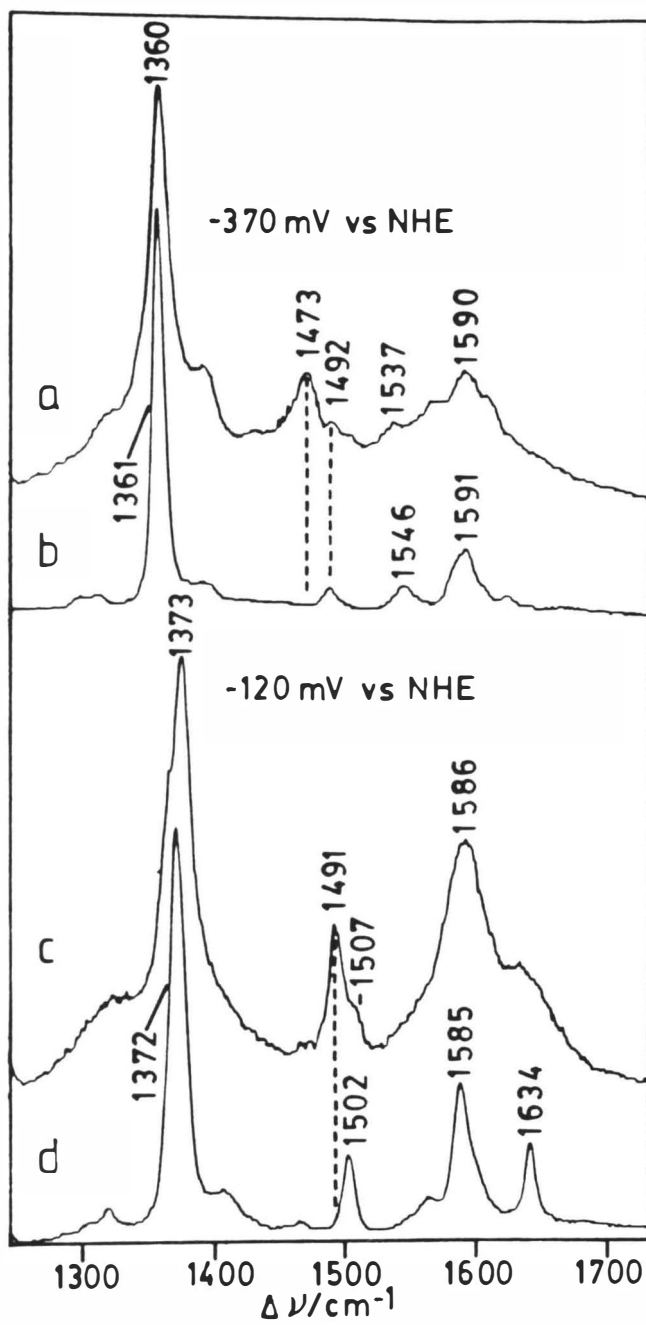
1492 cm^{-1} band possibly indicates the time course of protein denaturation observed at this metal surface. The increased intensity of additional bands at 1578 cm^{-1} (ν_2) and 1625 cm^{-1} (ν_{10}), characteristic frequencies of penta-coordinate high-spin ferriheme complexes (154,157), are also indicative of increased protein denaturation with time. The rapid decay of SERRS spectra with time, due to silver sol precipitation, along with the lack of reproducibility between experiments limited the usefulness of this approach for further application to this investigation.

2. Studies at Electrochemically Roughened Silver

Electrodes for Purified Cytochrome c.

Figure 22 presents SERRS results for purified cytochrome c at an electrochemically roughened silver surface. This figure shows SERRS spectra at applied potentials of -0.370 volts (Fig. 22a) and -0.120 volts (Fig. 22c) for 1 μM cytochrome c in 0.1 M Na_2SO_4 . The spectra in this figure are compared with resonance Raman (RR) spectra for 60 μM solutions of purified cytochrome c in the reduced (Figure 22b) and oxidized (Figure 22d) states. The 1373 cm^{-1} oxidation state marker band, ν_4 , in Figure 22c indicates that the adsorbed protein is mostly in the oxidized state at an applied potential of -0.120 volts. This is evident by comparison with the ν_4 band at 1372 cm^{-1} of the oxidized RR spectrum, Figure 22d. The ν_4 band of the adsorbed protein, Figure 22c, is shown to shift to 1360 cm^{-1} as the applied

Figure 22. Comparison of SERRS and resonance Raman spectra of purified cytochrome c in 0.1 M Na₂SO₄ at 413.1 nm excitation wavelength. Laser power: 2 mW at the silver electrode surface. (a): SERRS spectra at -0.370 volts adsorption potential. (b): RR spectra of 60 μM ferrocytochrome c. (c): SERRS spectra at -0.120 volts adsorption potential. (d): RR spectra of 60 μM ferricytochrome c.



potential is changed to -0.370 volts, Figure 22a. This frequency is indicative of a reduced form of the adsorbed protein at this potential by comparison with the ν_4 frequency at 1361 cm^{-1} of the reduced RR spectrum, Figure 22b. It is clear that the protein adsorbed on the roughened silver surface is undergoing oxidation and reduction as the potential of the working electrode is varied. Extensive denaturation is indicated for the adsorbed cytochrome c since it exists in the oxidized state at an applied potential of -0.120 volts, Figure 22c. This is concluded because the applied potential in Figure 22c is more than 0.350 volts negative of cytochrome c's formal potential in solution at pH 7 ($E^\circ = +0.260$ volts (194)). If adsorbed cytochrome c were in the native state it would have been reduced at the poised potential of -0.120 volts. Although highly purified cytochrome c samples were used in this study the results that are given with respect to potential in Figure 22 are the same as those obtained by Cotton et al. (3) using non-purified commercial cytochrome c samples.

Another observation in relation to the comparison between RR and SERRS spectra in Figure 22 is the spin state of the protein after adsorption. As was shown earlier in Figure 20, with silver sols suspensions of cytochrome c, the spin state marker band, ν_3 , is very sensitive to changes in protein alterations. This frequency is dependent on the oxidation state, spin-state, and coordination of the heme

iron (154,157). Such dependence of ν_3 is very useful in establishing disturbances of the native protein structure upon binding to the silver electrode surface. A comparison of the native RR spectra and SERRS spectra of Figure 22 indicates that both the reduced and oxidized forms of adsorbed cytochrome c are in the penta-coordinate high spin state. This is evident by the shift of ν_3 bands to lower frequency upon adsorption of this protein at the silver electrode surface. This band shifts from 1502 cm^{-1} for the oxidized RR spectra (Figure 22d) to 1491 cm^{-1} in the SERRS spectra (Figure 22c). A similar shift in this band is also seen in the reduced form of the adsorbed protein. In this case ν_3 shifts from 1492 cm^{-1} for the reduced RR spectra (Figure 22b) to 1473 cm^{-1} in the SERRS spectra (22a). The spin state conversion, from low spin in aqueous solution to high spin when adsorbed, would be consistent with the SERRS spectra taken at low temperature by Hildebrandt and Stockburger (193) using silver hydrosols. They observed a reversible thermal spin state dependency as the temperature was changed. At cryogenic temperature, -196°C , adsorbed cytochrome c was predominantly in the low spin state, while at room temperature it was partially populated by the high spin form. From such behavior it is suggested that the two conformational states of adsorbed cytochrome c existed in equilibrium on the silver surface.

Potentials less negative than those given in Figure 22,

will be necessary in order to effectively evaluate the conformational dynamics associated with the quasi-reversible electron transfer reactions of cytochrome c previously described by the voltammetric experiments in Figure 18. It is important to note that the experiments of both Figure 18 and Figure 22 were carried out at a roughened silver electrode using purified cytochrome c samples. Since the SERRS signal became very weak at potentials less negative than -0.070 volts, in order to carry out SERRS experiments at such positive potentials it was necessary to increase the concentration of purified cytochrome c. However, the weakening of the SERRS signal at positive potentials was not observed for commercial and oligomeric forms of cytochrome c, providing convincing evidence of the irreversible adsorption of the oligomeric form at this electrode.

The results of SERRS experiments for 6 μM purified cytochrome c at potentials ranging from -0.370 to +0.280 volts in 0.1 M Na_2SO_4 are shown in Figure 23. The same features that were observed in Figure 22 can be seen in this figure as well. Both the reduced (Figure 23a) and oxidized (Figure 23f) adsorbed cytochrome c molecules are shown to contain the same two conformational states observed in Figure 22. Despite the presence of these two conformational states, it was possible to obtain Nernst plots for this adsorbed protein, Figure 24. This figure illustrates the

Figure 23. Potential dependence of SERRS spectra for 6 μM purified cytochrome c in 0.1 M Na_2SO_4 at 413.1 nm excitation wavelength. Laser power: 2 mW at the silver electrode surface. Adsorption potentials in volts are as follows: (a) -0.370; (b) -0.270; (c) -0.170; (d) -0.070; (e) +0.030; (f) +0.280.

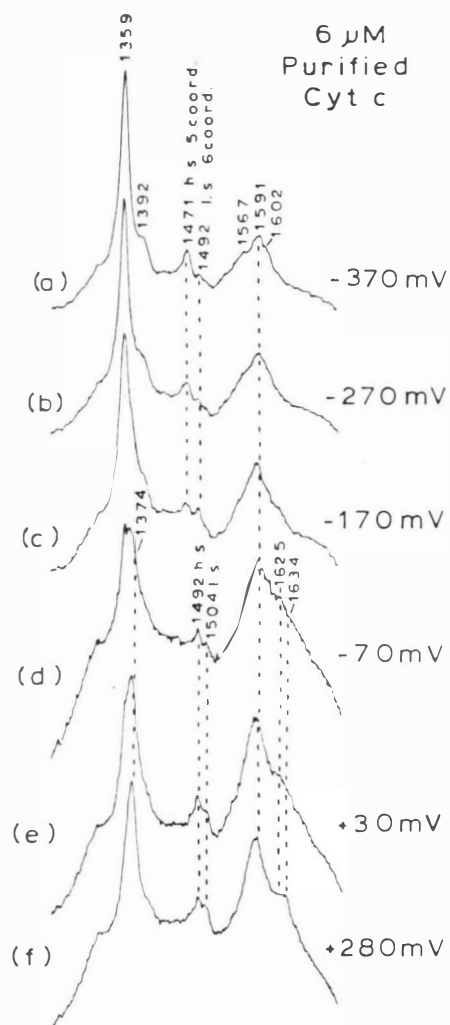
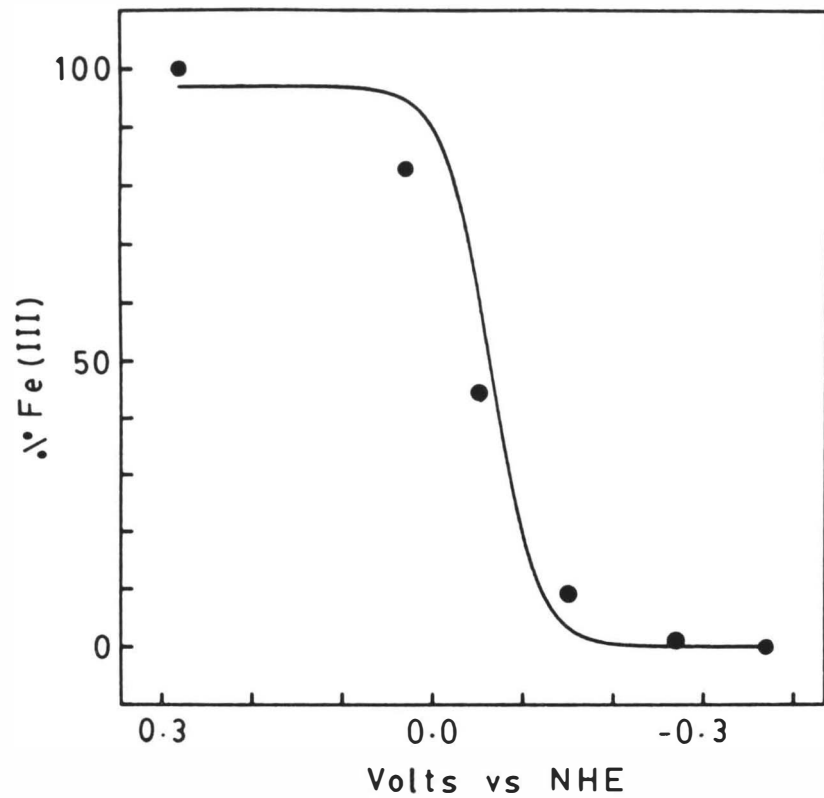


Figure 24. Fractional reduction of adsorbed cytochrome c as a function of electrode potential of SERRS spectra from Figure 23. Circles in this figure represent experimental responses calculated from ν_4 intensity ratios at 1359 cm^{-1} and 1374 cm^{-1} , solid line represents Nernstian response with $E^{\circ'} = -0.065$ volts.



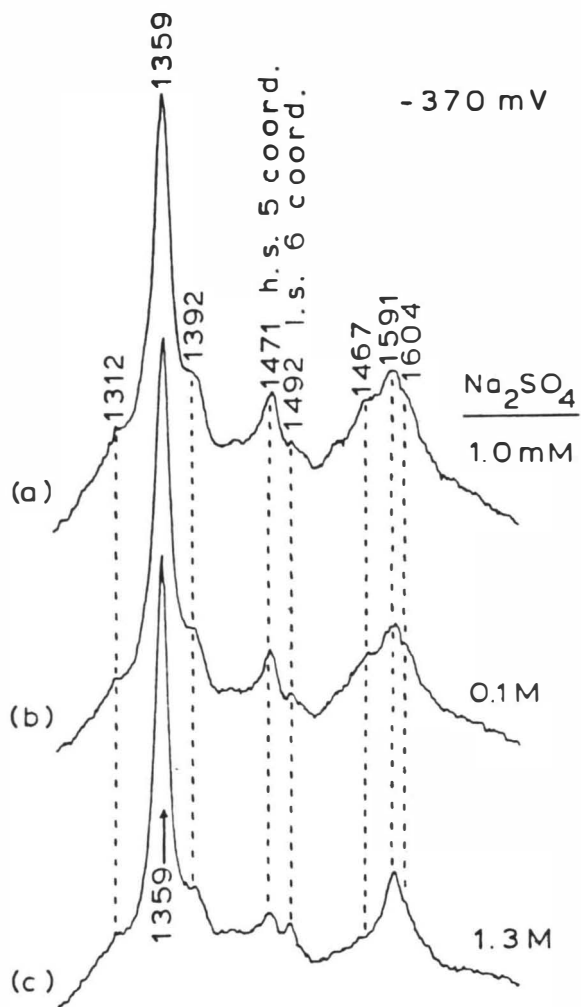
fractional reduction of surface species, as estimated from the SERRS intensity ratios of the ν_4 bands (1359 cm^{-1} and 1374 cm^{-1}) of Figure 23, as a function of electrode potential. The close agreement of the experimental (circles) and simulated (solid line) Nernstian response with $E^{\circ'} = -0.065$ volts indicates that the adsorbed protein is denatured. This Nernstian response can now be compared to the DCVA response of purified cytochrome c in Figure 18. From this comparison it can be concluded that a quasi-reversible electron transfer reaction is occurring for cytochrome c at a silver electrode in the presence of an irreversibly and strongly adsorbed layer of denatured cytochrome c. These observations are crucial since they are contrary to previous studies which have associated irreversible electron transfer kinetics with strong irreversible adsorption of this protein (133,206).

3. Effect of Electric Field on Spin State of Cytochrome c

Cytochrome c's structural change upon adsorption has been interpreted by Hildebrandt and Stockburger (193) in terms of electrostatic forces at the silver electrode/solution interface. These electrostatic forces occur due to charge differences between the electrode and electrolyte solution resulting in what is called the inner or compact double layer. The thickness of this layer can vary between ≈ 0 and 100 \AA depending on the charge and concentration of electrolyte solution, with more compact double layers resul-

ting at higher electrolyte concentrations. The intensity of electric fields across this double layer is relatively high (up to 10^6 volts/cm) and decays exponentially with distance from the electrode surface. Such electric fields were believed to be associated with the drastic conformational distortions observed for cytochrome c upon adsorption at silver surfaces (193). Since the electric field gradient in the double layer can be varied with electrolyte concentration, it should be possible to examine the interaction of cytochrome c with this layer. The interaction of cytochrome c with the electrostatic forces of the double layer is illustrated in the SERRS spectra of Figure 25. The Na_2SO_4 electrolyte concentration was varied from 1.0 mM to 1.3 M in order to alter the strength of the electric field developed at the double layer. The cytochrome c sample (1 μM), electrode and electrode potential (-0.370 volts) remained the same in order to limit possible errors between SERRS spectra in this experiment. By comparing the intensity of the spin state marker bands, shown at 1471 cm^{-1} and 1492 cm^{-1} in Figure 25, it is evident that the adsorbed cytochrome c is affected by the change in electrolyte concentration. The higher intensity of the 1471 cm^{-1} band in Figures 25a and 25b indicates that the SERRS spectra observed at low to moderate electrolyte concentrations are predominately that of a penta-coordinate high spin denatured form of cytochrome

Figure 25. SERRS spectra for 1 μM purified cytochrome c at a silver electrode as a function of electrolyte concentration. All spectra were obtained with the same electrode at the following conditions: 413.1 nm excitation wavelength, laser power 2 mW, and -0.370 volts electrode potential. Na_2SO_4 electrolyte concentrations are as follows: (a) 1.0 mM; (b) 0.1 M; (c) 1.3 M.

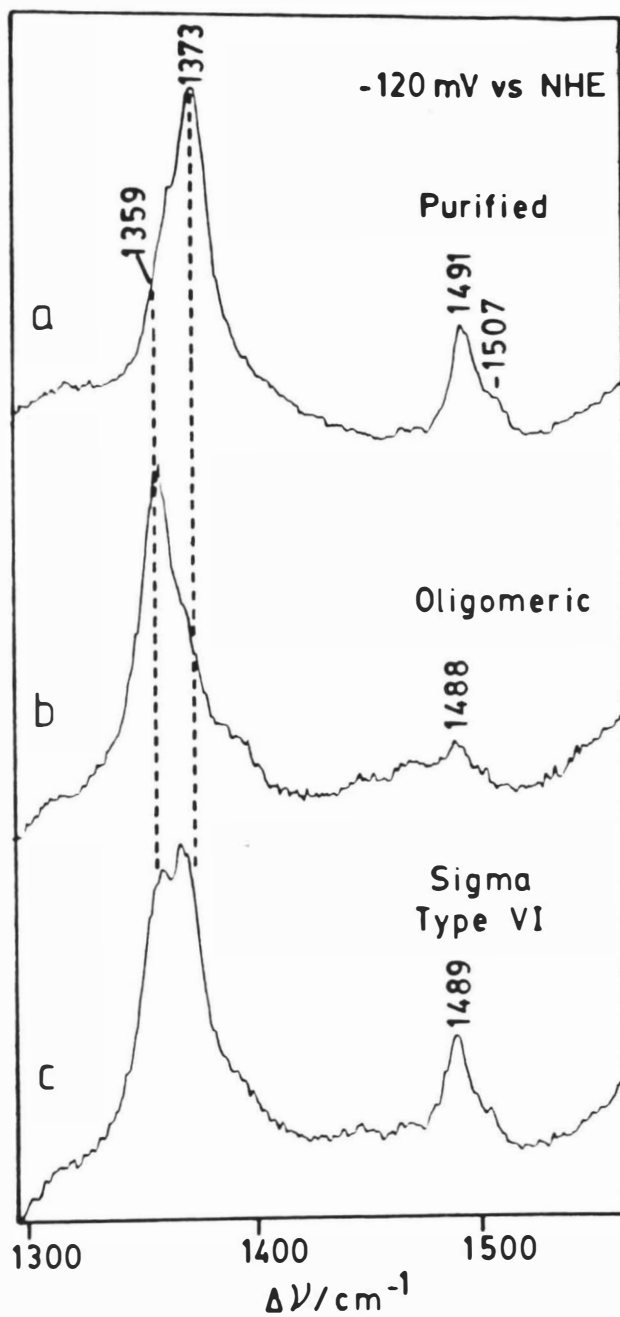


c. However at higher electrolyte concentrations, Figure 25c, the small difference in the intensities of the 1471 cm^{-1} and 1492 cm^{-1} bands indicates the presence of both native and denatured forms of cytochrome c. Therefore it can be concluded that the spin state of cytochrome c is clearly sensitive to the charge distribution within the electrical double layer. When high electrolyte concentrations are used, the effect of the double layer on the protein decreases. This is due to the increased compactness of the charge distribution within the double layer at such concentrations. However, at low to moderate electrolyte concentrations this charge distribution is more diffuse, affecting hydrogen bonds and electrostatic forces between amino acid residues holding cytochrome c together. The disruption of such intramolecular electrostatic forces can cause the protein to lose some of its native fold, thus destabilizing the closed heme crevice's conformation. This destabilization of the heme crevice may cause the protein to lose an axial ligand, most likely methionine 80, resulting in the penta-coordinate high spin signals obtained in SERRS spectra for cytochrome c.

4. Importance of Sample Purification on SERRS Experiments.

The preceding studies have dealt only with purified cytochrome c, however, in this section results of SERRS studies performed on purified and non-purified samples will be described. Such studies can establish the integrity of

Figure 26. Effects of sample purification on SERRS spectra of cytochrome c in 0.1 M Na₂SO₄ at a silver electrode, using 413.1 nm excitation wavelength and laser power of 2 mW. All spectra were obtained with an electrode potential of -0.120 volts. The samples used are as follows: (a) purified; (b): oligomeric; (c): commercial (as received).



the cytochrome c samples used. Figure 26 is a comparison of SERRS spectra for purified (native), oligomeric and commercial (non-purified) samples of cytochrome c obtained at an applied potential of -0.120 volts. The 1373 cm^{-1} oxidation state marker band in Figure 26a indicates that the purified form is 90% oxidized. On the other hand, the oligomeric form is in the reduced state as evidenced by the 1359 cm^{-1} band in Figure 26b. In the commercial (non-purified) sample, Figure 26c, the bands at 1373 cm^{-1} and 1359 cm^{-1} are of the same magnitude indicating the presence of both native and oligomeric forms. It is imperative to note that the amount of oligomeric form present in commercial samples is \approx 1% or less. The strong intensity of the 1359 cm^{-1} band in Figure 26c, is therefore indicative of strong adsorption of the oligomeric form as compared to the native form (Figure 26a). The presence of the oligomeric form in non-purified cytochrome c samples should therefore be taken into account in previous SERRS studies (3,147,193, 202,203).

CHAPTER IV - SUMMARY AND CONCLUSIONS

This investigation has now established that stable quasi-reversible heterogeneous electron transfer can occur for cytochrome c at bare silver electrodes. The lack of facile responses previously observed at this electrode (3,147) has been attributed to the small amount of oligomeric form present in both commercial and purified/lyophilized cytochrome c samples. Oligomeric cytochrome c was shown to rapidly and irreversibly adsorb on the silver electrode surface preventing further electron transfer with the native cytochrome c in solution. These findings agree with later studies of cytochrome c (207) which show that quasi-reversible heterogeneous electron transfer at metal electrodes is not unique to bare silver electrodes. Indeed, stable quasi-reversible heterogeneous electron transfer of cytochrome c, using purified/non-lyophilized samples, has been observed at gold, platinum and mercury electrodes.

SERRS spectroscopic studies, conducted under the same experimental conditions as the voltammetric studies above, have indicated that the quasi-reversible heterogeneous electron transfer reactions of cytochrome c occur in the presence of an irreversibly adsorbed layer of protein. The adsorbed protein has been shown to be denatured based on the

more than 0.300 volt negative shift in the formal potential relative to native cytochrome c in solution. The spin state change, from low spin hexa-coordinate in solution to high spin penta-coordinate upon adsorption, is also indicative of a denatured form residing on the electrode surface. Such conformational changes are possibly due to the intense electric field gradient at the electrode/solution interface, causing disruption of the intramolecular forces which stabilize the native conformation of cytochrome c.

The intense electric field observed at the electrode/solution interface has been described by Hildebrandt and Stockburger (193) as being comparable strength to that observed at the mitochondrial membrane. Since the electric field strengths at the electrode and mitochondrial membrane are of the same magnitude, Hildebrandt and Stockburger (193) have concluded that the changes in cytochrome c's spin state, caused by the intense electric fields at the electrode, are analogous to changes occurring at the mitochondrial membrane. According to this interpretation, electron transfer reactions of cytochrome c at the mitochondrial membrane may be affected by changes in this protein's spin state. However, contrary to Hildebrandt and Stockburger's interpretation (193), the work presented in this dissertation indicates that the denatured (i.e., high spin) protein adsorbed at a silver electrode has no adverse effect on the electron transfer rate with native cytochrome c in solution.

Therefore this work has shown that the spin state and coordination changes observed for heme proteins upon adsorption (binding), may not have a critical effect on their electron transfer rate.

The detailed mechanism by which cytochrome c, as well as other heme proteins, can transfer electrons in vivo is still a matter of discussion. However, based on the results presented and the literature discussed in this dissertation it is now possible to examine several proposed mechanisms for electron transfer of heme proteins. The first few mechanisms are based on electrostatic/orientational interactions which were believed to be necessary in order to overcome the steric restrictions placed upon the heme group by the protein envelope. The last mechanism to be discussed is based on the results obtained in studies which have shown that size rather than orientation is the controlling factor in electron transfer reactions of heme proteins.

According to the mechanism proposed by Koppenol et al. (59,60), the interaction between the positive end of cytochrome c's dipole moment with the electric fields generated by its physiological redox partners, cytochrome bc₁ (reductase) and cytochrome aa₃ (oxidase), properly guides cytochrome c into an orientation suitable for electron transfer. After cytochrome c's solvent exposed heme edge is directed towards the reductase and oxidase complexes, the negatively charged carboxyl groups on these complexes can

interact by electrostatic attraction with the positive lysine residues surrounding cytochrome c's heme crevice. Such an orientational mechanism is thought to be necessary in order to increase the number of productive encounters of cytochrome c with its physiological redox partners.

Based on this mechanism of in vivo electron transfer, Albery et al. (120) have also proposed a similar mechanism for the electron transfer reactions of cytochrome c at electrode surfaces. In Albery's mechanism (120), the electrostatic interaction between an electrode and the ring of positive charged lysine residues surrounding the solvent exposed heme edge of cytochrome c, is the rate determining step. According to this model, functional groups on the electrode surface are necessary in order for the protein to achieve the proper orientation just prior to electron transfer. Another important feature in Albery's model (120) is the ability of these groups to bind transiently with cytochrome c. Such weak binding interactions were believed to be necessary in order for cytochrome c to readily dissociate from the electrode surface after the electron transfer step. This was thought to be necessary in order to describe a process which reflects the turnover rates observed in vivo for this protein (26-30).

More recent results question the importance of orientation effects in describing rates of electron transfer of heme proteins. According to Mathews (208), the variation of

cytochrome c's dipole moment upon derivatization of various lysine residues does not account for the large differences in reaction rates observed by Koppenol and Margoliash (60) for in vivo electron transfer reactions. In later studies (207) at indium oxide electrodes heterogeneous electron transfer reactions of several heme proteins of similar size (cytochrome c, cytochrome c₃, and cytochrome c₅₅₃) were compared. These studies found no differences among the electron transfer rates of the three cytochromes even though their dipole moments are not the same. Such results provide additional evidence that a particular orientation of the protein is not necessary in order for an electron transfer reaction to take place.

From the studies mentioned above it seems more likely that electron transfer rates are controlled by the protein's size rather than its orientation. This dependence is observed when electron transfer rates of cytochrome c and cytochrome c₅₅₃ were compared to the rates for myoglobin (207). In this study the electron transfer rate obtained for myoglobin was three orders of magnitude lower than that observed for the two cytochromes. The differences in electron transfer rates among heme proteins has been explained by a tunneling mechanism. This mechanism predicts that a 2-3 Å change in the distance from the heme group to the electrode surface will result in an order of magnitude change in electron transfer rate (209). Since the distance

from the heme group to the surface of the molecule is approximately 22Å in myoglobin, whereas in the cytochromes it is less than 15 Å, the three order of magnitude difference in electron transfer rates is in agreement the difference predicted by the tunneling mechanism.

In conclusion, the work presented in this dissertation has shown several aspects that need to be considered when modeling heterogeneous electron transfer reactions of heme proteins at electrode surfaces. First, the integrity of the sample must be established, particularly when using bare metal electrodes, since they have a tendency to be easily fouled by solution impurities. Second, electron transfer can occur in the presence of an irreversibly adsorbed layer of denatured protein on the electrode surface. This is contrary to the general belief that strong irreversible adsorption leads to slow, irreversible electron transfer. Third, electrostatic/orientational effects are not necessary since electron transfer rates are more dependent on size rather than charge. Therefore from the size dependence of electron transfer rates, a more current mechanism of electron transfer might be related to a tunneling effect.

REFERENCES

REFERENCES

1. Bowden, E. F.; Hawkridge, F. M.; Blount, H. N., J. Electroanal. Chem., 1984, 161, 355-376.
2. Koller, K. B.; Hawkridge, F. M., J. Am. Chem. Soc., 1985, 107, 7412-7417.
3. Cotton, T. M.; Schultz, S. G.; van Duyne, R. P., J. Am. Chem. Soc., 1980, 102, 7960-7962.
4. Hinnen, C.; Parsons, R.; Niki, K., J. Electroanal. Chem., 1983, 147, 329-337.
5. Fleischmann, M.; Hendra, P. J.; McQuillan, A. J., J. Chem. Phys. Lett., 1974, 26, 163-168.
6. Rich, P. R., Faraday Discuss. Chem. Soc., 1982, 74, 349-364.
7. Prince, R. G., Bioscience, 1985, 35, 22-26.
8. Rieske, J. S., Biochim. Biophys. Acta, 1976, 456, 195-247.
9. Bosshard, H. R.; Zürcher, M.; Schägger, H.; von Jagow, G., Biochem. Biophys. Res. Commun., 1979, 89, 250-258.
10. Erecińska, M.; Davis, J. S.; Wilson, D. F., J. Biol. Chem., 1980, 255, 9653-9658.
11. Azzi, A., Biochim. Biophys. Acta, 1980, 594, 231-252.
12. Malmström, B. G., Biochim. Biophys. Acta, 1979, 547, 281-303.
13. Martin, C. T.; Scholes, C. P.; Chan, S. I., J. Biol. Chem., 1985, 260, 2857-2861.
14. Reinhammer, R.; Malkin, R.; Jensen, P.; Karlsson, B.; Andreasson, L. -E.; Aasa, R.; Vangard, T.; Malmström, B. G., J. Biol. Chem., 1980, 255, 5000-5003.
15. Karlsson, B.; Aasa, R.; Vangard, T.; Malmström, B. G., FEBS Lett., 1981, 131, 186-188.
16. Powers, L.; Chance, B.; Ching, Y.; Angiolillo, P., Biophys. J., 1987, 51, 300a.
17. Cline, J.; Reinhammer, B.; Jensen, P.; Venters, R.; Hoffman, B., J. Biol. Chem., 1983, 258, 5124-5128.

18. Palmer, G.; Babcock, G. T.; Vickery, L. E., Proc. Natl. Acad. Sci. USA, 1976, 73, 2206-2210.
19. Powers, L.; Chance, B.; Ching, Y.; Angiolillo, P., Biochim. Biophys. Acta, 1981, 34, 465-498.
20. Blumberg, W. E.; Peisach, J. In "Cytochrome Oxidase", King, T.E., Ed.; Elsevier/North-Holland, Amsterdam, 1979; 153-159.
21. Einarsdottir, O.; Caughey, W.S., Biochem. Biophys. Res. Commun., 1984, 124, 836-842.
22. Einarsdottir, O.; Caughey, W. S., Biochem. Biophys. Res. Commun., 1985, 129, 840-847.
23. Hill, B. C.; Greenwood, C.; Nicholls, P., Biochim. Biophys. Acta, 1986, 853, 91-113.
24. Palmer, G., Pure Appl. Chem., 1987, 59, 749-758.
25. Marcus, R. A.; Sutin, N., Biochim. Biophys. Acta, 1985, 811, 265-322.
26. Gibson, Q.; Greenwood, C.; Wharton, D. C.; Palmer, G., J. Biol. Chem., 1965, 240, 888-894.
27. Veerman, E. C. I.; Wilms, J.; Casteleijin, G.; Van Gelder, B. F., Biochim. Biophys. Acta, 1980, 590, 117-127.
28. Wilms, J.; Veerman, E. C. I.; König, B. W.; Dekker, H. L.; Van Gelder, B. F., Biochim. Biophys. Acta, 1981, 635, 13-24.
29. Wilms, J.; Dekker, H. L.; Boelens, R.; Van Gelder, B. F., Biochim. Biophys. Acta, 1981, 637, 168-176.
30. Veerman, E. C. I.; van Leeuwen, J. W.; van Buuren, K. J. H.; Van Gelder, B. F., Biochim. Biophys. Acta, 1982, 680, 134-141.
31. Beinert, H.; Shaw, R. W.; Hansen, R. E., J. Biol. Chem., 1978, 253, 6637-6640.
32. Peterson, L. C.; Cox, R. P., Biochim. Biophys. Acta, 1980, 590, 128-137.
33. Antonini, G.; Brunori, M.; Colosimo, A.; Malatesta, F.; Sarti, P., J. Inor. Biochem., 1985, 23, 289-293.

34. Greenwood, C.; Wilson, M. T.; Brunori, M., Biochem. J., 1974, 137, 205-215.
35. Mitchell, P., Science, 1979, 206, 1148-1159.
36. Brown, L. R.; Wüthrich, K., Biochim. Biophys. Acta, 1977, 468, 398-410.
37. Roberts, H.; Hess, B., Biochim. Biophys. Acta, 1977, 462, 215-234.
38. Hochman, J.; Ferguson-Miller, S.; Schindler, M., Biochemistry, 1985, 24, 2509-2516.
39. Bosshard, H. R.; Zürcher, M.; Schagger, H.; von Jagow, G., Biochem. Biophys. Res. Commun., 1979, 89, 250-258.
40. Ferguson-Miller, S.; Brautigan, D. F.; Margoliash, E., J. Biol. Chem., 1976, 251, 1104-1115.
41. Paléus, S.; Neilands, J. B., Acta Chem. Scand., 1950, 4, 1024-1030.
42. Margoliash, E.; Smith, E. L.; Kreil, G.; Tuppy, H., Nature (London), 1961, 192, 1125-1127.
43. Takano, T.; Trus, B. L.; Mandel, N.; Mandel, G.; Kallai, O. B.; Swanson, R.; Dickerson, R. E., J. Biol. Chem., 1977, 252, 776-785.
44. Kendrew, J. C., Sci. Am., 1961, 205, 96-111.
45. Dickerson, R. E.; Takano, T.; Eisenberg, D.; Kallai, O. B.; Samson, L.; Margoliash, E., J. Biol. Chem., 1971, 246, 1511-1535.
46. Takano, T.; Dickerson, R. E., Proc. Natl. Acad. Sci. U.S.A., 1980, 77, 6371-6375.
47. Moore, G. R.; Williams, R. J. P., Eur. J. Biochem., 1980, 103, 533-541.
48. Stellwagen, E., Nature, 1978, 275, 73-74.
49. Wüthrich, K., Proc. Natl. Acad. Sci. U.S.A., 1969, 63, 1071-1078.
50. Keller, R. M.; Wüthrich, K., Biochim. Biophys. Acta, 1978, 533, 195-208.

51. Moore, G. R.; Huang, Z. X.; Eley, C. G. S.; Barker, H. A.; Williams, G.; Robinson, M. N.; Williams, R. J. P., Faraday Discuss. Chem. Soc., 1982, 74, 311-329.
52. Gupta, R. K.; Koenig, S.H., Biochem. Biophys. Res. Commun., 1971, 45, 1134-1143.
53. Margalit, R.; Schejter, A., Eur. J. Biochem., 1973, 32, 492-499.
54. Moore, G. R.; Harris, D. E.; Leitch, F. A.; Pettigrew, G. W., Biochim. Biophys. Acta, 1984, 764, 331-342.
55. Takano, T.; Dickerson, R. E., J. Mol. Biol., 1981, 153, 79-94.
56. Osheroff, N.; Borden, D.; Koppenol, W. H.; Margoliash, E., J. Biol. Chem., 1980, 255, 1689-1697.
57. Barlow, G. H.; Margoliash, E., J. Biol. Chem., 1966, 241, 1473-1477.
58. Rush, J. D.; Lan, J.; Koppenol, W. H., J. Am. Chem. Soc., 1987, 109, 2679-2682.
59. Koppenol, W. H.; Vroonland, C. A. J.; Braams, R., Biochim. Biophys. Acta, 1978, 503, 499-508.
60. Koppenol, W. H.; Margoliash, E., J. Biol. Chem., 1982, 257, 4426-4437.
61. Marcus, R. A.; Sutin, N., Inorg. Chem., 1974, 14, 213-216.
62. Wherland, S.; Gray, H. B., Proc. Natl. Acad. Sci. U.S.A., 1976, 73, 2950-2954.
63. Gupta, R. K.; Koenig, S. H.; Redfield, A. G., J. Magn. Reson., 1972, 7, 66-73.
64. Gupta, R. K., Biochim. Biophys. Acta, 1973, 292, 291-294.
65. Hodges, H. L.; Holwerda, R. A.; Gray H. B., J. Am. Chem. Soc., 1974, 96, 3132-3137.
66. McArdle, J. V.; Gray, H. B.; Creutz, C.; Sutin, N., J. Am. Chem. Soc., 1974, 96, 5737-5741.
67. Ewall, R. X.; Bennett, L. E., J. Am. Chem. Soc., 1974, 96, 940-942.

68. Ahmed, A. J.; Millet, F., J. Biol. Chem., 1981, 256, 1611-1615.
69. Butler, J.; Davies, D. M.; Sykes, A. G.; Koppenol, W. H.; Osheroff, N.; Margoliash, E., J. Am. Chem. Soc., 1981, 130, 469-471.
70. Butler, J.; Chapman, S. K.; Davies, D. M.; Sykes, A. G.; Speck, S. H.; Osheroff, N.; Margoliash, E., J. Biol. Chem., 1983, 258, 6400-6404.
71. Moore, G. R.; Eley, C. G. S.; Williams, G., Adv. Inorg. Bioinorg. Mech., 1984, 3, 1-96.
72. Smith, H. T.; Staudenmayer, N.; Millet, F. S., Biochem., 1977, 16, 4971-4974.
73. Ahmed, A. J.; Smith, H. T.; Smith, M. B.; Millet, F. S., Biochem., 1978, 17, 2479-2483.
74. Ferguson-Miller, S.; Brautigan, D. L.; Margoliash, E., J. Biol. Chem., 1978, 253, 149-159.
75. Smith, M. B.; Stonehuerner, J.; Ahmed, A. J.; Staudenmayer, N.; Millet, F., Biochim. Biophys. Acta, 1980, 592, 303-313.
76. Osheroff, N.; Brautigan, D. L.; Margoliash, E., J. Biol. Chem., 1980, 255, 8245-8251.
77. König, B. W.; Osheroff, N.; Wilms, J.; Muijer, A. O.; Dikker, H. L.; Margoliash, E., FEBS Lett., 1980, 111, 395-398.
78. Veerman, E. C. I.; Wilms, J.; Dikker, H. L.; Muijsers, A. O.; van Buuren, K. J. H.; van Gelder, B. F.; Osheroff, N.; Speck, S. H.; Margoliash, E., J. Biol. Chem., 1983, 258, 5739-5745.
79. Smith, H. T.; Ahmed, A. J.; Millet, F., J. Biol. Chem., 1981, 256, 4984-4990.
80. Smith, L.; Davies, H.; Reichlin, M.; Margoliash, E., J. Biol. Chem., 1973, 248, 237-243.
81. Dickerson, R. E.; Timkovitch, R., in "The Enzymes" Vol. XI (Boyer, P.D., ed.) Academic Press, New York, 1975, 397-547.
82. Smith, H. T.; Millet, F., Biochem., 1980, 19, 1117-1120.

83. Theorell, H.; Akeson, A., J. Am. Chem., Soc. 1941, 63, 1818-1820.
84. Lambeth, D.; Campbell, K.; Zand, R.; Palmer, G., J. Biol. Chem., 1973, 248, 8130-8136.
85. Serre, P. -A.; Haladjian, J.; Bianco, P., J. Electroanal. Chem., 1981, 122, 327-336.
86. Greenwood, C.; Wilson, M. T., Eur. J. Biochem., 1971, 22, 5-10.
87. Nicholls, P., Biochim. Biophys. Acta, 1974, 346, 261-310.
88. Bosshard, H. R., J. Mol. Biol., 1981, 153, 1125-1149.
89. Myer, Y. P.; Srivastava, R. B.; Kumar, S.; Raghavendra, K., J. Prot. Chem., 1983, 2, 13-42.
90. Eaton, W. A.; Hockstrasser, R. M., J. Chem. Phys., 1967, 46, 2533-2539.
91. Shechter, E.; Saludjian, P., Biopolymers, 1967, 5, 788-790.
92. Wilting, J.; van Buuren, K. J. H.; Braams, R.; van Gelder, B. F., Biochim. Biophys. Acta, 1975, 376, 285-297.
93. Schejeter, A.; George, P., Biochem., 1964, 8, 1045-1049.
94. Hines, R. M.; Kreishman, G. P., Bioelectrochem. Bioenerg., 1981, 8, 309-314.
95. Myer, Y. P.; Thallam, K. K.; Pande, A., J. Biol. Chem., 1980, 255, 9666-9673.
96. Myer, Y. P.; Pande, A.; Saturno, A. F., J. Biol. Chem., 1981, 256, 1576-1581.
97. Ikai, A.; Fish, W. W.; Tanford, C., J. Mol. Biol., 1973, 73, 165-184.
98. Kaminsky, L. S.; Miller, V. J.; Davison, A. J., Biochem., 1973, 12, 2215-2220.
99. Tsong, T. W., Biochem., 1976, 15, 5467-5473.

100. Schejter, A.; Glauser, S. C.; George, P.; Margoliash, E., Biochim. Biophys. Acta, 1963, 73, 641-643.
101. Horecker, B. L.; Kornberg, A., J. Biol. Chem., 1946, 165, 11-20.
102. Horecker, B. L.; Stannard, J. N., J. Biol. Chem., 1948, 172, 589-597.
103. Myer, Y. P., J. Biol. Chem., 1968, 243, 2115-2122.
104. Harbury, H. A.; Loach, P. A., J. Biol. Chem., 1960, 235, 3640-3645.
105. Copeland, R. A.; Spiro, T. G., Biochem., 1985, 24, 4960-4968.
106. Cohen, J. S.; Fischer, W. R.; Schechter, A. N., J. Biol. Chem., 1974, 249, 1113-1118.
107. Minikami, S.; Titani, K.; Ishikura, H., J. Biochem. (Tokyo), 1957, 46, 121-127.
108. Salemme, F. A., Ann. Rev. Biochem., 1977, 46, 299-329.
109. Mayo, S. L.; Ellis, Jr., W. R.; Crutchley, R. J.; Gray, H. B., Science, 1986, 233, 948-952.
110. Simone, M. J.; Heineman, W. R.; Kreishman, G. P., J. Colloid Interface Sci., 1982, 86, 295-298.
111. Simone, M. J.; Kreishman, G. P., Anal. Biochem., 1983, 132, 142-146.
112. Bosshar, H. R.; Zürrer, M., J. Biol. Chem., 1980, 255, 6694-6699.
113. Moore, G. R.; Williams, R. J. P.; Chien, J. C. W.; Dickinson, L. C. D., J. Inorg. Biochem., 1980, 12, 1-15.
114. Wendoloski, J. J.; Matthew, J. B.; Weber, P. C.; Salemme, F. R., Science, 1987, 238, 794-796.
115. Liang, N.; Pielak, G. J.; Mauk, A. G.; Smith, M.; Hoffman, B. M., Proc. Natl. Acad. Sci. U.S.A., 1987, 84, 1249-1252.
116. Rackovsky, S.; Goldstein, D. A., Proc. Natl. Acad. Sci. U.S.A., 1984, 81, 5901-5905.

117. Yeh, P.; Kuwana, T., Chem. Lett., 1977, 1145-1148.
118. Eddowes, M. J.; Hill, H. A. O., J. Chem. Soc., Chem. Commun., 1977, 771-772.
119. Landrum, H. L.; Salmon, R. T.; Hawkrige, F. M., J. Am. Chem. Soc., 1977, 99, 3154-3158.
120. Albery, W. J.; Eddowes, M. J.; Hill, H. A. O.; Hillman, A. R., J. Am. Chem. Soc., 1981, 103, 3904-3910.
121. Heineman, W. R.; Norris, B. J.; Goelz, J. F., Anal. Chem., 1975, 47, 79-84.
122. Kuwana, T.; Heineman, W. R., Acc. Chem. Res., 1976, 9, 241-248.
123. Allen, P. M.; Hill, H. A. O.; Walton, N. J., J. Electroanal. Chem., 1984, 178, 69-86.
124. Chao, S.; Robbins, J. L.; Wrighton, M. S., J. Am. Chem. Soc., 1983, 105, 181-188.
125. Bianco, P.; Haladjian, J., J. Electroanal. Chem., 1987, 223, 201-214.
126. Taniguchi, I.; Toyosawa, K.; Yamaguchi, H.; Yasukouchi, K., J. Chem. Soc., Chem. Commun., 1982, 1032-1033.
127. Bancroft, E. E.; Blount, H. N.; Hawkrige, F. M., Biochem. Biophys. Res. Commun., 1981, 101, 1331-1336.
128. Bancroft, E. E.; Blount, H. N.; Hawkrige, F. M., In "Electrochemical and Spectrochemical Studies of Biological Redox Components", Kadish, K. M., Ed.; American Chemical Society, Washington, DC, 1982; 23-49.
129. Bowden, E. F.; Hawkrige, F. M.; Blount, H. N., In "Electrochemical and Spectrochemical Studies of Biological Redox Components", Kadish, K. M., Ed.; American Chemical Society, Washington, DC, 1982; 159-171.
130. Butler, J. A. V., Trans. Faraday Soc., 1924, 19, 729-733.
131. Butler, J. A. V., Trans. Faraday Soc., 1924, 19, 734-739.

132. Erdey-Gruz, T.; Volmer, M., Z. Phys. Chem., Abt. A, 1930, 150, 203-211.
133. Bowden, E. F.; Hawkrige, F. M.; Chlebowski, J. F.; Bancroft, E. E.; Thorpe, C.; Blount, H. N., J. Am. Chem. Soc., 1982, 104, 7641-7644.
134. Harmer, M. A.; Hill, H. A. O., J. Electroanal. Chem., 1984, 170, 369-375.
135. King, B. C.; Hawkrige, F. M., J. Electroanal. Chem., 1987, 237, 81-92.
136. Koller, K. B.; Hawkrige, F. M.; Fauque, G.; LeGall, J., Biochem. Biophys. Res. Commun., 1987, 145, 619-624.
137. Armstrong, F. A.; Hill, H. A. O.; Oliver, B. N., J. Chem. Soc., Chem. Commun., 1984, 976-977.
138. Arnold, D. J.; Gerchario, K. A.; Anderson, C. W., J. Electroanal. Chem., 1984, 172, 379-382.
139. Besto, S. R.; Klapper, M. H.; Anderson, L. B., J. Am. Chem. Soc., 1972, 94, 8197-8204.
140. Serre, P. -A.; Haladjian, J.; Bianco, P., J. Electroanal. Chem., 1981, 122, 327-336.
141. Kutznetsov, B. A., Bioelectrochem. Bioenerg., 1981, 8, 681-690.
142. Scheller, F., Bioelectrochem. Bioenerg., 1977, 4, 490-499.
143. Haladjian, J.; Bianco, P.; Serre, P. A., Bioelectrochem. Bioenerg., 1979, 6, 555-561.
144. Kôno, T.; Nakamura, S., Bull. Agric. Chem. Soc. Jpn., 1958, 22, 399-403.
145. Tarasevich, M. R.; Bogdanovskaya, V. A., Bioelectrochem. Bioenerg., 1976, 3, 589-595.
146. Kuznetsov, B. A. Mestechkina, N. M.; Izotov, M. V.; Karuzina, I.; Karyakin, A. V.; Archakov, A. I., Biochemistry (Engl. Transl.), 1979, 44, 1234-1239.
147. Cotton, T. M.; Kaddi, D.; Iorga, D., J. Am. Chem. Soc., 1983, 105, 7462-7464.

148. Armstrong, F. A.; Hill, H. A. O.; Walton, N. J., Quart. Rev. Biophys., 1986, 18, 261-322.
149. Reed, D. E.; Hawkridge, F. M., Anal. Chem., 1987, 59, 2334-2339.
150. Tang, J.; Albrecht, A. C., In "Raman Spectroscopy", Szymanski, H. A., Ed.; Plenum Press: New York, 1970; Vol. 2, Chapt. 2.
151. Spiro, T. G.; Streckas, T. C., Proc. Natl. Acad. Sci. U.S.A., 1972, 69, 2622-2626.
152. Albrecht, A. C., J. Chem. Phys., 1961, 34, 1476-1484.
153. Albrecht, A. C.; Hutley, M. C., J. Chem. Phys., 1971, 55, 4438-4443.
154. Spiro, T. G.; Streckas, T. C., J. Am. Chem. Soc., 1974, 96, 338-345.
155. Spiro, T. G., In "Iron Porphyrins"; Lever, A. B. P. and Gray, H. B., Eds.; Addison-Wesley: Reading, MA, 1983; Vol. 2, 89-160.
156. Spiro, T. G.; Burke, J. M., J. Am. Chem. Soc., 1976, 98, 5482-5489.
157. Callahan, P. M.; Babcock, G. T., Biochemistry, 1981, 20, 952-958.
158. Spiro, T. G., Biochim. Biophys. Acta, 1975, 416, 169-189.
159. Birke, R. L.; Lombardi, J. R.; Sanchez, L. A., In "Electrochemical and Spectroelectrochemical Studies of Biological Redox Components", Kadish, K. M., Ed.; American Chemical Society, Washington, DC, 1982; 69-107.
160. van Duyne, R. P., In "Chemical and Biochemical Application of Lasers"; Moore, C. B., Ed.; Academic Press: New York, 1979; Vol.4, Chapter 5.
161. Creighton, J. A.; Albrecht, M. G.; Hester, R. E.; Matthew, J. A. D., Chem. Phys. Lett., 1978, 55, 55-58.
162. Creighton, J. A.; Blachford, C. G.; Albrecht, M. G., J. Chem. Soc. Faraday Trans., 1979, 75, 790-795.

163. Murray, C. A., In "Surface Enhanced Raman Scattering"; Chang, R. K., Furtak, T. E., Eds.; Plenum: New York, 1982; pp. 203-221.
164. Otto, A., In "Light Scattering in Solids"; Cardona, M., Guntherodt, G, Eds.; Springer-Verlag: New York, 1984; Vol. 4, pp. 289-418.
165. Watanabe, T.; Kawanami, O.; Honda, K.; Pettinger, B., Chem. Phys. Lett., 1983, 102, 565-570.
166. Roy, D.; Furtak, T. E., Chem. Phys. Lett., 1986, 124, 299-303.
167. Roy, D.; Furtak, T. E., Phys. Rev. B, 1986, 34, 5111-5117.
168. Lippitsch, M. E., Chem. Phys. Lett., 1981, 79, 224-226.
169. Brautigan, D.L.; Ferguson-Miller, S.; Margoliash, E., Methods Enzymol., 1978, 53D, 131-132.
170. Margoliash, E.; Schejter, A., Adv. Protein Chem., 1966, 21, 113-286.
171. Margoliash, E., Biochem. J., 1954, 56, 535-543.
172. Margoliash, E. Frohwirt; N.; Wiener, E., Biochem. J., 1959, 71, 559-564.
173. Lumry, R.; Solbakken, A.; Sullivan, J.; Reyerson, L. H., J. Am. Chem. Soc., 1962, 84, 142-149.
174. Morton, R. A.; Bohan, T. L., Can. J. Biochem., 1971, 49, 328-331.
175. Aviram, I.; Schejter, A., Biopolymers, 1972, 11, 2141-2145.
176. Van Buuren, K.J.H.; Van Gelder, B.F.; Wilting, J.; Braams, R., Biochim. Biophys. Acta, 1974, 333, 421-429.
177. Pyun, C.H.; Park, S.M., Anal. Chem., 1986, 58, 251-256.
178. Hill, R., In "Modern Methods of Plant Analysis," Peach, K. and Tracey, M.V. (Editors), Springer-Verlag, New York (1956) Vol 1, p.393.
179. Nicholson, R.S., Anal. Chem., 1965, 37, 1351-1355.

180. Sevcik, A., Collect. Czech. Chem. Commun., 1948, 13, 349-377.
181. Bancroft, E.E.; Sidwell, J.S.; Blount, H.N., Anal. Chem., 1981, 53, 1390-1394.
182. Albertson, D.E.; Blount, H.N.; Hawkridge, F.M., Anal. Chem., 1979, 51, 556-560.
183. Bancroft, E.E.; Blount, H.N.; Hawkridge, F.M., Anal. Chem., 1981, 53, 1862-1866.
184. Evans, J.F.; Blount, H.N., J. Am. Chem. Soc., 1978, 100, 4191-4196.
185. Bard, A.J.; Faulkner, L.R., "Electrochemical Methods," Wiley, New York, 1980, pp. 563-567.
186. Woodward, F.E.; Woodward, W.S.; Reilley, C.N., Anal. Chem., 1981, 53, 1251A-1266A.
187. Kissinger, P.T.; Reilley, C.N., Anal. Chem., 1970, 42, 12-15.
188. Theorell, H., Biochem. Z., 1936, 285, 207-218.
189. Matsuda, H.; Ayabe, Y., Z. Elektrochem., 1955, 59, 494-503.
190. Koller, K. B., Ph.D. Dissertation, Virginia Commonwealth University, Richmond, VA, 1986.
191. Suh, J. S.; Dilella, D. P.; Moskovits, M., J. Phys. Chem., 1983, 87, 1540-1544.
192. Hendra, P. J.; Loader, E. J., Chem. Ind. (London), 1968, 718-719.
193. Hildebrandt, P.; Stockburger, M., J. Phys. Chem., 1986, 90, 6017-6024.
194. Cusanovich, M. A., In "Bioorganic Chemistry," van Tamelen, E.E. (Editor), Academic Press, New York (1978) Vol. IV, pp. 117-145.
195. Armstrong, N.R.; Vanderborgh, N.E.; Quinn, R.K., J. Phys. Chem., 1976, 80, 2740-2745.
196. Hopfield, J. J., Proc. Natn. Acad. Sci. USA, 1974, 71, 3640-3644.

197. Trasatti, S., Electrochim. Acta, 1983, 28, 1083-1093.
198. Christie, J.H.; Lauer, G.; Osteryoung, R.A., J. Electroanal. Chem., 1964, 7, 60-72.
199. Robinson, R. S.; McCurdy, C. W.; McCreery, R. L., Anal. Chem., 1982, 54, 2356-2361.
200. Kolb, D. M.; Kötzt, R., Surf. Sci., 1977, 64, 96-108.
201. Furtak, T. E.; Lynch, D. W., J. Electroanal. Chem., 1977, 79, 1-17.
202. Taniguchi, I.; Iseki, M.; Yamaguchi, H.; Yasukouchi, K., J. Electroanal. Chem., 1984, 175, 341-348.
203. Smulevich, G.; Spiro, T.G., J. Phys. Chem., 1985, 89, 5168-5173.
204. Koller, K. B.; Hawkridge, F.M., J. Electroanal. Chem., 1988, 239, 291-306.
205. Paul, K. -G., Acta Chem. Scand., 1950, 4, 239-244.
206. Hill, H. A. O., Pure & Appl. Chem., 1987, 59, 743-748.
207. Sun, S.; Reed, D. E.; Cullison, J. K.; Rickard, L. H.; Hawkridge, F. M., submitted for publication in Microchim. Acta.
208. Mathews, F. S., Prog. Biophys. Molec. Biol, 1985, 45, 1-56.
209. Marcus, R. A.; Sutin, N., Biochim. Biophys. Acta, 1985, 811, 265-322.

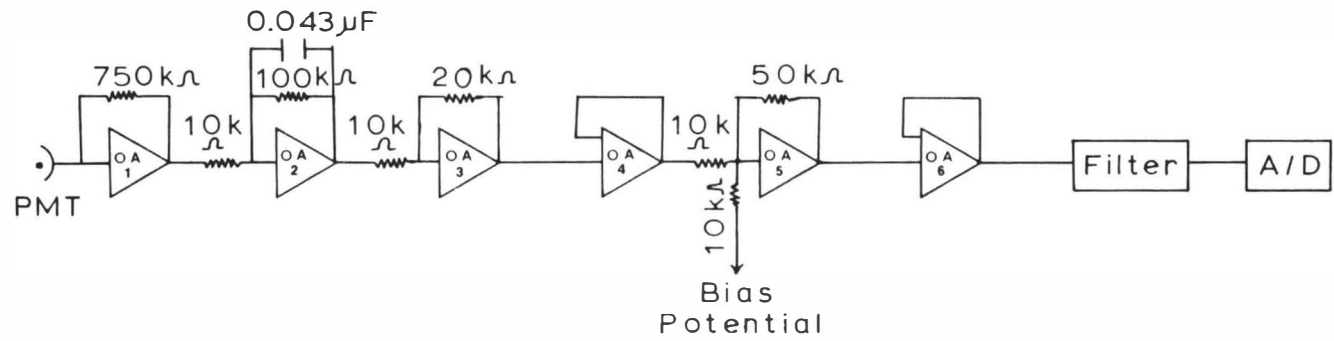
APPENDIX I

DATA ACQUISITION SYSTEMS

A. Setup of the Spectroelectrochemical System.

In both DCVA and SPS/CA experiments, acquisition of optical signals was carried out with the aid of a UNC computer interfaced to a single-beam spectroelectrochemical system. Figure 27 shows the schematic diagram used for converting the optical intensity into an absorbance profile. The first step is to convert the PMT current to a voltage signal using the current follower, OA1. This signal was then passed to a gain amplifier, OA2. A capacitor was placed in parallel with the feedback resistor of OA2 in order to partially filter the noise of the system. How much filtering is performed on the signal is related to the RC time constant (capacitance times feedback resistor). Increases in the RC time constant will lead to smoother signals. However, the magnitude of the RC constant should be limited since excessive smoothing will cause severe signal distortion. The RC time constant used for DCVA and SPS/CA experiments were 0.1 and 4.3×10^{-3} seconds, respectively. The partially smoothed signal is then inverted and amplified by passing through OA3.

Figure 27 Schematic diagram for converting optical intensity into absorbance. OA in this diagram represents operational amplifiers.



At the beginning of an experiment the voltage signal of OA3 is adjusted, by the gain on this amplifier, to equal ≈ 1.0 volt. This amplified voltage of the PMT now represents the initial intensity of the sample, P0, just prior to applying a potential perturbation to the working electrode. This voltage is then passed by a coaxial cable to the port of A/D convertor #3 on the computer interface card and is used in the calculation of the sample absorbance in DCVA and SPS/CA programs. The initial signal ensuing from OA3 is inverted and offset to ≈ 50 mV by applying a bias potential to the gain amplifier OA5. During an experiment, this configuration will cause the voltage from OA5 to increase, while that from OA3 to decrease. By adjusting the resistors on OA5, it is possible to amplify the signal in order to cover the 0-1 volt range of the A/D convertor. In DCVA experiments this signal is filtered prior to entering A/D port #1, using an analog fourth-order Butterworth active filter with a cutoff frequency of ca. 50 Hz.

The data processing, acquisition and control of DCVA and SPS/CA experiments was carried out by the use of two programs written in BASIC for the UNC computer: DCVA and SPSCA7. In order to calculate the absorbance in these programs the total gain, G, from OA4 to the input of the A/D convertor #1 needs to be calculated with the bias on OA5 off. In addition the dark current, D, must be determined for these calculations. This is carried out by turning a

filter wheel placed in front of the monochrometer. This wheel contains an opaque filter in position one and no filter in position three. By rotating the filter wheel from position three to position one, the dark current can be measured at OA3.

B. Computational Algorithms for DCVA and SPS/CA Experiments

In DCVA experiments, once the data has been acquired and converted to an absorbance signal, it is passed twice through a 5-point moving average smoothing routine before taking the derivative (1). The derivative in this program is obtained from the difference, in both the absorbance and potential, between two neighboring data points. Following derivatization, the signal is passed through a 25-point smoothing routine (1). These computations for DCVA experiments are based on published algorithms of Bancroft et al. (2).

For SPS/CA experiments it was necessary to correct the results for changes in reflectivity of the metal-electrolyte interface. This general procedure for obtaining background corrected SPS/CA responses is as follows: First, the absorbance spectra of the electrolyte alone is obtained. The same potential perturbations are then applied to a sample containing both electrolyte and cytochrome c. The difference between these two responses is the background corrected SPS/CA. These background corrected files can then

be used to determine heterogeneous electron transfer kinetic parameters. In order to calculate such parameters, $k_{f,h}$ must be determined for each overpotential. These values are obtained from working curves generated by the SPSCA7 program using equations derived by Bancroft et al. (3).

```
PROGRAM TITLE SPSCA7
10  CLEAR; PLOT (0,1,1)
20  DIM A(200),A1(200),A2(200),I(20),A4(200),D4(200),
    T(200),B(3200),C(3200),$F(30).$F1(30),S9(20)
30  REM  THIS IS A BACKGROND CORRECTED SPSCA PROGRAM
40  REM  THIS PROGRAM TAKES DATA POINTS AT A RATE OF 20
    pts./sec.
50  REM  THIS PROGRAM IS DESIGNED FOR THE UNC LAB
    COMPUTER.
60  REM  INITIAL CURRENT VOLTAGE OUTPUT MUST BE BIASED TO
    APR.
70  REM  0.05 VOLTS POSITIVE.  ALL CURRENT TO OUTPUT MUST
    BE BETWEEN
80  REM  0 TO 1 VOLTS.
90  REM  CHANNEL 1          ABSORBANCE
100 REM  DAC CHANNEL 3      E INPUT TO POTENTIOSTAT
110 REM  1 INDICATES YES RESPONSE, 0 INDICATES NO
120 PRINT"IF YOU WANT TO RETRIEVE A DISK FILE ENTER 1"
130 INPUT X6
140 IF X6=1 THEN GOSUB 870
150 IF X6=1 THEN GOTO 340
160 PRINT%%  "INPUT MONTH, DAY, YEAR, RUN NO."
170 INPUT C1,C2,C3,C4
180 PRINT"INPUT INITIAL VOLTAGE IN MV";INPUT V1
190 DAC(3)=V1*5E-5+.5
```

```
200 PRINT"INPUT TIME LIMIT FOR DATA ACQUISITION (SEC)";  
    INPUT T  
  
210 REM TIME INCLUDES 1 SEC DELAY TO FIRST TIME  
  
220 PRINT%%"PLOT HAS MAX DIM OF 5X5 INCHES"  
  
230 PRINT"INPUT SECONDS PER DIVISION"  
  
240 INPUT S  
  
250 S1=S*10  
  
260 ERAS;PRINT"INPUT DARK CURRENT (IN VOLTS)"; INPUT D  
  
270 PRINT"INPUT VOLTAGE IN MV FOR STEP"  
  
280 INPUT V  
  
290 V2=V*5E-5+.5  
  
300 PRINT"INPUT VOLTAGE IN MV TO RETURN TO"  
  
310 INPUT V3  
  
320 V3=V3/.996  
  
330 GOSUB 750  
  
340 PRINT"WANT ABSORBANCE VERSUS TIME PLOT?"  
  
350 INPUT N1  
  
360 IF N=1 THEN GOSUB 930  
  
370 ERAS;PRINT"WANT THIS DATA STORED ON DISK?"  
  
380 INPUT N8  
  
390 IF N8=1 THEN GOSUB 1970  
  
400 ERAS;PRINT"WANT TO CORRECT POTENTIAL STEP FOR  
    BACKGROUND REFLECTANCE?";INPUT N31  
  
410 IF N31=1 THEN GOTO 430  
  
420 GOTO 540
```

```
430 Q4=K;FOR N=0 TO Q4;A2(N)=A(N);NEXT N
440 ERAS;PRINT"INPUT FILENAME TO RETRIEVE BACKGROUND
REFLECTANCE STEP";INPUT $F1
450 GET '$F1 ON(1)
460 GET S9(B) A(Z) END 470
470 C1=S9(0);C2=S9(1);C3=S9(2);C4=S9(3);S=S9(4);
S1=S9(5);T=S9(6);V=S9(7);V1=S9(8);V2=S9(9);
V3=S9(10);K=S9(11);W=S9(12)
480 FOR N=0 TO Q4;A(N)=A2(N)-A(N);NEXT N
490 W=Q4
500 ERAS;PRINT"WANT ABSORBANCE VERSUS TIME PLOT FOR
REFLECTANCE CORRECTED STEP?";INPUT N32
510 IF N32=1 THEN GOSUB 930
520 ERAS;PRINT"WANT THIS DATA STORED ON DISK?";INPUT N33
530 IN N33=1 THEN GOSUB 1970
540 ERAS;PRINT"WANT ABSORBANCE VERSUS SQUARE ROOT OF TIME
PLOT?";INPUT N10
550 IF N10=1 THEN GOSUB 1140
560 ERAS;PRINT"WANT CALCULATION OF NABS VS.
LOG10(SQR(T/D))?";INPUT N9
570 IF N9=1 THEN GOSUB 1340
580 ERAS;PRINT"WANT NABS VS. LOG10(KF(SQR(T/D))) FROM
WORKING CURVE?";INPUT N11
590 IF N11=1 THEN GOSUB 1550
```

```
600 ERAS;PRINT"INPUT 0 TO STOP OR 1 TO CONTINUE TO NEXT
    CALCULATION";INPUT O
610 IF O=0 GOTO 2140
620 IF O=1 GOTO 120
630 ERAS;PRINT"PRESS SPACE BAR TO INITIATE EXPERIMENT"
640 X=KEY(K); IF X<>160 GOTO 640
650 ERAS;PRINT"***** ACQUIRING DATA *****"
660 K=((T)*20)+9)
670 I=IADC(0)(0);PO=IADC(3)(.1)
680 FOR N=0 TO 9
690 A(N)=IADC(1)(.1)
700 NEXT N
710 A(0)=IADC(0)[1](0);DAC(3)=V2
720 FOR N= 10 TO K
730 A(N)=IADC(1)(0.05)
740 NEXT N
750 DAC(3)=V3*5E-5+.5
760 B=(A(0)+A(1)+A(2)+A(3)+A(4)+A(5)+A(6)+A(7)+A(8)+
    A(9))/10
770 FOR N=0 TO K
780 A(N)=A(N)-B
790 NEXT N
800 ERAS;PRINT"INPUT GAIN FOR ABSORBANCE";INPUT G
810 FOR N=0 TO K
820 A(N)=-LOG10(((P0-(A(N)*(1/G)))-D)/(P0-D))
```



```
830 NEXT N
840 W=K
850 ERAS
860 RETURN
870 PRINT"INPUT FILE NAME TO RETRIEVE"
880 INPUT $F1
890 GET '$F1
900 GET S9(B) A(Z) END 910
910 C1=S9(0);C2=S9(1);C3=S9(2);C4=S9(3);S=S9(4);
    S1=S9(5);T=S9(6);V=S9(7);V1=S9(8);V2=S9(9);
    V3=S9(10);K=S9(11);W=S9(12)
920 RETURN
930 REM      ABSORBANCE VERSUS TIME PLOT
940 PRINT%%"MAXIMUM ABSORBANCE= ",A(W), "AU"
950 PRINT%%"INPUT ABSORBANCE UNITS PER DIVISION"
960 INPUT U
970 U1=U*10
980 PLOT(0,(0.05/S1)*10,.1+A(10)/U1)
990 PLOT(1,(0.05/S1)*10,.1+A(10)/U1)
1000 FOR N=10 TO K
1010 PLOT(1,(0.05/S1)*N,.1+A(N)/U1)
1020 NEXT N
1030 PLOT(0,(0.05/S1)*K,.1+A(K)/U1)
1040 PLOT(0,1,1)
1050 PRINT"WANT TO FRAME GRAPH"
```

```
1060 INPUT W1
1070 IF W1=1 THEN GOSUB 2030
1080 IF W1=0 THEN RETURN
1090 PLOT(0,.05,.9)(3)"A VS. T"
1100 PLOT(0,.05,.85)(3)"X=",S,"SEC/DIV"
1110 PLOT(0,.05,.80)(3)"Y=",U,"AU/DIV"
1120 PLOT(0,1,1)
1130 RETURN
1140 REM      ABSORBANCE VERSUS SQUARE ROOT OF TIME PLOT
1150 PRINT%%"MAXIMUM ABSORBANCE=",A(W),"AU"
1160 PRINT%%"INPUT ABSORBANCE UNITS PER DIVISION"
1170 INPUT U2
1180 U3=U2*10
1190 PLOT(0,SQR((0.05/S1)*10),.1+A(10)/U3)
1200 PLOT(1,SQR((0.05/S1)*10),.1+A(10)/U3)
1210 FOR N=10 TO K
1220 PLOT(1,SQR((0.05/S1)*N),.1+A(N)/U3)
1230 NEXT N
1240 PLOT(0,SQR((0.05/S1)*K),.1+A(K)/U3)
1250 PLOT(0,1,1)
1260 PRINT"WANT TO FRAME GRAPH";INPUT W8
1270 IF W8=1 THEN GOSUB 2050
1280 IF W8=0 THEN RETURN
1290 PLOT(0,.05,.9)(3)"A VS. SQR(T)"
1300 PLOT(0,.05,.85)(3)"X=",SQR(S),"SQR(SEC)/DIV"
```

```
1310 PLOT(0,.05,.80)(3)"Y=",U2,"AU/DIV"
1320 PLOT(0,1,1)
1330 RETURN
1340 REM    CALCULATION OF NABS VS. LOG10(SQR(T/D))
1350 PRINT"INPUT DIFFUSION COEFF. ";INPUT D
1360 FOR N=0 TO K
1370 A1(N)=A(N)
1380 NEXT N
1390 PRINT"INPUT FILE NAME TO RETRIEVE DIFFUSION CONTROL
        STEP";INPUT $F1
1400 GET '$F1
1410 GET S9(B) A(Z) END 1420
1420 C1=S9(0);C2=S9(1);C3=S9(2);C4=S9(3);S=S9(4);
        S1=S9(5);T=S9(6);V=S9(7);V1=S9(8);V2=S9(9);
        V3=S9(10);K=S9(11);W=S9(12)
1430 FOR N=10 TO K
1440 A4(N)=A1(N)/A(N)
1450 D4(N)=LOG10(SQR(((N-9)*(0.05))/D))
1460 NEXT N
1470 TYPE TAB(2),"TIME(INSEC.)",TAB(16),"NABS",TAB(26),
        "LOG10(SQR(T/D))"
1480 TYPE
1490 FOR T1=1 TO (2*T)
1500 N=(T1/.1)+9
1510 T2=T1/2
```

```
1520 TYPE%Z%TAB(2),T2,%Z4%TAB(15),A4(N),TAB(25),D4(N)
1530 NEXT T1
1540 RETURN
1550 REM      WORKING CURVE CALCULATION
1560 PRINT"INPUT STANDARD POTENTIAL(IN VOLTS)";INPUT E0
1570 PRINT"INPUT STEP POTENTIAL (IN VOLTS)";INPUT E1
1580 PRINT"INPUT TEMP.(IN DEG KELVIN)";INPUT T3
1590 TYPE"WORKING CURVE CALCULATIONS"
1600 TYPE
1610 TYPE"STANDARD POTENTIAL=",E0,"VOLTS"
1620 TYPE"STEP POTENTIAL=",E1,"VOLTS"
1630 TYPE"OVERPOTENTIAL=", (E1-E0),"VOLTS"
1640 TYPE"TEMPERATURE =",T3,"KELVIN"
1650 TYPE
1660 TYPE TAB(2),"TIME(INSEC.)",TAB(16),"NABS",TAB(26),
      "LOG10(KF*(SQR(T/D)))"
1670 TYPE
1680 FOR Q=0 TO 1500
1690 S2=EXP(2.30258*(Q/800-2))
1700 R=S2*(1+EXP(96485*(E1-E0)/(8.31441*T3)))
1710 Z1=1/(1+(.32759*R))
1720 Z=(.25482*Z1-.28449*Z1^2+1.421141*Z1^3-1.45315*Z1^4
      +1.061*Z1^5)
1730 B(Q)=(S2*1.77246/(2*R*R))*((2*R/1.77246)+(Z)-1)
1740 C(Q)=LOG10(S2)
```

```
1750 NEXT Q
1760 FOR T1=1 TO (2*T)
1770 N=(T1/.1)+9
1780 T2=T1/2
1790 FOR Q=0 TO 1500
1800 IF B(Q)>=A4(N) GOTO 1820
1810 NEXT Q
1820 TYPE%Z%TAB(2),T2,%Z4%TAB(15),B(Q),%4E%TAB(25),C(Q)
1830 NEXT T1
1840 TYPE
1850 TYPE TAB(2),"TIME (IN SEC)",TAB(16)"LOG10(KF)"
1860 TYPE
1870 FOR T1=1 TO (2*T)
1880 N=(T1/.1)+9
1890 T2=T1/2
1900 FOR Q=0 TO 1500
1910 IF B(Q)>=A4(N) GOTO 1930
1920 NEXT Q
1930 LOGKF=C(Q)-D4(N)
1940 TYPE%Z%TAB(2),T2,%4E%TAB(16),LOGKF
1950 NEXT T1
1960 RETURN
1970 PRINT"INPUT FILE NAME FOR THIS DATA"
1980 INPUT $F
```

```
1990 S9(0)=C1;S9(1)=C2;S9(2)=C3;S9(3)=C4;S9(4)=S;S9(5)=
      S1;S9(6)=T;S9(7)=V;S9(8)=V1;S9(9)=V2;S9(10)=V3;
      S9(11)=K S9(12)=W
2000 PUT '$F
2010 PUT S9(20) A(200) END
2020 RETURN
2030 PLOT(0,0,0)
2040 M=.025
2050 FOR L=1 TO 4
2060 FOR N=1 TO 10
2070 IF L=1 THEN PLOT(1,N/10,0);PLOT(1,N/10,M);
      PLOT(1,N/10,0)
2080 IF L=2 THEN PLOT(1,1,N/10);PLOT(1,1M,N/10);
      PLOT(1,1,N/10)
2090 IF L=3 THEN PLOT(1,1-N/10,1);PLOT(1,M,1-N/10);
      PLOT(1,0,1-N/10)
2100 IF L=4 THEN PLOT(1,0,1-N/10);PLOT(1,M,1-N/10);
      PLOT(1,0,1-N/10)
2110 NEXT N;NEXT L
2120 PLOT(0,1,1)
2130 RETURN
2140 STOP
```

```
PROGRAM TITLE      "DCVA"
10  ERAS;PLOT(0,1,1);DAC(3)=0.5;DIMA(1550),E5(1550),
    A1(1550),O(11),P(30),$F5(7),$F6(7)
20  PRINT "WANT TO RETRIEVE DATA FROM DISK?(YES=1)";
    INPUT N
30  IF N=1 THEN GOSUB 350
40  IF N=1 THEN GOTO 410
50  ERAS;PRINT"INPUT INITIAL POTENTIAL (IN MV's),
    APPROXIMATE SCAN RATE (IN MV/SEC), AND ABSORBANCE
    GAIN";INPUT E1,S5,G
60  IF S5=1 THEN Z=0.5
70  IF Z=0.5 THEN GOTO 150
80  IF S5=2 THEN Z=0.25
90  IF Z=0.25 THEN GOTO 20
100 IF S5>2 THEN Z=0.10
110 IF Z=0.100 THEN GOTO 150
120 ERAS;PRINT"PUT P0 CABLE IN A/D 3 AND TURN FILTER WHEEL
    TO POSITION 1."
130 PRINT"WHEN POTENTIAL HAS STABILIZED PRESS SPACE BAR TO
    OBTAIN DARK CURRENT.";Q=KEY(160)
140 I=IADC(0)(0);D=IADC(3)(.1)
150 ERAS;PRINT"LEAVE P0 CABLE IN A/D 3 AND TURN FILTER
    WHEEL TO POSITION 3."
```

```
160 PRINT"WHEN POTENTIAL HAS STABILIZED PRESS SPACE BAR TO
    OBTAIN P0.";Q=KEY(160)
170 I=IADC(0)(0);P(0)=IADC(3)(.1)
180 ERAS;PRINT"***** ACQUIRING DATA *****"
190 I=IADC(0)(0);E5(0)=IADC(2)(.1)
200 DAC(3)=0.75
210 FOR V5=0 TO 1550;T5=V5+1
220 A(V5)=IADC(1)(Z);E5(T5)=IADC(2)(Z)
230 IF E5(T5)>=E5(0) GOTO 250
240 NEXT V5
250 DAC(3)=0.5;ERAS;PRINT"FINISH ACQUIRING DATA"
260 QE=ABS(E5(10)-E5(11));S5=(QE*1000)/(Z*2.0)
270 E3=MINX(T5)E5(0);E2=(E1/1000)-(E5(0)-E5(E3));E2=E2*100
280 ERAS;PRINT;"DO YOU WANT TO STORE DATA?";INPUT N;IF N=1
    THEN GOSUB 300
290 GOTO 410
300 ERAS;PRINT"INPUT FILENAME FOR THIS DATA";INPUT $F5
310 O(0)=E1;O(1)=E2;O(2)=E3;O(3)=S5;O(4)=T5;O(5)=G;
    O(6)=P0;O(7)=Z;O(8)=D
320 PUT '$F5 ON(1)
330 PUT O(11) A(1550) E5(1550) END
340 RETURN
350 REM     ROUTINE TO RETRIEVE DATA
360 ERAS;PRINT"INPUT FILENAME TO RETRIEVE DATA";INPUT $F6
370 GET '$F6 ON(1)
```



```
380 GET O(B) A(D) E5(D) END 390
390 E1=O(0);E2=O(1);E3=O(2);S5=O(3);T(5)=O(4);G=O(5);
    P0=O(6);Z=O(7);D=O(8)
400 RETURN
410 A0=(A(0)+A(1)+A(2)+A(3)+A(4)+A(5)+A(6)+A(7)+A(8)+
    A(9))/10
420 FOR V5=0 TO T5;A(V5)=A(V5)-A(0);NEXT V5
430 FOR V5=0 TO T5;A(V5)=-LOG10(((P0-(A(V5)/G))-D)/(P0-
    D));NEXT V5
440 SUM=0.0
450 FOR M=0 TO E3-1;SUM=SUM+((ABS(E5(M)E5(M+1)))
    *1000);NEXT M
460 DE=SUM/E3
470 ERAS;PRINT"WANT TO PLOT ABSORBANCE CONVERTED
    CVA?";INPUT N; IF N=1 THEN GOTO 490
480 GOTO 520
490 FOR V5=1 TO T5;E5(V5)=E5(V5)-((S5*Z)/1000);NEXT V5
500 GOSUB 870
510 ERAS;PRINT"WANT TO SMOOTH CVA?";INPUT N;IF N=1 GOSUB
    590
520 ERAS;PRINT"WANT TO CALCULATE DCVA?";INPUT N;IF N=1
    THEN GOSUB 540
530 ERAS;PRINT"WANT TO PLOT DCVA?(YES=1)";INPUT N;IF N=1
    THEN GOSUB 870
540 REM SUBROUTINE FOR 1st DERIVATIVE
```

```
550 FOR V5=0 TO T5
560 A(V5)=(A(V5+1)-A(V5))/DE
570 NEXT V5
580 RETURN
590 REM      SUBROUTINE FOR 5-POINT MOVING AVERAGE
600 ERAS;PRINT"INPUT NUMBER OF TIMES YOU WOULD LIKE TO
        APPLY 5-POINT MOVING AVERAGE TO CVA"; INPUT Q5
610 ERAS;PRINT "NOW SMOOTHING DATA WITH 5-POINT MOVING
        AVERAGE"
620 FOR Z5=1 TO Q5
630 FOR V5=5 TO T5-4
640 A1(V5)=(A(V5+5)+A(V5+4)+A(V5+3)+A(V5+2)+A(V5+1)+A(V5)
        +A(V5-1)+A(V5-2)+A(V5-3)+A(V5-4)+A(V5-5))/11
650 NEXT V5
660 FOR V5=5 TO T5-4
670 A(V5)=A1(V5)
680 NEXT V5
690 NEXT Z5
700 RETURN
710 REM      25-POINT SMOOTHING ROUTINE
720 ERAS;PRINT "NOW SMOOTHING DCVA WITH 25-POINT SMOOTH"
730 M=T5-24
740 FOR Z6=1 TO 25
750 FOR L=1 TO 24
760 J=L-1;P(L)=A(J);NEXT L
```

```
770 FOR L=0 TO M;J=L+24;FOR K=0 TO 23;K1=K+1
780 P(K)=P(K+1);NEXT K;P(24)=A(J)
790 W=467*(P(12))+462*(P(11)+P(13))+447*(P(10)+P(14))+422
    *(P(9)+P(15))
800 W=W+387*(P(8)+P(16))+343*(P(7)+P(17))+287*(P(6)+P(18)
    +222*(P(5)+P(19))
810 W=W+147*(P(4)+P(20))+62*(P(3)+P(21))
820 W=W-33*(P(2)+P(22))-138*(P(1)+P(23))-253*(P(0)+P(24))
830 A1(L+12)=W/5175;NEXT L
840 FOR J=12 TO M;A(J)=A1(J);NEXT J
850 NEXT Z6
860 RETURN
870 REM      PLOT ROUTINE FOR CVA AND DCVA
880 A2=MAXX(E3) A(25);PRINT"CATHODIC PEAK MAXIMUM=",
    %4E%A(A2),"ABSORBANCE/MV"
890 A4= MINX(E3-100) A(E3);PRINT"ANODIC PEAK MINIMUM=",
    %4E%A(A4),"ABSORBANCE/MV";PRINT" "
900 PRINT"INPUT DA/DE UNITS PER INCH"
910 INPUT Y;Y1=Y*10;X=E5(0)E5(E3+1);PLOT(0,0,0.5+
    A(0)/Y1)
920 FOR R5=0 TO T5;PLOT (1,(E5(0)E5(R5))/X,0.5+
    A(R5)/Y1);NEXT R5
930 PLOT(0,1,1);PLOT(0,0,0);PLOT(0,0.04,0.90)(3),%3E%Y,
    "ABSORBANCE/MV" PLOT(0,0.04,0.85)(3),%22%5,"MV/SEC"
```

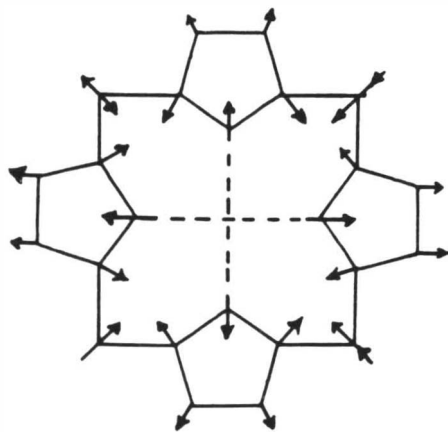
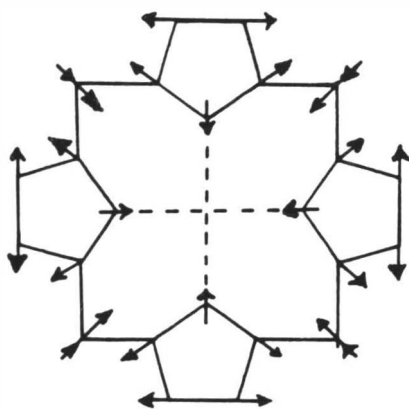
```
940 PLOT(0,0,0);PLOT(1,0.05,0.05);PLOT(0,0.05,0.05)(3),  
    %Z3%E1  
950 PLOT(0,1,0);PLOT(1,0.95,0.05);PLOT(0,0.80,0.05)(3),  
    %Z3%E2;PLOT(0,1,1)  
960 RETURN  
970 STOP
```

APPENDIX II

VIBRATIONAL MODES CORRESPONDING TO ν_3 AND ν_4
RR INDICATOR BANDS

The diagrams included in this appendix illustrate the molecular motions of the porphyrin which contribute to the observed normal vibrational modes of the RR indicator bands (ν_3 and ν_4). As shown in Figure 28 both ν_3 and ν_4 are totally symmetric (A_{1g}) vibrations. The ν_3 vibration is sensitive to changes in both oxidation state and spin state of the heme iron, while the ν_4 vibration is mainly sensitive to changes in oxidation state.

Figure 28 Molecular motions contributing to the observed normal vibrational modes of the ν_3 and ν_4 bands.

 \checkmark_3  \checkmark_4

APPENDIX REFERENCES

1. Savitzky, A.; Golay, M. J.E., Anal. Chem., 1964, 36, 1627-1634.
2. Bancroft, E. E.; Sidwell, J. S.; Blount, H. N., Anal. Chem., 1981, 53, 1390-1394.
3. Bancroft, E. E.; Blount, H. N.; Hawkrige, F. M., Anal. Chem., 1981, 53, 1862-1866.

VITA

